MODELLNG OF *DREISSENID* MUSSEL IMPACTS ON LAKE MICHIGAN

by

Chunqi Shen

A Dissertation Submitted in
Partial Fulfillment of the
Requirements of the Degree of

Doctor of Philosophy
in Engineering

at

The University of Wisconsin-Milwaukee

August 2016

ABSTRACT

MODELLING OF *DREISSENID* MUSSEL EFFECTS ON LAKE MICHIGAN

by

Chunqi Shen

The University of Wisconsin-Milwaukee, 2016
Under the Supervision of Professor Qian Liao

Invasive *dreissenid* mussel appear to have profoundly altered Great Lakes food webs and nutrient cycles during the past several decades. Recent declines of phytoplankton were supposed to be highly related with the increase of mussel population. These phytoplankton declines were further found to be coincident with declines in the abundance of planktivorous fish. In addition, the resurgence of *Cladophora* in Great lakes was estimated to be associated with the high density colonization of mussels. More light is available at lake bottom due to the mussels' graze effect. The mussels further promote *Cladophora* growth by fertilizing it with nutrient-rich excrement. And their shells provide hard rocky surface on which the algae can grow.

Numerical models were applied in this thesis to investigate the ecosystem of Lake Michigan, specifically to explore how invasive mussels affect the nutrient dynamics and distribution of phytoplankton. A 1D biophysical model was successfully developed for the mid-depth zone and it can be easily expanded to any other area with stable horizontal homogeneity. Coriolis force, momentum sink as well as wave effects were fully considered in order to well resolve the physical mixing. The phytoplankton simulation results of 2013 with the 1D model revealed significant reduction of the phytoplankton in the water column with the mussels incorporated at the bottom, 24% and 8% reduction for spring and summer respectively.

The mussels' filtering effect over lake wide was investigated with the 3D biophysical model as well. The physical parameters were solved with FVCOM while the biological part was simulated based on the NPZD model. For the simulation in 2012, the total amount of phytoplankton for the whole lake was estimated to decreased by 6% in spring and 2% in summer with mussel model included. A high concentration layer of nutrient and low concentration layer of phytoplankton were observed with the existence of mussels which was in agreement of the recent field observations. Meanwhile, the vertical distribution of phytoplankton with and without mussels along the Lake Ferry Express transect was discussed for the nearshore and offshore exchange. The mussels in our simulation results proved an important role in keeping a low concentration of phytoplankton in the offshore area where no mussel colonization was found. Finally, The *Cladophora* particle tracking simulation was conducted based on the physical FVCOM output for the Sleeping Bear Dune national park area. The model results suggested the sloughed dead *Cladophora* particles were very likely to deposit at the nearby but deeper area comparing with their original positions.

TABLE OF CONTENTS

LIST OF FIGURES

LIST OF TABLES

ACKNOWLEDGEMENTS

It was such an amazing time and important experience for the past four years. I am particularly grateful to my advisor, Dr. Qian Liao who not only supported my study, but also directed me in the whole research work. He has set me such a good example I want to follow, being knowledgeable, humorous and optimistic. His kindness and patience made the study relaxing and fun. It would be never too much to express my gratitude for his help. I have learned so much from him as a scientist and a professional.

Many thanks to Dr. Harvey Bootsma. Without him, I can never finish my thesis work. He provided me with so many insights and guidance on my research work. His enthusiasm, kindness and knowledges made him a so respectable scientist. Thank you so much to the other committee members, Dr. Hector Bravo, Dr. Yin Wang and Dr. Ryoichi Amano who provided a lot of comments and suggestion to better my work.

I am so grateful to my colleagues in Environmental Hydraulics Lab, Mr. Tong Jin, Ms, Wei Li, Dr. Binbin Wang, Ms. Xinxin Wang, for their companion and help on the work. It was them who made my life abroad much easy and colorful. I do share so many great memories with them. Good luck for all of them in the future.

At last, I would like to express my sincere gratitude to my family. Thank you to my parents for their understanding on my study abroad and their support on my daily life. All my achievement is inseparable to their cultivation. Many thanks to my sister for the encouragement and comfort when I was down. It was so great to have them and let me feel the warm and happiness.

Thanks to all other people who helped me on my work and daily life. I do appreciate that!

Chapter 1

1. INTRODUCTION AND BACKGROUND

1.1 Impacts of Invasive Dreissenid Mussels on the Ecosystem of Great Lakes

During the past several decades, *Dreissenid* mussels (*Dreissena polymorpha* [zebra mussel] and *Dreissena rostiformis bugensis* [quagga mussel]) have successfully established massive populations in the benthos of the Laurentian Great Lakes (Bunnell, 2009; Karatayev, 2014; Nalepa, 2009, 2010). One of the most direct effects is that the highly growing mussel will clog the intake pipes and damage underwater infrastructures, resulting in substantial costs for the maintaining work (Connelly, 2007; Limburg, 2010). More importantly, profound water-quality impacts and ecosystem influences have been recognized especially in shallow nearshore areas (Hecky, 2004). For example, compared to the *pre-dreissenid* period, increased water clarity has been observed due to their filtering activities (Auer, 2010; Limburg, 2010). It is estimated that the spring chlorophyll have dropped 50% and primary production has decreased 70% since the mid-1990s in Lake Michigan (Fahnenstiel, Pothoven et al. 2010). Vanderploeg (2010) indicated that the grazing effects of *dreissenid* mussels played an important role in the disappearance of the spring phytoplankton bloom in Lake Michigan. The decline is much obvious near the bottom of the water column. Recent field experiments showed that a 1-m thick concentration boundary layer which has a relative low phytoplankton biomass compared to the upper water column can be created in shallow areas (Ramcharan and Turner, 2010). The decline in the abundance of the *Diporeia* and plankton is further found to be coincident with declines in the abundance of planktivorous fish (Vanderploeg, 2002; Strayer, 2004; Pothoven and Madenjian, 2008; Bunnell, 2009; Nalepa, 2010).

Due to their nutrient requirement and the influence of food quality on excretion and egestion, invasive zebra and quagga mussels appear to have greatly altered the food web and nutrient cycle in Great Lakes (Hecky, 2004; Newell, 2004; Prins, 1998; Vaughn, 2008). The observed summer harmful algal blooms (HABs) in Lake Erie consisting primarily of the toxic colonial cyanobacterium Microcystis has been attributed to mussels through their selective rejection of the large toxic colonies of this species (Vanderploeg, 2001; Raikow, 2004). While it is well known that the spatial and temporal distributions of nutrient are largely controlled by internal recycling and water-sediment fluxes, besides the cutting of the external nutrient loading, mussels have added more complexity to the nutrient cycle in Great lakes. As the lab experiment shows, in P rich water system, mussels tend to increase P availability as soluble P while in P poor system, they will excrete little P in order to maintain a sustainable concentration in their tissue (Hecky, Smith et al. 2004). In the particle-depleted boundary layer above mussel colonies in the nearshore bottom, high dissolved nutrient concentration is often observed. Through a model study which incorporates mussel filter feeding activities, Dayton et al. (2014) found a concentration boundary layer of soluble reactive phosphorus (SRP) established at the bottom of Good Harbor Bay in Lake Michigan under quiescent conditions. Particulate phosphorus (PP) that egested by mussel or the deposit of the dead *Cladophora* will be stored in nearshore sediments, further enhancing P retention in the nearshore (Bootsma and Liao, 2013; Hecky, 2004). In addition, if this portion of P can't be recycled in time, it will lead to a net loss of P concentration in water and would affect productivity of the entire food web.

The growth and abundance of *Cladophora* in Lake Michigan was once considered to be under control since the phosphorus concentrations have dropped to a relatively low level after the phosphorus loading regulations in the late 1970s (Mida, 2010; Pauer, 2011; Chapra and Dolan,

2012). However, associated with the invasion of mussel, the resurgence of *Cladophora* is being observed at a large scale, especially in northeast Lake Michigan (Auer, 2010; Higgins, 2008). Frequent outbreaks of *Cladophora* create beach fouling and the contamination of drinking water, which have caused serious concerns of the ecosystem and human health (Auer, 2010; Higgins, 2008; Whitman, 2003). It is postulated that the increased water clarity allows more light penetration into the shallow water bottom, supporting the growth of *Cladophora*. Mussels themselves can be a favorable solid substrate for the establishment of *Cladophora*. In addition, it was found excretion of P from nearshore mussels can provide sufficient nutrient for *Cladophora* growth through the summer (Fillingham, 2015; Bootsma, 2009; Dayton, 2014). According to the calculation by Ozersky et al. (2009) in Lake Ontario, mussels can supply more soluble phosphorus than is required to support *Cladophora* growth.

During most of the *post-dreissenid* period, zebra mussels have been the dominant species. They grow primarily on hard substratum, confined primarily in the nearshore areas where the lake bottom is rocky. As a result, investigation of the mussels' effects on the ecosystem had been focused in the nearshore zone. Hecky et al. (2004) suggested that *dreissenid* mussels can efficiently retain the nutrients within the nearshore zone at the expense of offshore areas, potentially depleting pelagic resources and supporting the growth of nuisance algae in the nearshore water. This has been well known as the "nearshore shunt" hypothesis. However, since the mid-1990s, zebra mussels have been gradually replaced by the quagga mussel in Great Lakes (Nalepa, 2015; Rowe, 2015). Quagga mussel can establish on soft substrate and more tolerate to cold water compared with zebra mussels which are limited to had substrates and warm environment. As a result, quagga mussels have rapidly expanded from nearshore to offshore areas. The mid-depth sink hypothesis proposed by Vanderploeg (2010) assumes that, for the

sandy coastal area, wave actions and sandy substrate prevent colonization by *dreissenids*, and the tributary loads and primary production that they stimulated move from inshore to mid-depth regions where phytoplankton are first intercepted by mussels.

1.2 Hydrodynamic Environment

An accurate representation of the hydrodynamic environment is a key to precisely quantify the dynamics of ecosystem in Great Lakes. During the summer stratification season, the thermocline prevents dissolved oxygen produced by plant photosynthesis in the warm waters of epilimnion from reaching the cold hypolimnion, which will strongly influence the cycling of numerous elements in aquatic systems (Tyner, 2013). Mixing condition has been proved as a critical factor that affects the filtration and food capture of mussels. Vanderploeg et al. (2010) estimated the potential water column clearance rates of the quagga mussel community in Lake Michigan. And their results showed that in-situ clearance rates will depend not only on mussel filtration capacity, but also on the delivery rate of phytoplankton to the benthos, which is controlled to a large degree by vertical mixing. It has also been demonstrated that in the shallow waters without strong thermal stratification, the effective clearance rates can be much lower than the potential one when mixing is weak (Yu and Culver, 1999; Ackerman, 2001; Edwards, Rehmann, 2005). The field measurements in Good Harbor indicated that the turbulence condition is critical to the development or disruption of the concentration boundary layer of SRP at the bottom of water column (Dayton and Auer, 2014). In Lake Erie, the effect of *dreissenid* mussels on phytoplankton abundance was found to be moderated by a particulate boundary layer above mussel beds due to limited vertical mixing rates (Boegman, 2008; Zhang, 2008).

To explore the potential impact of the mussel on the lake-wide nutrient and ecosystem dynamics, vertical and horizontal advections are also critical parameters to be explored. Even the distribution of the mussel benthic colonization shows significant spatial heterogeneity, horizontal advection and dispersion tend to extend their influences beyond their colonized area since the availability of nutrients to phytoplankton will depend largely on hydrodynamic conditions (Cha, 2011; Bocaniov, 2014; Jonsson, 2014). Jonsson (2014) found an optimal bottom flow velocity exists for the maximum filtering activities of the mussels. A recent study conducted in the mid-depth hypolimion water of Lake Michigan shows that quagga mussels' phosphorus grazing rates were observed to be several times greater than passive particulate P sinking rates (Mosley and Bootsma, 2015). This may be explained by that boundary layer mixing due to internal waves and horizontal transport can enhance food delivery and support quagga mussel growth in profunda water. Furthermore, hydrodynamic conditions are important in determining bottom shear stress, which will be crucial in estimating the sediment resuspension and the *Cladophora* slough rate (Madon, 1988).

1.3 Physcial-Biogeochemical Lake Models

While the effects of invasive *dreissenids* on the ecosystem of Great Lakes are being well observed and investigated, the detailed mechanisms by which nutrient and ecosystem alterations occur are still elusive. Further research to test the validity of various conceptual models and hypothesis as well as to provide quantitative measurements are of strong necessity. Many previous work focused on shallow, weakly stratified environments, partly due to the lack of offshore *in-situ* measurement (Boegman, 2008; Zhang, 2008), it is still not very clear how mussels in the pelagic water, which are more abundant now, will affect the lake system at the

basin scale. Numerical models which combine hydrodynamic, biological and chemical processes are considered as efficient and economical tools here to quantify the impact of mussels on lake ecosystems.

Several ecological models with *dreissenid* mussels incorporated have recently been applied in large lakes. A two-dimensional ecological model based on a hydrodynamic-water quality model (CE-QUAL-W2) was constructed (Zhang, Culver et al. 2008) to investigate the *dreissenids* impact on plankton populations in Lake Erie. The result shows that impacts of *dreissenid* grazing on non-diatom algae and diatoms are different and this selectively feeding on specific phytoplankton is highly possible to contribute to harmful algal blooms in Lake Erie. Boegman et al. (2008) also applied the CE-QUAL-W2 model to explore the impact of vertical mixing and weak stratification over zebra mussels in Western Lake Erie. Results indicated that mussel grazing effect reduced under the condition when wind speed is less than 6 m/s while stratification is sufficient enough to suppress vertical mixing. Grazing effect increased significantly when wind speed is above 6 m/s. Similarly, a three-dimensional hydrodynamic model (ELCOM) coupled with a biological module (CAEDYM) was calibrated by Schwalb et al. (2014) with field data from Lake Simcoe. The model is applied to examine the expected impact of mussels on the distribution of phytoplankton and nutrients. With the same bio-physical model, Leon (2011) investigated the impacts of *dreissenid* mussels and nutrient loads to the algal biomass in Lake Erie while Bocaniov et al. (2013) focused on the nearshore shunt and the decline of the phytoplankton spring bloom after invasion of *dreissenid* mussels in Lake Erie. In a 1-D column simulation based on the 3D FVCOM physical results, Rowe et al. (2015) found that the mussel filtering substantially reduced the magnitude of the spring phytoplankton bloom in

east Lake Michigan while their impact was strongly suppressed in the summer with stratification. All the research work above highlighted an important role of mussels in the ecosystems.

Although a great amount of numerical modelling work has been conducted to explore the effect of the mussels in the ecosystem, most of them focused on the 1D vertical water column and did not take full consideration of the horizontal advection/dispersion effect to resolve the whole lake or large scale influence (Rowe, 2015). Some 2D and 3D models did successfully quantify the mussel's effects in Lake Erie (Boegman, 2008; Zhang, 2008; Schwalb, 2013; Leon, 2011). However, litter research is done to explore these effects in Lake Michigan, especially on the effects of nearshore and offshore exchange. Meanwhile, it is also necessary to understand how the *Cladophora* will influence the nutrient and food web dynamics given their abrupt resurgence associated with mussel. *Cladophora* growth models parameterized with water temperature, nutrient and photosynthetically available radiation have been validated for Lake Huron and these models effectively predicted the reduction of *Cladophora* growth in the nearshore zone with the decrease of external source loading (Auer, 2010; Higgins, 2008). Recent modeling studies in the five Great Lakes after the invasion of mussels all proved the role of mussels in promoting the growth of *Cladophora* (Higgins, 2006, 2012; Malkin, 2008; Tomlinson, 2010). However, little work has been done to couple the hydrodynamic model with the growth model. Such a coupling is critically important since, as mentioned above, the hydrodynamic environment is an important factor that controls the nutrient distribution pattern. In addition, considering their massive population and short life period, the path way and destination of the dead *Cladophora* mats after being sloughed and suspended from the bottom should be of great concern especially for the recreational beaches and water intake pipes.

1.4 Research Objective

My thesis study will focus on Lake Michigan. Although certain models have been applied to Lake Erie to assess the effects of mussels, lake-wide biophysical research for Lake Michigan is largely missing. In my research, three questions will be addressed. 1) How will the mussel influence nutrient dynamics and phytoplankton concentration in south mid-depth region of Lake Michigan? I will investigate the "mid-depth sink" theory by model simulations with and without mussels. 2) If and how the nearshore benthic mussels can affect the exchange on nutrient and energy flux between the nearshore and offshore areas of Lake Michigan? 3) How does the hydrodynamic environment influence the slough of *Cladophora* mats and the following fate and transport.

The mid-depth sink theory hypothesizes that the extension of quagga mussel to deep area away from the nearshore sandy bed creates a sink for the particle and phytoplankton in the mid-depth area of the southern Lake Michigan water. I will examine this theory through a one dimensional biophysical model for mid-depth region to evaluate the mussels' filtering activities and the effect on distribution of phytoplankton for both stratified and unstratified seasons. Based on the "nearshore phosphorus shunt" and "mid-depth sink" hypotheses associated with a small number of offshore field measurement, the phosphorus concentration of pelagic zone was found to be suppressed to a low level. To investigate the nearshore offshore exchange and the whole lake nutrient and energy dynamics, a three-dimensional coupled hydrodynamic-biogeochemical model will be established to estimate the lake-wide effects of invasive mussels. Although phosphorus loading regulation in Great Lakes has been enforced for several decades, *Cladophora* growth has been observed well even away from tributary point sources (Bootsma and Liao, 2013; Dayton, 2014). To develop a tool for better management of contamination and

prevention of potential threats to the public health, a Lagrangian particle tracking model will be developed and applied in my thesis research to predict the fate and transport of the sloughed *Cladophora* mats.

The dissertation consists of six chapters. In summary, chapter 1 is the background and literature study of the dreissenid mussels and their ecological impacts to Great Lakes. The model development and setup is presented in chapter 2 including the formulization of external forcing conditions for the model and the structure of 1D and 3D biophysical models. Chapter 3 describes the results of one-dimensional mid-depth region model. The model validation, physical mixing process and transportat of nutrient and phytoplankton are presented. Chapter 4 presents lake-wide results from the coupled 3-D Finite Volume Coastal Ocean Model (FVCOM) and biogeochemistry model. The hydrodynamic output from the FVCOM is also used to develop a particle tracking module, which is applied to study the fate and transport of *Cladophora* in the Sleeping Bear Dunes (SBD) national park area. The particle trajectory simulation results are described in Chapter 5. Chapter 6 is the conclusions and discussion of this research.

Chapter 2

2. MODEL DEVELOPMENT AND SETUP

2.1 External Forcing

2.1.1 Meteorological Data for Model

The 1D model site is close to the Milwaukee harbor and located in a mid-depth region (55 m) of Lake Michigan where quagga mussel population density is high and several filed deployments were performed during the last several years (Fig. 2.1). Field observations were

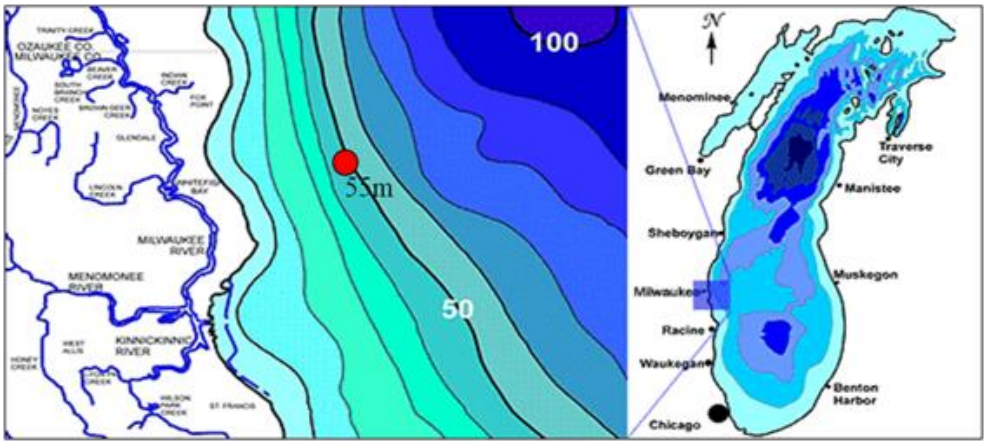

Fig. 2.1 Site positon (red dot) in Lake Michigan for 1D model.
Depth contours are given in 10-meter intervals

carried out for 3 months at this site between 21 June and 18 September in 2012 (DOY 173-262). A thermistor chain at the study site was deployed to record the temperature profiles from 0.25 m above bottom to 49 m above bottom with an interval of 4 m. The thermistors were sampled every 5 minutes. At the same time, an upward-looking Acoustic Doppler Profiler (ADP, 250 kHz) was mounted with a tripod at the bottom to record the north and east direction velocities from 6.1 m

to 48.1 m above bottom with a 2 m interval. The water surface temperature at the 55 m site is obtained through the satellite-based measurements for Lake Michigan from NOAA's Coast Watch Program (http://coastwatch.glerl.noaa.gov/ftp/glsea/) on a daily basis and will be used as a tool to validate the thermal output at the top of the water column.

A bulk aerodynamic formulation is used to estimate the heat and momentum fluxes over the water surface as the main driving force for the 1D model. As the flux calculation is based on the meteorology data, however, no direct meteorological measurement is available at the model site. Then, the overland meteorological data such as wind, air temperature, cloud cover and dew point measured at selected land-based meteorological stations was interpolated to the study site. The locations of the overland stations are shown in Fig.2.2.

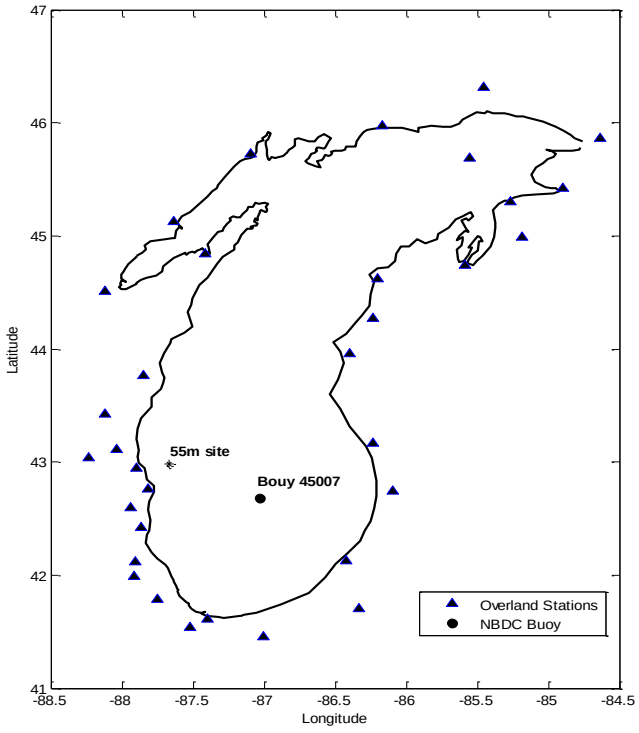

Fig.2.2 Overland stations around Lake Michigan and Buoy site (45007) location

The detail procedure of interpolation follows that presented by Beletsky and Schwab (Beletsky and Schwab, 2001). It consists of 3 steps: height adjustments, overland/over lake adjustment and interpolation. The height profile equation for air temperature and wind speed is as follows:

$$u(z) = (u_*/k)[\ln(\frac{z}{z_0} - \psi_m)] \quad (1)$$

$$T_a(z) = T_0 + (T_*/k)[\ln(\frac{z}{z_0} - \psi_h)] \quad (2)$$

where, u is the wind speed, z is vertical coordinate, u_* is the friction velocity, k is the Von Karman constant, T_a is the air temperature, T_* is the scaling temperature, ψ_m and ψ_h are the stability height coefficient. Overland and over lake adjustment is also important. The wind speed over water directly interpolated from the land is often underestimated due to the difference of roughness over land and water. The adjustment equation is expressed as:

$$u_w = u_l(1.2 + \frac{1.85}{u_l})\left[1 - \left(\frac{\Delta T}{|\Delta T|}\right)(\frac{\Delta T}{1920})^{1/3}\right] \quad (3)$$

where u_w is the wind speed over water, u_l is the wind over land, ΔT is the difference of air temperature and water surface temperature. One difference from the equation in our procedure is that we applied a different coefficient to calculate the air temperature over water.

$$T_a = aT_{al} + (1 - a)T_w \quad (4)$$

where T_a is the estimated temperature over water, T_{al} is the interpolated air temperature from land stations and T_w is lake- surface water temperature. Here, instead of assigning a equal to 0.4, we found a value 0.2 is better according to calibration with buoy measurements available on the lake (see below). The final interpolation is based on a multi-quadric interpolation procedure as presented by Nuss and Titley (Nuss and Titley, 1994):

$$H(X) = \sum_{i=1}^{N} \alpha_i Q(X - X_i) \quad (5)$$

where, N is the number of stations, α_i is the weighting coefficient for each station, Q is the distance function and with the form as:

$$Q_i(x,y) = -(\frac{|x-x_i|^2+|y-y_i|^2}{c^2}+1)^{1/2} \quad (6)$$

where, c is the influence distance and is set 10km here. To calibrate the interpolation process, we first interpolate the overland data to Buoy 45007 which locates in south Lake Michigan and

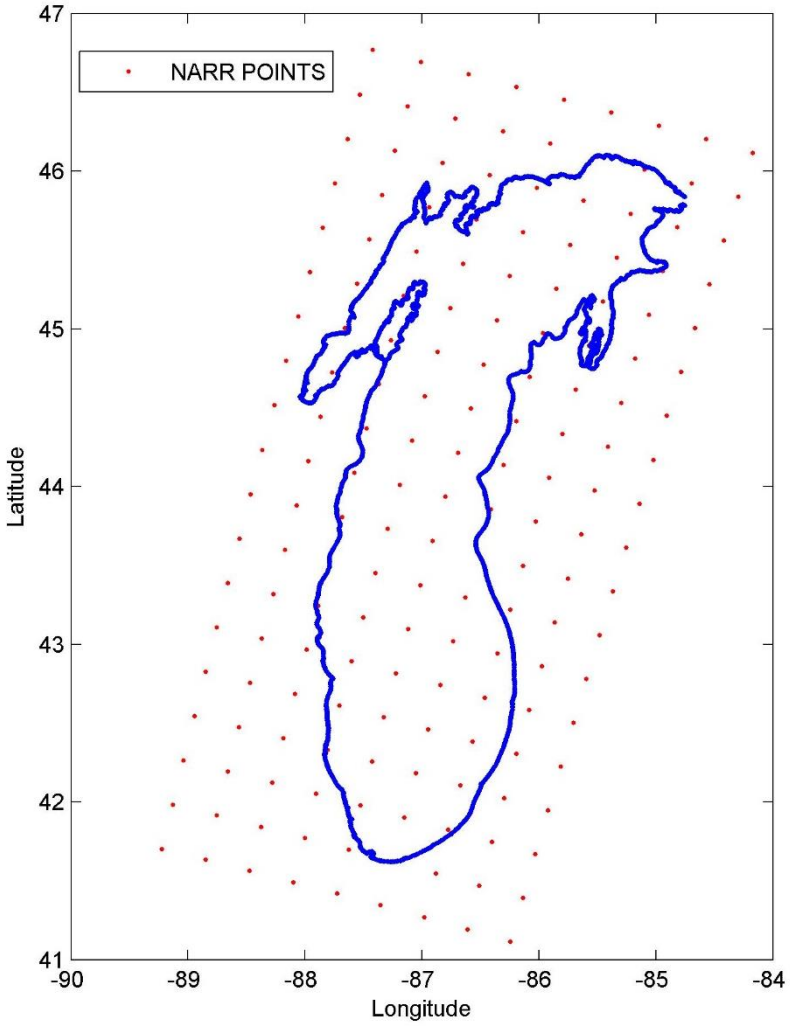

Fig.2.4 NARR forcing interpolation points

the interpolated data is found with a good match with the observation (Fig.2.3).

For the 3D model, however, meteorological forcing is calculated based on data downloaded directly from the North American Regional Reanalysis (NARR) database, which covers the entire area of Lake Michigan (Fig.2.4). Atmospheric forcing variables are the same as those described for the 1D model. NARR is 32-km-resolution and 3-hourly intervals data set derived from the NCEP Eta meteorological model with assimilation of observational data from surface, upper atmosphere and remote sensing sources, including Great Lakes buoy data and satellite-derived surface temperature.

2.1.2 Momentum and Heat Flux

The main external momentum flux for the 1D transport model is wind stress and can be calculated with Eq. (7):

$$\tau_{x,y} = C_d \rho_a (u, v) U \tag{7}$$

Where ρ_a is the surface air density, U is the wind speed, u, v are the east and north components of the wind. C_d is the drag coefficient. The surface drag coefficient depends on several parameters such as winds, waves, surface roughness and. In our model, an empirical formula is applied which depends on the wind speed only. The value of C_d is between 0.0012-0.0021 with the form of Eq. (8):

$$C_d = \begin{matrix} 0.0012 & U \leq 11 m/s \\ 0.001(0.49 + 0.065U) & 11 < U < 25\ m/s \\ 0.0021 & U \geq 25 \end{matrix} \tag{8}$$

Surface heat fluxes include 4 parts and can be calculated as:

$$H = H_{sr} + H_{lr} + H_s + H_l \tag{9}$$

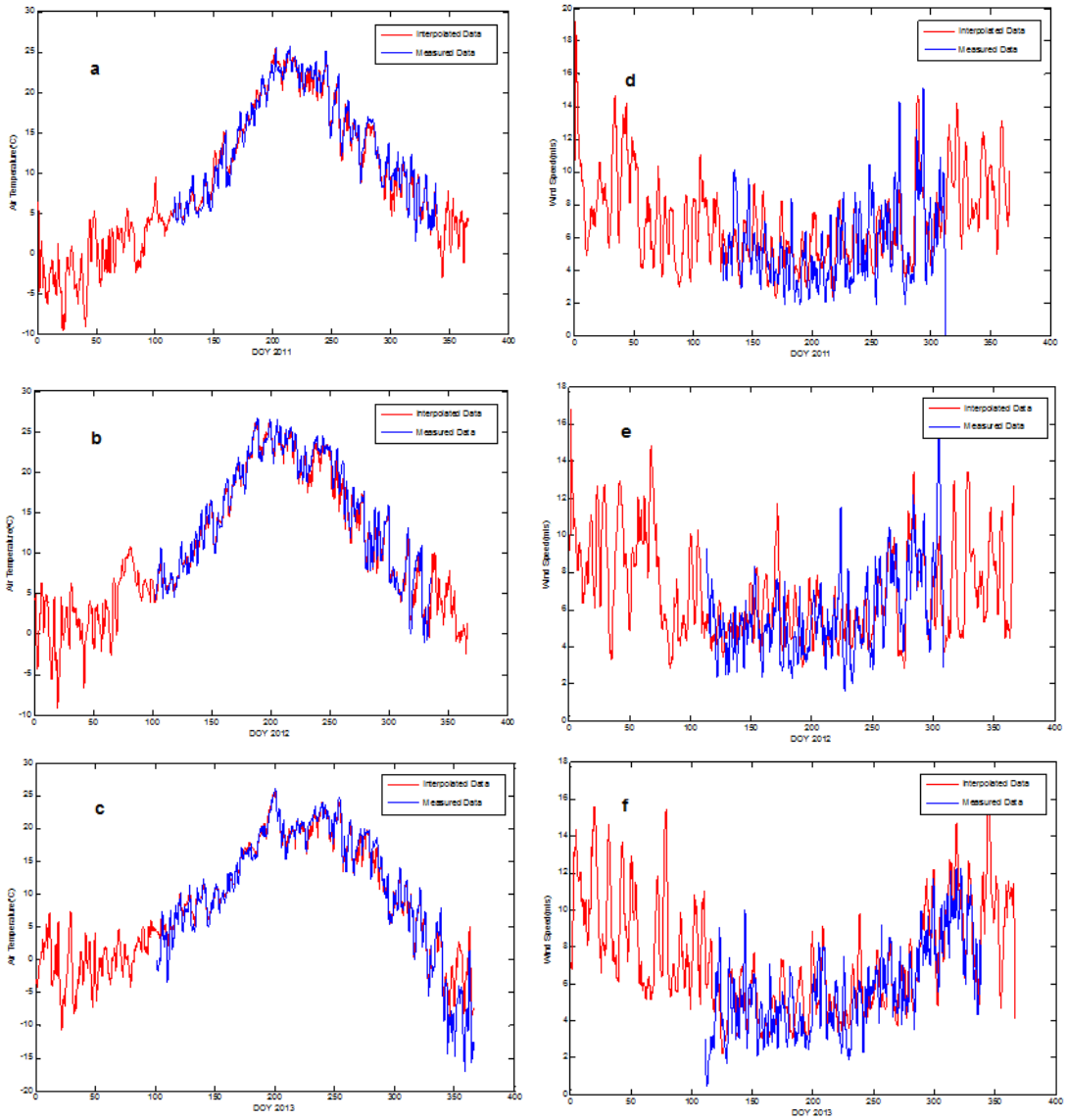

Fig.2.3 Comparison between the measurement (red) and interpreted data (blue) at the buoy 45007 site. a-c are the air temperature from 2011-2013, d-e are wind speed from 2011-2013

where, H_{sr} is the shortwave radiation from the sun, $H_{lr}$is the longwave radiation, H_l is the latent heat flux due to evaporation and condensation, H_s is the sensible heat flux due to heat conduction. The calculation procedure follows the method described by McCormick and Meadows (McCormic and Meadows, 1998) and Rosati (Rosati, A., Miyakoda, K., 1998). The radiation at the top of the atmosphere:

$$Q_0 = \frac{J_0}{a^2} cosz \tag{10}$$

$$a^2 = 1 + 0.033\cos(2\pi J/365) \tag{11}$$

$$cosz = sin\emptyset sin\delta + cos\emptyset cos\delta cosh \tag{12}$$

where J_0 is the solar constant – 1350J/s/m^2, a^2 is the earth-sun distance corrector factor, J is Julian day, $\emptyset$ is the latitude, δ is the sun decline angle and h is the sum's hour angle. And the direct short wave component reaching the water surface is expressed as:

$$Q_{dir} = Q_0 \tau^{secz} \tag{13}$$

where τ is the atmosphere transmission coefficient, set as 0.7. The diffuse radiation under cloudless conditions may be approximated by assuming that when scatter of radiation occurs, half is scattered downward and half upward. So we have:

$$Q_{diff} = ((1 - A_a)Q_0 - Q_{dir})/2 \tag{14}$$

$$Q_{tot} = \ Q_{dir} \ + \ \ Q_{diff} \tag{15}$$

where, A_a is attenuation coefficient, set as 0.09. In addtion, the emiprical formula F(C) for cloud cover range from 1 in clear sky and 0.36 (Beletsky and Schwab, 2001) is applied here.

$$H_{sr} = QtotF(C) = Qtot(1 - aC - bC^2 + cC^3) \tag{16}$$

where *a* is 0.38, *b* is 0.38, *c* is 0.12.

The net longwave radiation is the sum of the upward and downward longwave radiation.

$$H_{lr} = \varepsilon\sigma T_w^4 \left(0.39 - 0.05 e_a^{\frac{1}{2}}\right) F(C) + 4\varepsilon\sigma T_w^3 (T_w - T_a) \quad (17)$$

where ε is the emissivity (0.97), σ is the Stefan-Boltzmann constant, e_a is the atmospheric vapor pressure (mb). The sensible and latent heat flux can be expressed as:

$$H_s = \rho_a C_p C_h |v| (T_w - T_a) \quad (18)$$

$$H_l = \rho_a C_e |v| (e_{sat}(T_w) - r e_{sat}(T_a)(0.622/p) \quad (19)$$

where, C_p is the heat capacity, C_h, C_e are the turbulent exchange coefficient, T_w is the water surface temperature, T_a is the air temperature, e_{sat} is the saturation vapor pressure. The shortwave radiation is the primarily source to heat input to the water body. Since it can penetrate into the water body, this term is treated as an external source in the temperature transport equation. The shortwave reaching water surface is generally influenced by the geological location, time of the year and the cloud cover condition. The calculated solar radiation is compared with the recorded value at Chicago O'Hare airport in 2012. The comparison is in Fig. 2.5. It can be found that the calculated value, in general, matches well with the measured one,

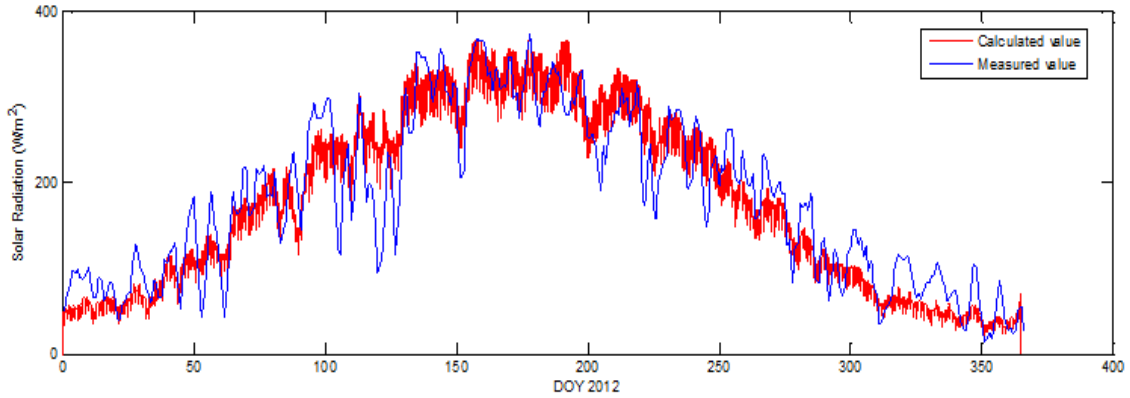

Fig.2.5 Solar radiation comparison in 2012 at Chicago O'Hare airport. Measurement (blue), calculation value (red) (W/m^2).

however, the fluctuation is relatively large for the observed measurements and it is very likely that the cloud cover is not as continuous as other meteorological parameters, thus interpolation may result with significant errors. In Fig.2.6, the cumulative net surface heat flux over the year

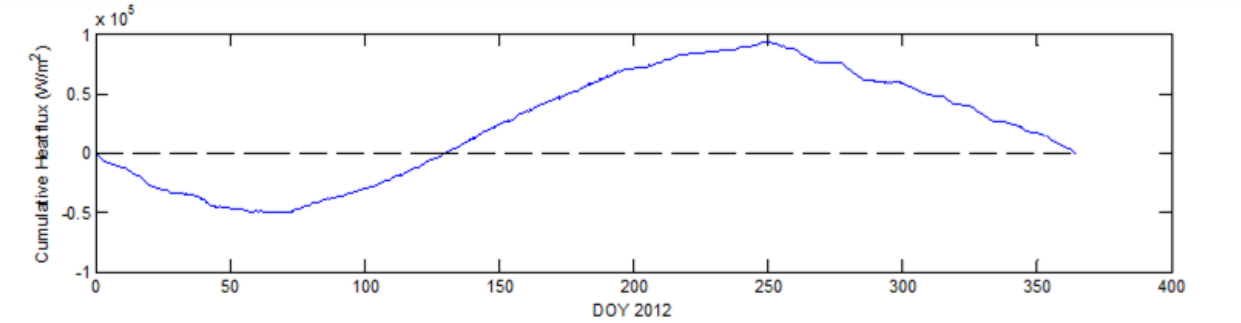

Fig. 2.6 Calculated Cumulative total heat flux in 2012 at model site (W/m^2)

2012 is given which indicates a nearly zero net heat flux over one year. For a long term scale, annual heat balance should be estimated and this result proved the calculation of the other 3 parts of heat flux are reasonable from another degree.

The shortwave flux downwards into the water column is approximated by:

$$SW = \mathrm{SW}_0(\mathrm{Re}^{z/a} + (1 - \mathrm{R})\mathrm{e}^{z/b}) \quad (20)$$

This equation has been widely used in numerical studies with *a* and *b* the attenuation length for longer and shorter wavelength components and *R* is the percent of total flux that is associated with the longer wavelength irradiance, SW_0 is the surface shortwave radiation. These coefficients are: R: 0.55, a:0.35 m and b:3.5 m, for both 1D and 3D models.

2.2 Description of 1D Model

An important issue to model the ocean circulation is the full consideration of turbulence. Turbulence in the ocean leads to mixing. Vertical mixing process is critical to the scalar diffusion

and energy, momentum transfer. In this study, the Mellor-Yamada Level 2.5 (MY2.5) mixing scheme are employed as the turbulence closure model for both 1D and 3D models. It is a 2-equation second order moment scheme and has proved to be valid for a wide variety of engineering and geophysical flow applications (Mellor and Yamada, 1982). The "eddy" viscosity and diffusivity in the scheme are parameterized as:

$$D_v = qlS_H \tag{21}$$

$$K_v = qlS_M \tag{22}$$

Where q is the turbulence velocity scale, l is the turbulence length scale, S_M and S_H are the stability function which are parameterized by the Richardson number.

$$S_M = \frac{A_1\left(1-3C_1-6A_1B_1^{-1}\right)-S_H[G_H(18A_1^2+9A_1A_2)]}{1-9A_1A_2G_H} \tag{23}$$

$$S_H = \frac{A_2(1-6A_1B_1^{-1})}{1-(3A_2B_2+18A_1A_2)G_H} \tag{24}$$

where $(A_1, A_2, B_1, B_2, C_1)$ = (0.92,0.74,16.6,10.1,0.08) and G_H is the Richardson number:

$$G_H = -\frac{l^2}{q^2}\frac{g}{\rho_0}\frac{\partial\rho}{\partial z} \tag{25}$$

The turbulence intensity and its length scale are obtained prognostically by solving transport equations of q^2 and q^2l:

$$\frac{\partial q^2}{\partial t} = \frac{\partial}{\partial z}\left[K_q\frac{\partial q^2}{\partial z}\right] + 2K_v\left[\left(\frac{\partial u}{\partial z}\right)^2 + \left(\frac{\partial v}{\partial z}\right)^2\right] + \frac{2g}{\rho_0}D_v\frac{\partial\rho}{\partial z} - \frac{2q^3}{B_1 l} \tag{26}$$

$$\frac{\partial q^2 l}{\partial t} = \frac{\partial}{\partial z}\left[K_q\frac{\partial q^2 l}{\partial z}\right] + E_1 l\left(K_v\left[\left(\frac{\partial u}{\partial z}\right)^2 + \left(\frac{\partial v}{\partial z}\right)^2\right]\right) + E_1 l\frac{g}{\rho_0}D_v\frac{\partial\rho}{\partial z} - \frac{q^3}{B_1}\widetilde{W} \tag{27}$$

where the mixing coefficient K_q is estimated as $0.41K_v$. $\widetilde{W}$ is a wall proximity function that can be defined as:

$$\widetilde{W} = 1 + \frac{E_2 l}{\kappa^2}\left(\frac{1}{-z} + \frac{1}{H-z}\right) \tag{28}$$

The 1D model adapts a staggered grid arrangement as depicted in Fig.2.7. The water column is divided into N equally-spaced cells. Velocity components and temperature are assigned on the

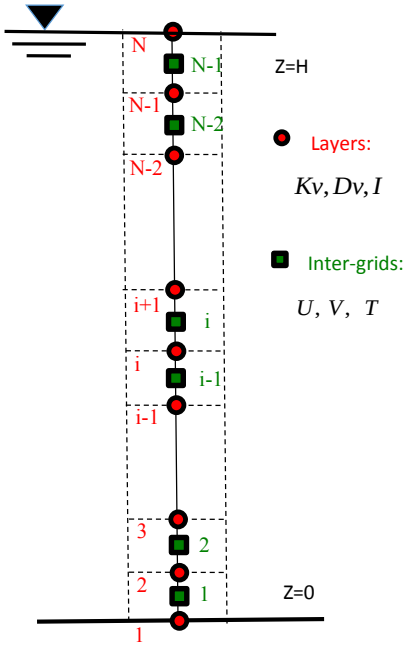

Fig.2.7 vertical stagger grid structure of 1D model

center of cells (green squares) and the "eddy" viscosity and diffusivity are located at the cell interfaces (red circles).

The 1D model solves 5 physical variables simultaneously: the East and North velocity components (U and V, respectively), the temperature T and the turbulence parameters q^2 and $q^2 l$ in Eq. (26) and (27) as well as the phytoplankton concentration. And considering the idealized situation of horizontal homogeneity, the following one-dimensional transport equations can be applied:

$$\frac{\partial U}{\partial t} - fv = \frac{\partial}{\partial z}\left(K_V \frac{\partial U}{\partial z}\right) + cU \tag{29}$$

$$\frac{\partial V}{\partial t} + fu = \frac{\partial}{\partial z}\left(K_V \frac{\partial V}{\partial z}\right) + cV \tag{30}$$

$$\frac{\partial \mathrm{T}}{\partial \mathrm{t}} = \frac{\partial}{\partial \mathrm{z}}\left(\mathrm{D_V}\frac{\partial \mathrm{T}}{\partial \mathrm{z}}\right) + \frac{\mathrm{I}}{\rho \mathrm{C_P}}\frac{\partial \mathrm{I}}{\partial \mathrm{z}} \tag{31}$$

$$\frac{\partial \mathrm{Phy}}{\partial \mathrm{t}} = \frac{\partial}{\partial \mathrm{z}}\left(\mathrm{D_V}\frac{\partial \mathrm{Phy}}{\partial \mathrm{z}}\right) + Source \tag{32}$$

Where $\mathrm{K_V}$ is the eddy viscosity, $\mathrm{D_V}$ is the eddy diffusivity, f is the Coriolis factor, c is a sink term, ρ is the water density, $\mathrm{C_P}$ is heat capacity, and I is the source of heat due to the penetrative solar radiation.

As discussed by Mellor (2000), artificial kinetic energy build up and augmentation of mixing are common problems associated with 1D mixing models, since lateral processes are not accounted for in the simplified 1D approach. A sinking term can be introduced in a 1D model to counteract this effect and it has been shown to improve the modeling results as compared to current meter measurements.

Surface waves, as an important source of turbulence production in oceans and large lakes, have attracted attention of scientists on the research of turbulent mixing and climate change (Wang, 2015; Hu and Wang, 2010). In this study, wave effects are included into the modeling to account for turbulence production due to surface wave breaking as well as the penetrative wave-turbulence interaction. Modeling parameters are adapted from those reported in the literature (Mellor and Blumberg, 2004; Huang and Qiao, 2010; Babanin and Onorato, 2012). A modified surface boundary condition for Eq. (26), (27) is required to represent the surface wave breaking for the numerical solutions:

$$q^2(0) = (15.8\alpha_{CB})^{2/3}{u_*}^2 \tag{33}$$

$$l(0) = 2 * 10^5 {u_*}^2/g \tag{34}$$

Where u_* is the surface friction velocity, α_{CB} is an empirical constant which is set to 100 in our model. For the wave-turbulence interaction, additional TKE dissipation rate (ε_w) and vertical

mixing coefficient (B_v), which are functions of surface wave parameters and the water depth, are required in the model (Huang and Qiao, 2010):

$$D_v = qlS_h + B_v \tag{35}$$

$$K_v = qlS_m + B_v \tag{36}$$

$$B_v = 10^5 \delta \frac{u_{s0}{u_*}^2}{g} e^{3kz} \tag{37}$$

In which, δ is the wave steepness, u_{s0} is the Stokes drift at water surface, z is the water depth. The additional dissipation rate generated from the wave current interaction is expressed as:

$$\varepsilon_w = 148\beta\sqrt{\delta}\frac{u_{s0}{u_*}^2}{L} e^{2kz} \tag{38}$$

In which, L is the wave length, β is an empirical constant and set as 1. This term will be incorporated into Eq. (10), (11) as the additional shear production term:

$$P = P_S + \varepsilon_w = \mathrm{K_v}\left[\left(\frac{\partial \mathrm{u}}{\partial \mathrm{z}}\right)^2 + \left(\frac{\partial \mathrm{v}}{\partial \mathrm{z}}\right)^2\right] + \varepsilon_w \tag{39}$$

For the boundary condition, on the surface, the shear stress is induced by the surface wind with the form:

$$\rho \mathrm{K_V}\frac{\partial \mathrm{U}}{\partial \mathrm{z}} = \tau_{\mathrm{wx}} \tag{40}$$

And near the bottom, the shear stress can be expressed as:

$$\rho \mathrm{K_V}\frac{\partial \mathrm{U}}{\partial \mathrm{z}} = \tau_{\mathrm{bx}} = \mathrm{C}\rho \mathrm{U}|\mathrm{U}| \tag{41}$$

where τ_{bx} is the bottom shear stress in east direction, C is the Chezy coefficient.

Similar to the velocity transport equation, the surface heat includes longwave heat flux, sensible heat flux and latent heat flux.

$$\rho \mathrm{C_P D_V}\frac{\partial \mathrm{T}}{\partial \mathrm{z}} = \mathrm{H_{SURF}} \tag{42}$$

And there is no flux to the bottom ground.

Boundary conditions for Eq. (26), (27) follow that described by Mellor and Yamada (1982), on the surface:

$$q^2(0) = (B_1)^{2/3} {u_*}^2 \tag{43}$$

$$q^2 l(0) = 0 \tag{44}$$

And at the bottom:

$$q^2(-H) = (B_1)^{2/3} \sqrt{{\tau_{bx}}^2 + {\tau_{by}}^2}/\rho \tag{45}$$

$$q^2 l(-H) = 0 \tag{46}$$

The vertical diffusion coefficient for the phytoplankton transport equation is defined as equal to the diffusivity of temperature. The source term for the phytoplankton is calculated firstly to update the concentration which will be ready to use in the mixing process. The source equation for the phytoplankton is:

$$Source = growth + sink - grzing + mortality \tag{47}$$

In which the sinking process and the grazing effect by zooplankton and mussel at bottom are the same as those for the 3D model, more detail can be found in the next section. However, the growth of phytoplankton in the 1D model is only light and temperature dependent and we assume that the nutrient is of sufficient supply since our focus is the phytoplankton in the spring and the beginning of summer.

2.3 Description of 3D Physical Model

FVCOM is an unstructured grid, finite volume, sigma coordinate terrain following ocean model that provides the capability of representing accurately the geometrical complexities that characterize the usually highly irregular water-land coastal environment such as inlets, islands and peninsulas. The spatial fluxes of momentum are discretized using a second-order accurate

finite volume method. A flux formulation for scalars is used in conjunction with a vertical velocity adjustment to enforce exact conservation of the scalar quantities. The horizontal diffusion is modeled with the Smagorinsky formulation. In short, the code solves numerically the following set of primitive equations as momentum, continuity, heat and density:

$$\frac{\partial \mathrm{u}}{\partial \mathrm{t}} + u\frac{\partial \mathrm{u}}{\partial \mathrm{x}} + v\frac{\partial \mathrm{u}}{\partial \mathrm{y}} + w\frac{\partial \mathrm{u}}{\partial \mathrm{z}} - \mathrm{fv} = -\frac{1}{\rho_0}\frac{\partial \mathrm{P}}{\partial \mathrm{x}} + \frac{\partial}{\partial \mathrm{z}}\left(\mathrm{K_m}\frac{\partial \mathrm{u}}{\partial \mathrm{z}}\right) + \mathrm{F}_u \tag{48}$$

$$\frac{\partial \mathrm{v}}{\partial \mathrm{t}} + u\frac{\partial \mathrm{v}}{\partial \mathrm{x}} + v\frac{\partial \mathrm{v}}{\partial \mathrm{y}} + w\frac{\partial \mathrm{v}}{\partial \mathrm{z}} + \mathrm{fu} = -\frac{1}{\rho_0}\frac{\partial \mathrm{P}}{\partial \mathrm{y}} + \frac{\partial}{\partial \mathrm{z}}\left(\mathrm{K_m}\frac{\partial \mathrm{v}}{\partial \mathrm{z}}\right) + \mathrm{F}_v \tag{49}$$

$$\frac{\partial \mathrm{T}}{\partial \mathrm{t}} + u\frac{\partial \mathrm{T}}{\partial \mathrm{x}} + v\frac{\partial \mathrm{T}}{\partial \mathrm{y}} + w\frac{\partial \mathrm{T}}{\partial \mathrm{z}} = +\frac{\partial}{\partial \mathrm{z}}\left(\mathrm{K_h}\frac{\partial \mathrm{T}}{\partial \mathrm{z}}\right) + \mathrm{F}_T \tag{50}$$

$$\frac{\partial \mathrm{u}}{\partial \mathrm{x}} + \frac{\partial \mathrm{v}}{\partial \mathrm{y}} + \frac{\partial \mathrm{w}}{\partial \mathrm{z}} = 0 \tag{51}$$

$$\rho = \rho(\mathrm{T}) \tag{52}$$

In which, x, y and z are the east, north and vertical axis in the Cartesian coordinate system, u, v and w are the corresponding velocity components. T is the temperature, ρ is the water density, f is the Coriolis effect to represent the rotation effect of the earth, g is the acceleration of gravity and Km and Kh are the vertical eddy viscosity and vertical thermal diffusion coefficient respectively.

In order to obtain a smooth representation of irregular variable bottom topography, the σ-coordinate transformation is applied in FVCOM as most other popular ocean circulation models. The σ-coordinate transformation is defined as:

$$\sigma = \frac{z-\mathcal{E}}{H+\mathcal{E}} = \frac{z-\mathcal{E}}{D} \tag{53}$$

Where σ scales from -1 at the bottom to 0 at the surface; D is the depth of the water column; Ɛ is the height of the free surface.

In a numerical model of general circulation of oceans, external gravity waves often travel much faster than the other motions in the system. FVCOM adopts a split mode technique to improve the efficiency of the numerical algorithm. First, the 2-D external mode is applied to solve the surface elevation and the average velocity can be obtained. The 3-D internal mode is then applied along the vertical direction to solve the diffusion processes implicitly.

The 3rd generation NOAA GLERL Great Lakes Coastal Forecasting System had adopted FVCOM as it can better model physical processes with an unstructured grid. In addition, FVCOM has been successfully implemented in a good number of cases for Great Lakes. Bai et al (2013) applied FVCOM-GL to simulate the circulation and thermal structure for all five Great Lakes from 1993 to 2008 and found all Great Lakes exhibit significant annual and inter-annual variations in current speed and temperature. A variety of meteorological forcing terms were used to assess the thermal structure of Lake Superior with FVCOM and the dynamic heat flux as well as the wind field from weather forecasting model are proved to be key points in improving the simulation results (Xue, 2015). FVCOM is also a useful tool for modeling the biogeochemistry by accurately reproducing the hydrodynamic conditions which largely controls the distribution pattern of ecological parameters in such aquatic systems. Luo et al (2012) simulated the 1998 spring bloom in Lake Michigan with a coupled physical-biological model and confirmed that the phytoplankton bloom is forced by the rapidly increased temperature and light intensity in spring. The FVCOM based Integrated Compartment Model (FVCOM-ICM) was implemented to investigate plankton dynamics with the inclusion of mussel invasion in Lake Erie and revealed that the effect of zooplankton predation on phytoplankton is stronger than that of the mussel grazing effect (Jiang, 2015).

This study has attempted to simulated whole Lake Michigan. Only internal cycle is considered in my research, so, no open boundary conditions are specified. Surrounding tributaries and the flow through the Straits of Mackinac are ignored from the model as well. To fully explore the nearshore offshore exchange for the biological module along with majority of the field measurement locating at shallow area, the mesh density of the lake gradually decreases from the lake boundary, with higher density at the nearshore zone and lower density in the deep central area. The mesh is first generated through Gmsh which is an open source code and adjusted with quality check with Matlab and SMS software. The triangular mesh contains 10492 nodes and 19813 triangles. 30 layers are divided in the vertical direction with high resolution

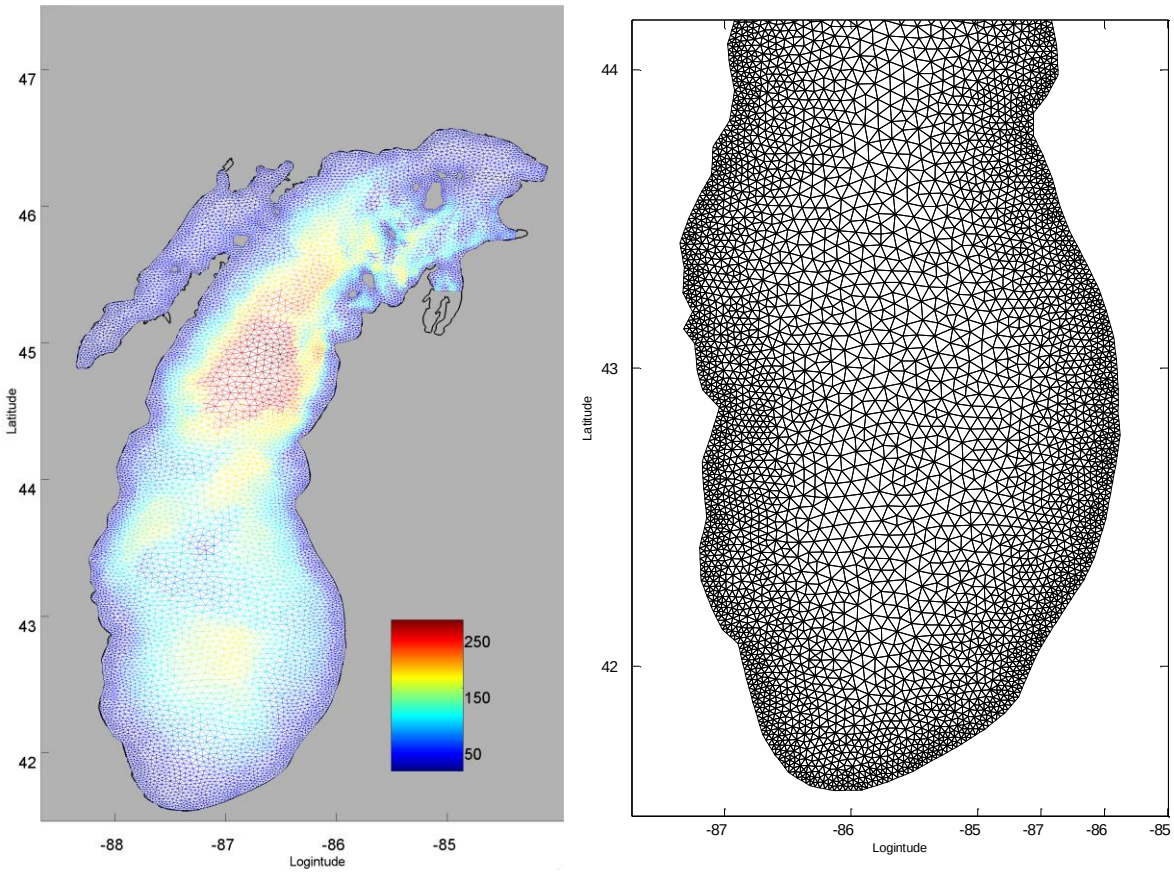

Fig.2.8 Triangle mesh of Lake Michigan for FVCOM

approaching the surface and the bottom to better resolve mixing process near the boundary. The minimum length of the boundary triangle is 0.8km and the maximum in the central part of the lake is around 6km (Fig.2.8).

The 3D simulation time period begins from March 1st 2012 and ends at the end of October during which the temperature is warm enough and almost no ice cover on Lake Michigan is found. To ensure model will converge and stable, the Courant-Friedrich Levy (CFL) stability criterion is applied that:

$$\Delta t_{\mathrm{E}} \leq \frac{\Delta L}{U+\sqrt{gD}} \tag{54}$$

where, ΔL is the side length of the triangle, U is the velocity, D is the local depth. The external mode time step is set to be 10s according to the minimum value of the CFL criterion. The split number is set as 10, which means the internal mode time step is 100s and runs every 10 external time steps.

2.4 Description of 3D Biological model

The biological NPZD (Nutrient, Phytoplankton, Zooplankton, Detritus) model with *dreissenid* mussel incorporated is derived from the Flexible Biological Module which is developed by the FVCOM team. Specifically, the model mainly contains two nutrient types (phosphorus and silicon), two phytoplankton groups (small and large), one zooplankton and one detritus group. In the NPZD model, soluble reactive phosphorus will be the major nutrient that controls the growth of both the two phytoplankton groups while silicon is the additional limit nutrient only for the large phytoplankton group. Moreover, to facilitate the calculation between different parameters, carbon is used as the standard unit except nutrient in the model.

The main equations are as below:

(1). Zooplankton:

$$\frac{\partial ZOO}{\partial t} = Grazing - Repiration - Mortality \quad (55)$$

The grazing function follows that proposed by Ivlev (1995):

$$Grazing_{PHY} = Gr * (1 - \exp(-sigma_{Phy} * Phy)) \quad (56)$$

$$Grazing_{Det} = Gr * (1 - \exp(-sigma_{Det} * Det)) \quad (57)$$

$$G_r = G_{max} * Zoo * \exp(-A_{tz} * |t - t_0|) \quad (58)$$

where, G_{max} is the maximum graze rate for specific zooplankton, A_{tz}: exponential coefficient for temperature function, t_0: optimal temperature, $sigma_{Phy}$: preference on phytoplankton, $sigma_{Det}$: preference on detritus.

$$Mortality_{Zoo} = \varepsilon Zoo \quad (59)$$

where ε is the mortality rate.

$$Repiration_{Zoo} = \gamma Zoo \quad (60)$$

where γ is the respiration rate.

(2). Phytoplankton:

$$\frac{\partial Phy}{\partial t} = Growth + Repiration + Mortality + Sinking + Grazing \quad (61)$$

$$Growth_{Phy} = (1 - d_{dom})\mu Phy \quad (62)$$

where, d_{dom} is the active DOM exudation, μ is the growth rate, Phy is the initial concentration of phytoplankton.

Here, the growth rate μ is a key parameter in controlling the growth of the phytoplankton which can be expressed as follow:

$$\mu = \mu\_max((1-\alpha)\mu_a + \alpha\mu_b) \tag{63}$$

μ_max is the maximum growth rate, α is the weighting coefficient (0-1) and μ_a, μ_b are empirically modeled as:

$$\mu_a = \mu(T)min(\mu(I), \mu(N)) \tag{64}$$

where, $\mu(T)$ is the temperature limitation function, $\mu(I)$ is the lighting limitation function and $\mu(N)$ is the nutrient limitation function.

$$\mu_b = \mu(T)\mu(I)min(\mu(N)) \tag{62}$$

And the temperature function is:

$$\mu(T) = exp(-A_{tz} * |t - t_0|) \tag{66}$$

where A_{tz} is the exponential decay rate, t_0 is the optimal water temperature for the max growth rate.

Based on the literature, several lighting limit function are available now and the PGH80_LIGHT function proposed by Platt (1980) is applied here:

$$\mu(I) = (1 - exp\left(-\frac{\alpha I}{\mu_{max}}\right)) * exp(-\frac{\beta I}{\mu_{max}}) \tag{67}$$

where, α and β are the light function coefficient, I is the light intensity.

The nutrient limitation function follows the classic Monod theory and has the form of:

$$\mu(N) = \frac{N}{N+KSN} \tag{68}$$

where, KSN is the half saturation concentration for the growth of phytoplankton.

$$Sinking_{Phy} = -w\frac{\partial Phy}{\partial z} \tag{69}$$

where, w is the sinking velocity. At the boundary, if we consider no source sinking from the water surface,

$$Sinking_{surf} = -1 * wPHY_{surf}/\Delta z \tag{70}$$

While no material sinking out from the bottom,

$$Sinking_{bot} = wPHY_{bot-1}/\Delta z \tag{71}$$

(3). Detritus:

The aggregation and disaggregation for the Detritus is simplified as balanced in the system, so the change of detritus can be expressed as:

$$\frac{\partial Det}{\partial t} = Mortality_{Zoo/Phy} - Graze - Dissolution + Sinking \tag{72}$$

$$Dissolution_{Det} = \eta Det \tag{73}$$

In which, η is the dissolution coefficient.

(4). Nutrient:

$$\frac{\partial N}{\partial t} = Repiration_{Zoo/Phy} - Uptake_{Phy} + Dissolution_{Det} \tag{74}$$

(5). *Dreissenid* mussel

Dreissenid mussels are incorporated into the NPZD model to investigate the effect of mussel to the ecosystem. The grazing by *dreissenid* mussel as well as the egestion and excretion only applied at the bottom layer of the model. Clearance rate is calculated as a function of local mussel density and water temperature based on empirical relationships. The egestion and excretion effects of mussel are calculated assuming a recycling efficiency of 80% and the egested and excreted material will be directly added into the bottom layer. Tyner (2015) fitted the mussel pumping rate relationship according to the Van't Hoff model based on the laboratory experiments. The volumetric pumping rate is calculated through dividing the carbon grazing rate with the average, available organic carbon concentration. This empirical formula is only temperature dependent and did not account for the size of mussel:

$$M_P = M_1 \exp(M_2 * T) \text{ (mL mg/DW/hr)} \quad (75)$$

Where M_1 and M_2 are both empirical constants. As the figure shown by Fillingham (2015), the

Figure from Fillingham (2015)

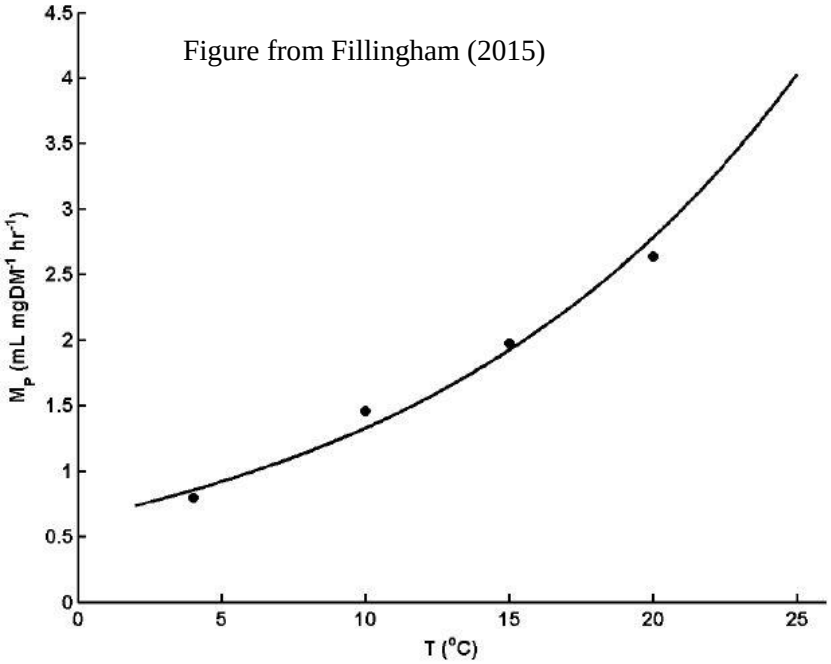

Fig.2.9 Mussel volumetric pumping rate as a function of temperature.

equation is in a good representation of the laboratory data (Fig. 2.9).

The biomass distribution of *dreissenid* mussel were obtained from samples collected with a grab in a sampling area of 0.046 m^2. The sample results of total 144 sites then are interpolated with a geostatistical model by Rowe et al (2015). For our simulation, the mussel density will be extracted from the map (Fig.2.10) and be interpolated to the mesh nodes with the natural neighbor method.

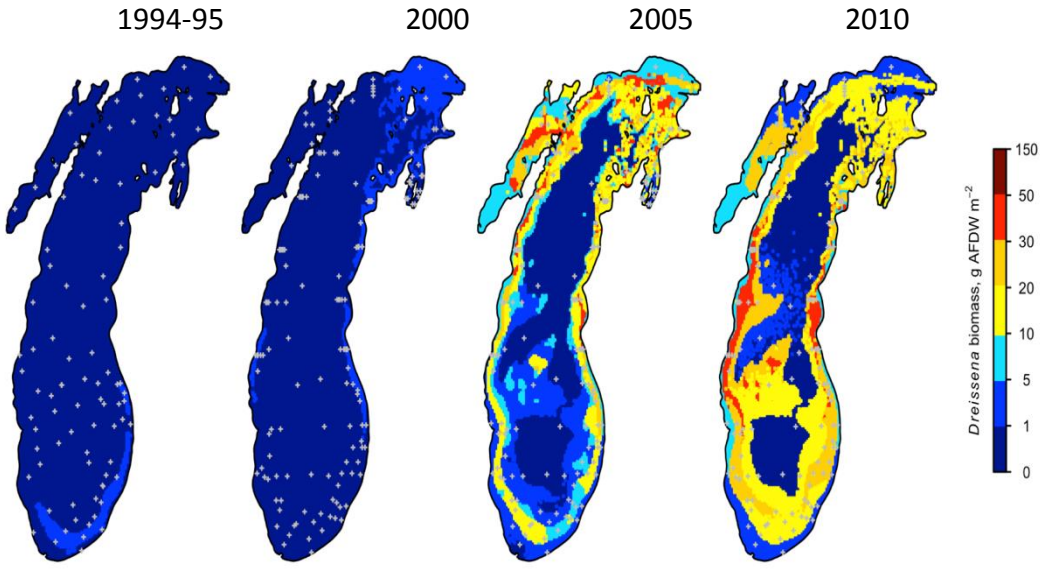

Fig.2.10 Mussel density (dry mass) from 1994-2010 (Obtained from M.D. Rowe (2015)).

Besides the reaction and mussel feeding process, the horizontal advection and diffusion process are directly linked to the 3D FVCOM physical model, in which the horizontal diffusivity is calculated with the Smagorinsky method while the vertical diffusivity is based on the Mellor-

Yamada 2.5 level model. At last, the simple conceptual diagram of the biology model is shown in Fig.2.11. Model variables are listed in table 2.1.

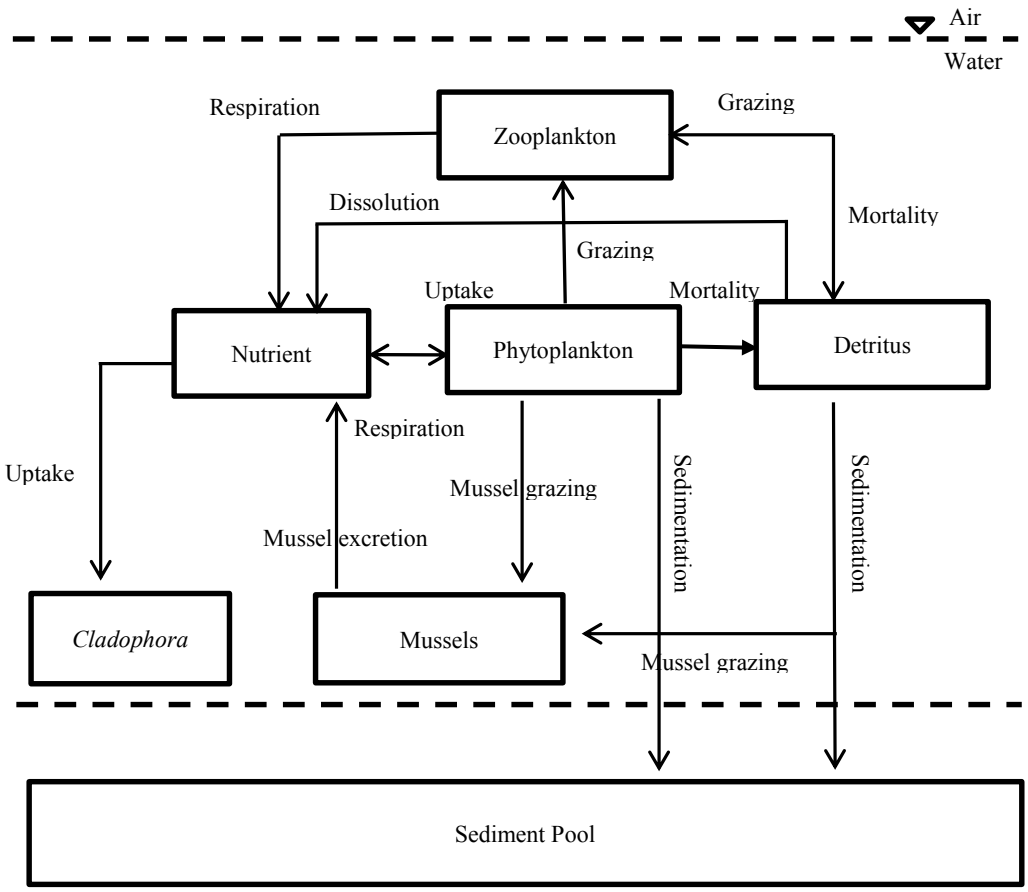

Fig.2.11 Conceptual diagram of the NPZD biological model

Table 2.1 List of the model parameters

Parameter	Definition	V	Unit
α_I	Light function coefficient	1.48e-6	mmolC//s/W
α	Weight function coefficient	0.5	Dimensionless
a_t	Temperature function coefficient	0.069	$(C)^{-1}$
αt_chl	Attenuation of CHL	0.04	$(MgCHL)^{-1}m^2$
αt_d	Attenuation of detritus	0.02	$(mmol)^{-1}m^2$
αt_w	Attenuation of water	0.08	m^{-1}
β	Light function coefficient	4.25e-8	mmolC $(s\ W)^{-1}$
d_{dom}	Active DOM exudation	0.1	dimensionless
ε_L	Mortality coefficient for large phyto	5.8e-8(0.05)	$s^{-1}(d^{-1})$
ε_S	Mortality coefficient for small phyto	5.8e-8(0.05)	$s^{-1}(d^{-1})$
ε_Z	Mortality coefficient for zooplankton	5.8e-8(0.05)	$s^{-1}(d^{-1})$
G_max	Maximum grazing rate by zooplankton	7.0e-6(0.6)	$s^{-1}(d^{-1})$
γ_Z	Zooplankton respiration rate	0.06	d
γ_S	Small phyto respiration rate	0.06	d^{-1}
γ_L	Large phyto respiration rate	0.06	d^{-1}
T_opt	Optimal temperature	20	C
μ_max(large)	Maximum growth for large phyto	1.85e-5(1.6)	$(s)^{-1}$
μ_max(small)	Maximum growth for small phyto	1.16e-5(1.0)	$(s)^{-1}$
w	Sinking velocity	5.78e-6(0.5)	m/s
KSN_pho(L)	Half saturation for P uptake by Phy(L)	0.20	mmol P m^{-3}

KSN_pho(S)	Half saturation for P uptake by Phy(S)	0.05	mmol P m^{-3}
KSN_sil(L)	Half saturation for silica uptake by Phy(L)	5.0	mmol sil m^{-3}
N2CP	Element ratio for phosphorus and phyto	1/200	dimensionless
M1	Coefficient for mussel model	0.633	
M2	Coefficient for mussel model	0.074	

2.5 *Cladophora* Particle Tracking Model

As mentioned above, associated with the invasive mussels, massive growth of *Cladophora* has been another environmental issue, especially in the north Lake Michigan and along the Wisconsin coastal line (Fig.2.12). Not only they can foul the beach, contaminate the drinking water and deplete the dissolve oxygen at bottom, but the dead mats provide a hotbed for bacteria and even virus as well. The *Cladophora* particle tracking model will be applied for the Sleeping Bear Dunes (SBD) national park area, where *Cladophora* was found with a massive density for some seasons and has caused many environment problems. During last several years, the *Cladophora* continued to influence this recreational area. A large amount of dead migratory birds and aquatic fish were found along the coastal line and scientists postulated that the *Cladophora*

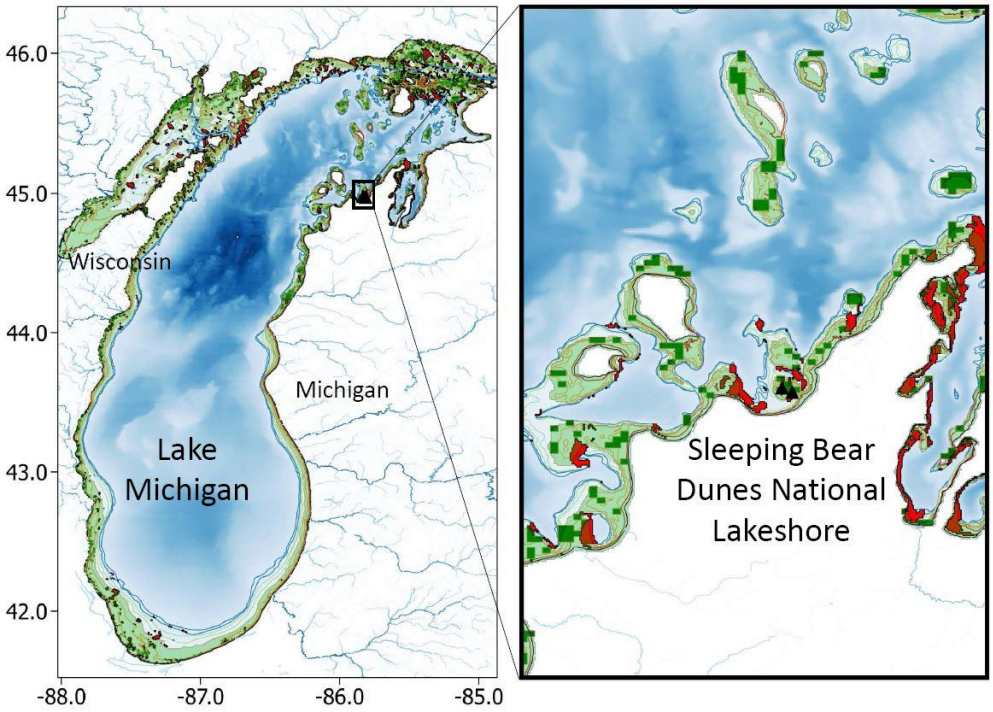

Fig.2.12 *Cladophora* distribution in Lake Michigan and the SBD area.

around this area may be highly responsible for these problems. Given the complicated bathymetry of the SBD area, we hypothesize that it's very likely the dead *Cladophora* moving following the local circulation pattern and deposit to the nearby deeper area where they can be accumulated.

This model mainly tracks the Cladophora trajectory in the hydrodynamic environment. The velocity field and mixing process are based on the output of FVCOM. The Lagrangian particle tracking model is developed to simulate the trajectories of sloughed *Cladophora*, i.e.,

$$\frac{d\vec{x}}{dt} = \vec{v}(\vec{x}(t), t) \tag{76}$$

Where $\vec{x}$ is the particle position at a time t, $\frac{d\vec{x}}{dt}$ is the rate of change of the particle position in time and $\vec{v}$ is the 3-D velocity field generated by the model. In our model, the 4th order 4-stage explicit Runge-Kutta method is employed to update the particle position:

$$\vec{\varepsilon}_1 = \vec{x}_n \tag{77}$$

$$\vec{\varepsilon}_2 = \vec{x}_n + 1/2\Delta t\vec{v}(\vec{\varepsilon}_1) \tag{78}$$

$$\vec{\varepsilon}_3 = \vec{x}_n + 1/2\Delta t\vec{v}(\vec{\varepsilon}_2)(60)\vec{\varepsilon}_4 = \vec{x}_n + 1/2\Delta t\vec{v}(\vec{\varepsilon}_3) \tag{79}$$

$$\vec{x}_{n+1} = \vec{x}_n + \Delta t(\frac{\vec{v}(\vec{\varepsilon}_1)}{6} + \frac{\vec{v}(\vec{\varepsilon}_2)}{3} + \frac{\vec{v}(\vec{\varepsilon}_3)}{3} + \frac{\vec{v}(\vec{\varepsilon}_4)}{6}) \tag{80}$$

Where Δt is the time step. $\vec{x}_n$ is the position of a particle at time t = t_n. The velocity field is linearly interpolated from the FVCOM output and in the vertical direction, a sinking velocity of 10m/hour for the particles is considered as well.

An important part for the *Cladophora* particle trajectory is to take the particle deposition and resuspension into full consideration. For our model, the bottom shear stress will be calculated at each time step to determine the condition for the resuspension of particles reached and deposited on the bottom. The bottom shear stress induced by surface wind-waves is simplified as the dominant stress in this coastal shallow area. Based on linear wave theory, the benthic shear stress (N/m^2) is calculated as a function of wave height and wave period as follows:

$$\tau_w = \rho\sqrt{\nu}\frac{W_H(2\pi/W_T)^{3/2}}{2sinh(k\cdot h)} \tag{81}$$

where ρ is the water density, v is the water viscosity, W_H is the wave height in m, W_T is the wave period, k is the wave number, and h is the water column depth. Data of wave height and period are downloaded from the NOAA GLERL website (Fig.2.13). The uniform wave data is applied for this area considering the relative small size of the simulated area.

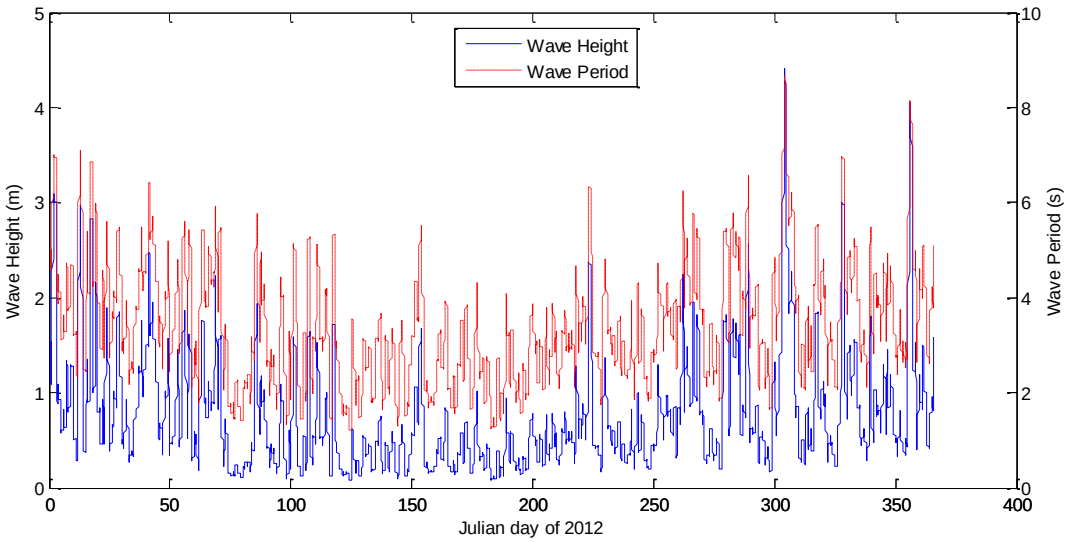

Fig. 2.13 Wave height and wave period for the SBD area.

In order to better resolve the hydrodynamic condition and reproduce more accurate velocity results, refined mesh for this area is used for FVCOM simulation (Fig.2.14).

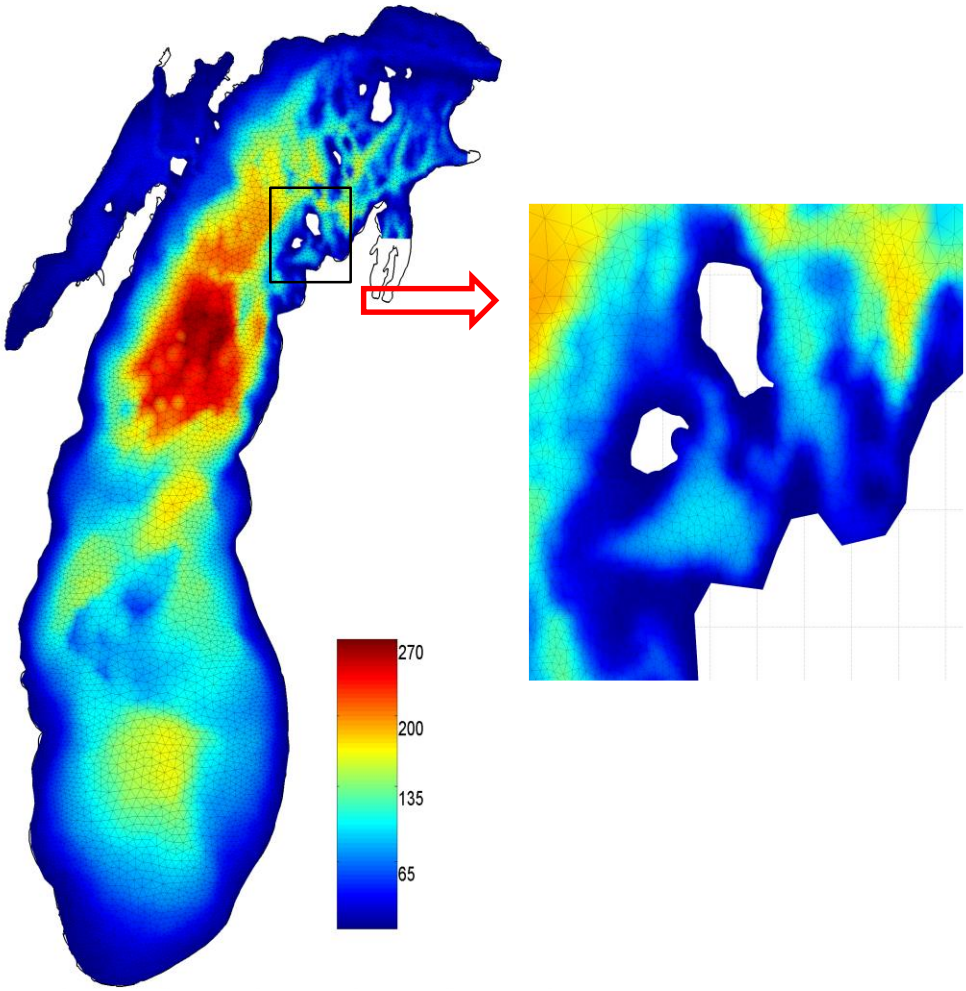

Fig. 2.14 Triangle mesh for Lake Michigan and local high density mesh for SBD area.

Chapter 3

3. A One-Dimension Transport Model

3.1 Physical Results

The surface heat flux driving force is usually pre-computed based on the satellite recorded water surface temperature or field measurement data and then is interpolated to the time series to run the model during our past research or popular 3D models. However, as described by Xue et al. (2015) in the investigation of thermal response to meteorological forcing in the 3D hydrodynamic model of Lake Superior, an important procedure to achieve better and accurate simulations is to derive instantaneous latent/sensible heat fluxes and upward longwave radiation based on the prognostic surface water temperature predicted by the model rather than to pre-calculate these three parts with known surface water temperature. It is believed that with much higher frequency in the calculation of the heat flux after each time step in the model run, the complex air-sea interactions, in certain degree, can be more accurately represented. To compare the difference, a five-year long simulation (2009-2013) is conducted with the heat flux calculated based on the two different methods. The comparison is made between the individual simulation results from the 1D model and the surface temperature data from GLSEA. With the pre-calculated heat flux, the mismatch between the model results and satellite data is clearly shown from the weak stratification in May to the end of each year. The mismatch seems to grow in the summer strong stratification period, especially for the year of 2009 and 2010. The summer results of 2009 showed an overly high surface water temperature while an overly low result was found for the 2010 case. Differently, the prognostically calculated heat flux did significantly improve the performance of the simulation. Within the five-year

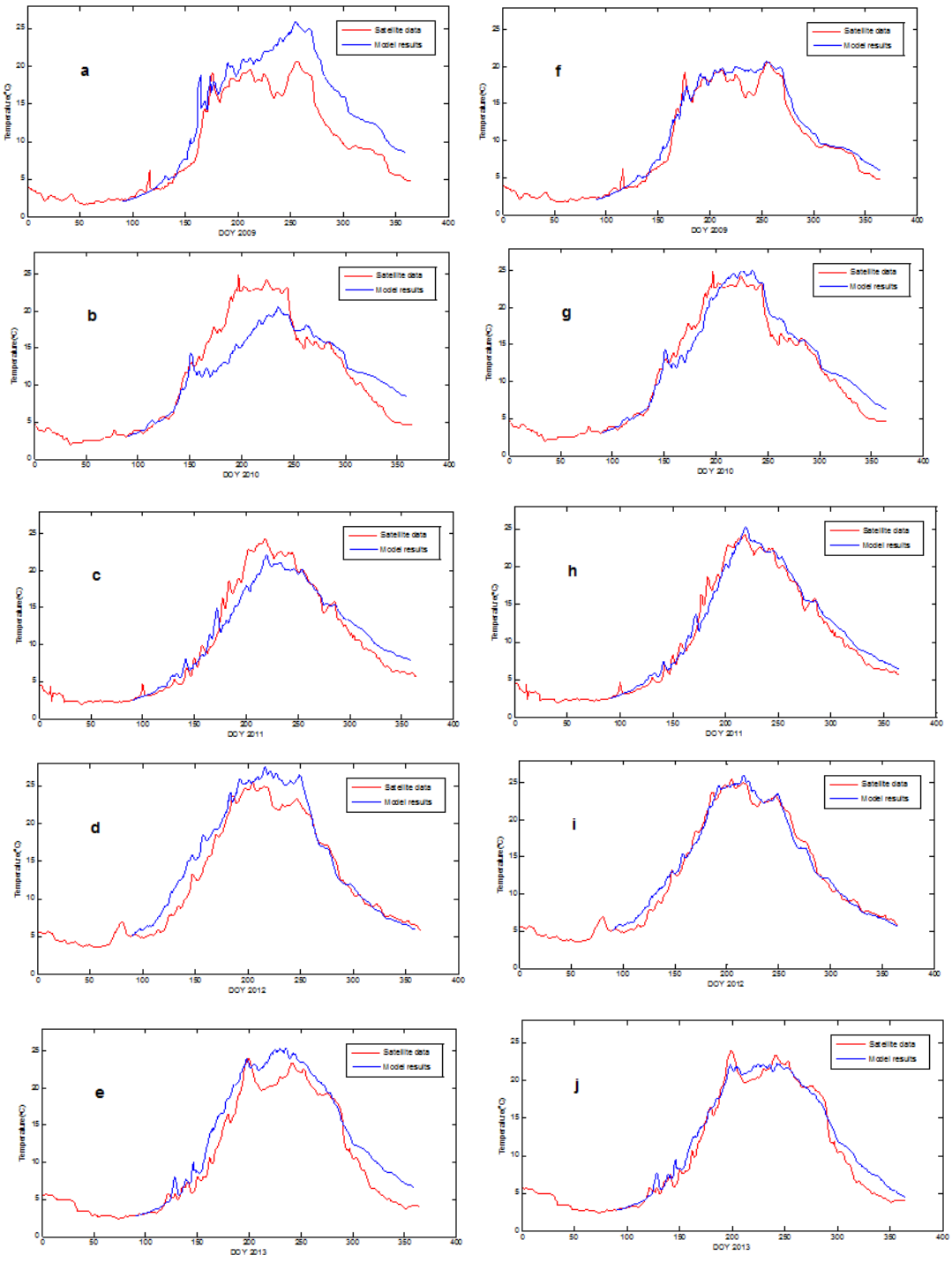

Fig. 3.1 Time series (2009-2013) of water surface temperature simulated (blue) in comparison to the GLSEA data (red). a-e is model results (2009-2013) based on the pre-computed heat flux. f-j is model results (2009-2013) based on dynamically calculated heat flux.

long simulation (2009-2013), good agreements between the simulation results and GLSEA data on surface water temperature (Fig.3.1) are found. However, with the limitation of 1D model where lateral transport processes are missing, some mismatch can be found, especially for the summer and fall of 2010.

As discussed in the momentum equation of the 1D model, to suppress the buildup of kinetic energy, a sink term is necessary to create a damping effect. For ocean simulation cases presented by Mellor (2000), an 8-inertial-day (c =8 day^{-1}) is applied in the 1D model. The velocity was found with a significant decrease during the whole water column while the increase of surface temperature is negligible. The model is tested for the year of 2012 when field data were available for Lake Michigan. A 3.0-inertial-day sink term value is applied to reproduce the same velocity magnitude compared to the observed velocity, although the simulated surface temperature increased slightly due to the sink term. In addition, the result with sink term agrees better with the satellite data from the fall convection period to the end of year. However, the velocity results showed improvement with that additional term (Fig. 3.2). The model velocity results at 5m and 10m depth are compared with the field measurement. Without the sink term, the magnitude of the velocity is found much larger than the measured data. Velocity result with the sink term is in a very reasonable scale and matches well during the observation period, especially before the downwelling period from DOY 175 to 223. To better illustrate the performance of the model on the velocity simulation, comparison of the shear production between the two are given in Fig.16. Shear production is in the form as:

$$P_S = \mathrm{K_v}\left[\left(\frac{\partial \mathrm{u}}{\partial \mathrm{z}}\right)^2 + \left(\frac{\partial \mathrm{v}}{\partial \mathrm{z}}\right)^2\right] \tag{66}$$

Since no direct eddy viscosity measurement is available, this term will be obtained from the model output. The comparison is made for the recorded observation period before the

downwelling event occurred when strong horizontal current was generated. The results displayed a good match, especially in the upper 10m while the comparison is not as good near the depth of the thermocline (Fig 3.3). Relative large mismatch is captured at DOY 225 when the strong downwelling due to the basin scale internal wave.

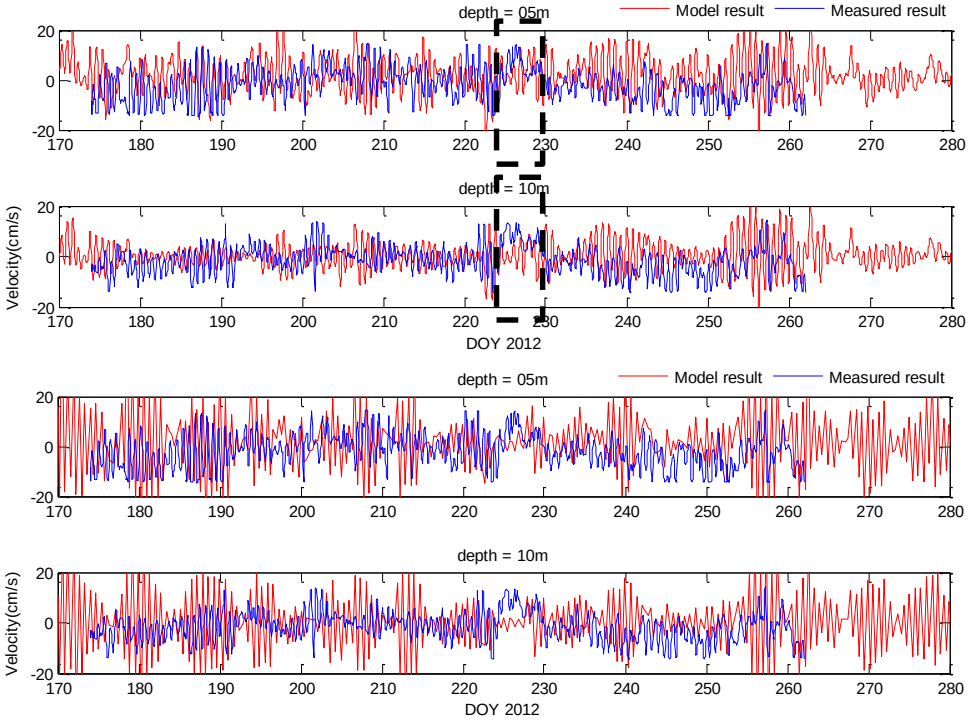

Fig.3.2 Eastward velocity comparison at depth 5 and 10m with (above) and without (below) sink term during the summer time, black dash square is the downwelling period

The difference between the simulated results and field measurement is still quite obvious. Since the model site is in a mid-depth region between the nearshore and offshore site, the cross shore and along shore currents due to coastal processes which are not represented by the 1D model will definitely have a strong effect on that site. And from the field measurement, there is indeed a strong west basin downwelling recorded during DOY 223-230 (with a corresponding upwelling on the east side) which is unusual since western (Wisconsin) coast is upwelling

favorable under the prevailing summer wind conditions and rotation effects of the Earth (Troy, 2012). As a result, the velocity after that time is theoretically difficult, if not impossible, for the 1D model to reproduce. The time variability of the velocity is investigated by estimating the spectra of measured and model velocities at the 10m depth (Fig. 3.4). Other depth results showed very similar spectral features. From the spectral analysis, the observation data displayed a distinctive peak at 17.5h which is attributed to the near-inertial Poincare wave in Lake Michigan during strong stratification period. Similar with the simple slab model (Choi, Troy, 2012), our 1D model also reproduced an inertial period which is believed that the model is based on an inertial timescales of the summer wind force and well reproduced the vertical thermal structure.

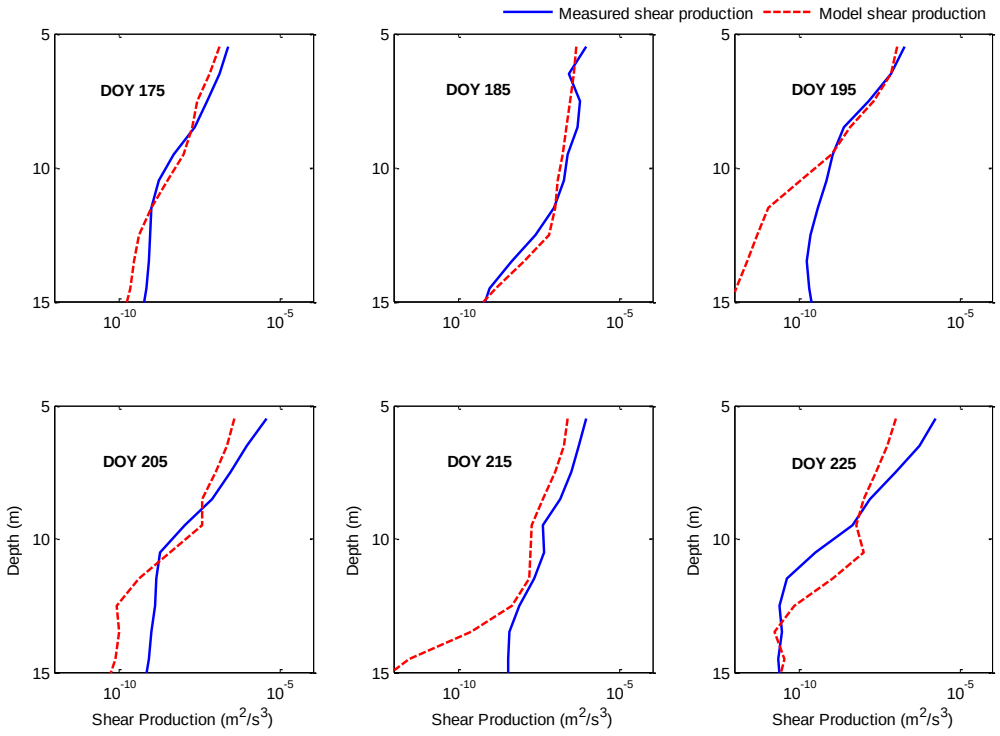

Fig. 3.3 Comparison of shear production before the downwelling period. Measurement (blue), model simulation (red).

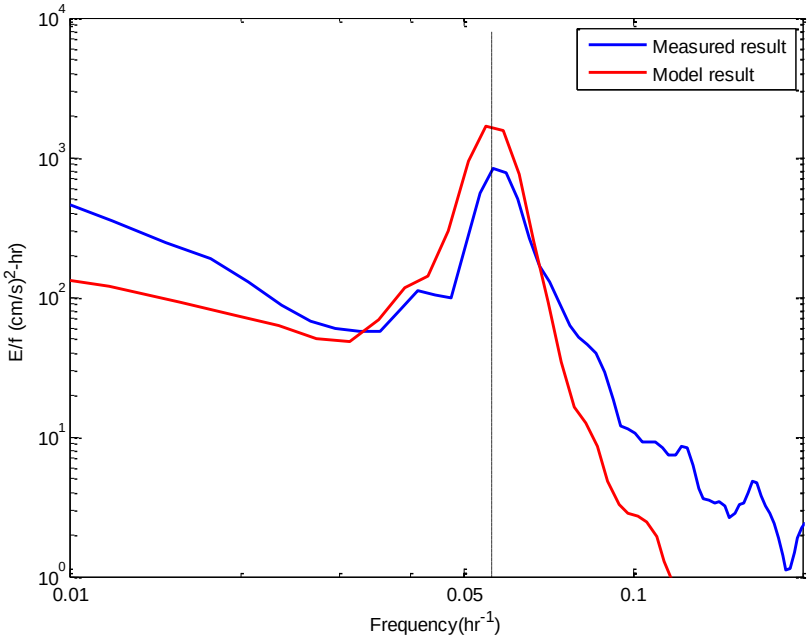

Fig.3.4 Spectral analysis of the eastern velocity component at 10m depth.

Surface wave is considered and tested in our model as well since it has been proved important in affecting the mixing depth in the ocean and Great Lakes (Craig and Banner, 1994; Wu, 2002, Babanin, 2006). Two effects, surface wave breaking and wave current interaction, are included in the 1D model. The results basically agree with those derived in the investigation of ocean in the literature (Fig 3.5). Surface wave breaking is associated with enhanced turbulence velocity at the upper layer as described in the boundary condition with Eq. 33, however, the enhanced surface layer mixing length (Eq. 34) also demonstrates the affected zone is limited in the order of the wave heights. In the summer strong stratification period, the mixing layer depth is deeper than the wave-breaking induced length scale, so the thermal structure is much like the one without wave effect as in the figure. Differently, the wave current effect will result in the additional dissipation to the whole water column in the exponential decay with depth and the

affect zone will be much deeper than the wave breaking effect. Extended mixing layer depth is found in our simulation results under the wave current effect with a corresponding decrease of the surface layer temperature. However, compared to the ocean simulation, wave effect is much small in Great Lakes due to the limited wave height and length.

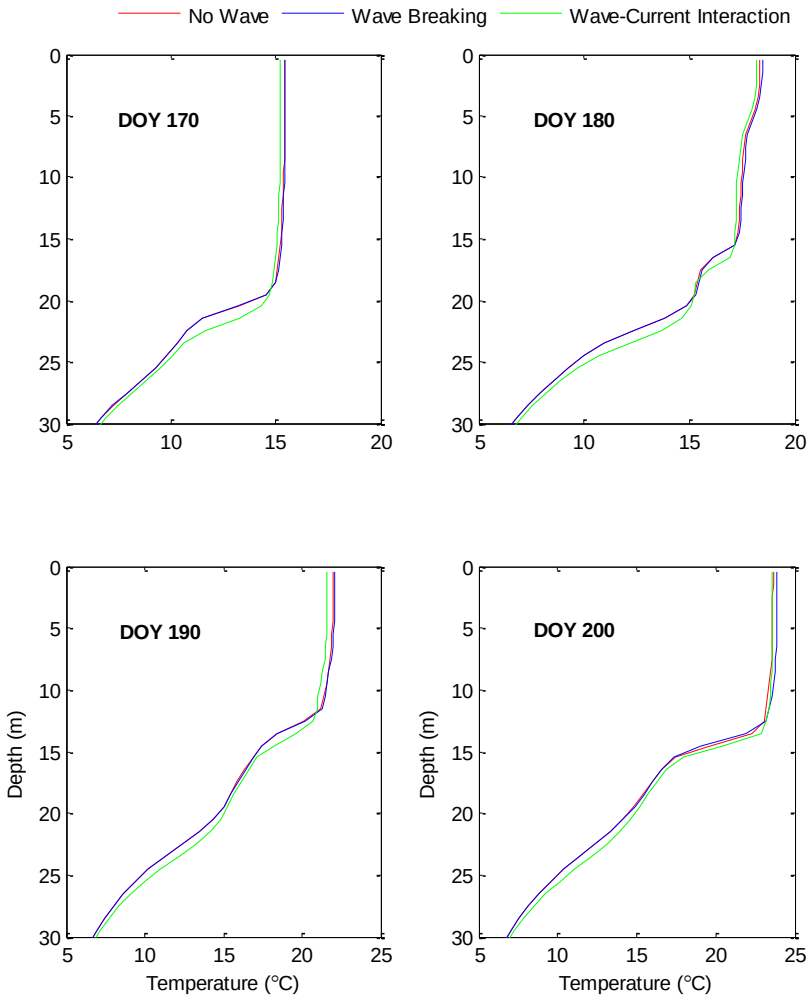

Fig. 3.5 Time series of thermal structure at the 55m site with waves effects. No wave (red), surface wave breaking (blue), wave current interaction (green)

At the beginning of summer in 2012 (DOY 170) during the field measurement, a PIV instrument was deployed at the same time and the dissipation rate at the vertical column was

derived through analyzing the micro velocity structure. Meanwhile, the dissipation from a Self-Contained Autonomous Micro Profiler (SCAMP) measurement is available as well. Energy dissipation results from the model are calculated with and without the wave effect (Fig. 3.6). As

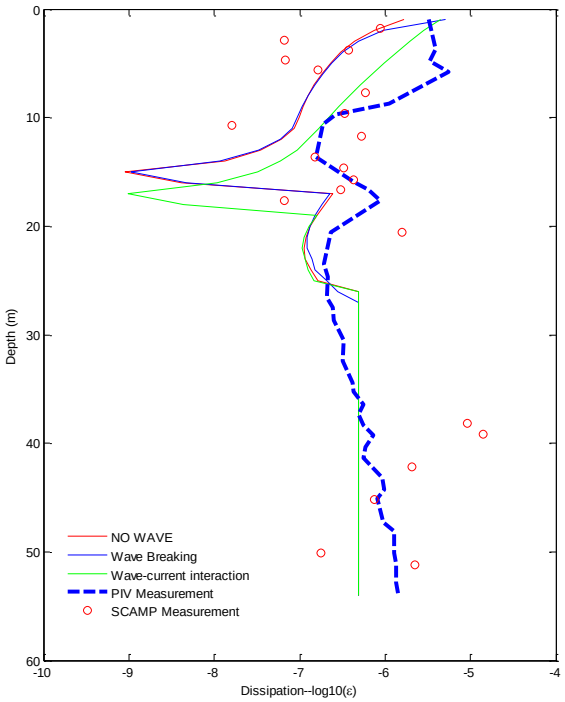

Fig.3.6 Comparison of vertical dissipation in June 20th in 2012. No wave (red), wave breaking (blue), wave current interaction (green), PIV measurement (blue dash), SCAMP measurement (red circle).

the figure shows, the model results agree well with the measurement, especially with the SCAMP results, reproducing a gradually decrease, then a sharp increase in the surface layer. Given the turbulence induced by the drop of the PIV system, it is reasonable to have a relative high value of PIV measurement, especially in the thermocline in which the dissipation is relative small due to the strong stratification. Near the thermocline, the model results are roughly one order less compared to the measurement and considering the small value at this location, it's comparably easy to be disturbed by the surrounding environment which cannot be captured by

our model. The wave effects are also clearly demonstrated in the figure. With an enhanced surface turbulence velocity and mixing length, the surface dissipation rate is much larger with the surface wave breaking effect and is in a good agreement with the PIV measurement. Dissipation results with wave current effect is comparably larger as well and an obvious mixing layer depth increase can be observed.

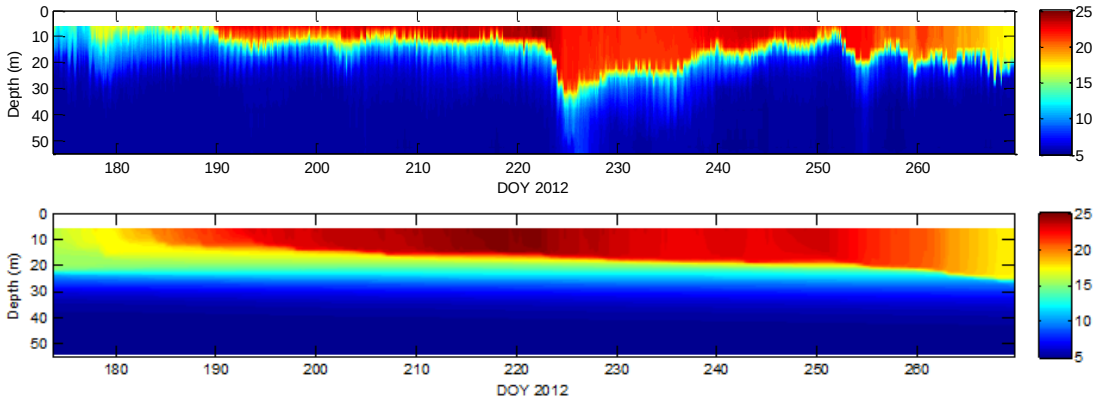

Fig. 3.7 Thermal structure between the field measurement (above) and simulated results (below).

Compared to the measured thermal structure in the whole summer of 2012, the modeled result is proved to be able to capture the main features, starting from the weak stratification to the fully developed thermcocline along with the warm up of water body and end with the convection overturn in the fall with the cooling process (Fig.3.7). Moreover, different to the smooth thermocline in the time series, the observed data indicated featured variation of the temperature with the internal wave effect which cannot be reflected in the 1D model. Moreover, the simulation result displayed a diffusive thermocline. The mismatch of the thermocline has been investigated as a common problem in the numerical simulations in Great Lakes. Similarly, in a 3D model simulation on the current and thermal structure in Lake Michigan by Beletsky

(Beletsky, 2006), simulated thermocline is found more diffusive and cannot be improved with the increasing vertical resolution or decreasing time step. An assumption is that some mechanisms such as the Langmuir circulation are not reflected in the model (Beletsky, 2006). At different depth in the vertical water column, the temperature time series of simulated and measured data are shown in Fig.3.8 and the two are in a good agreement at surface and bottom area except near the thermocline.

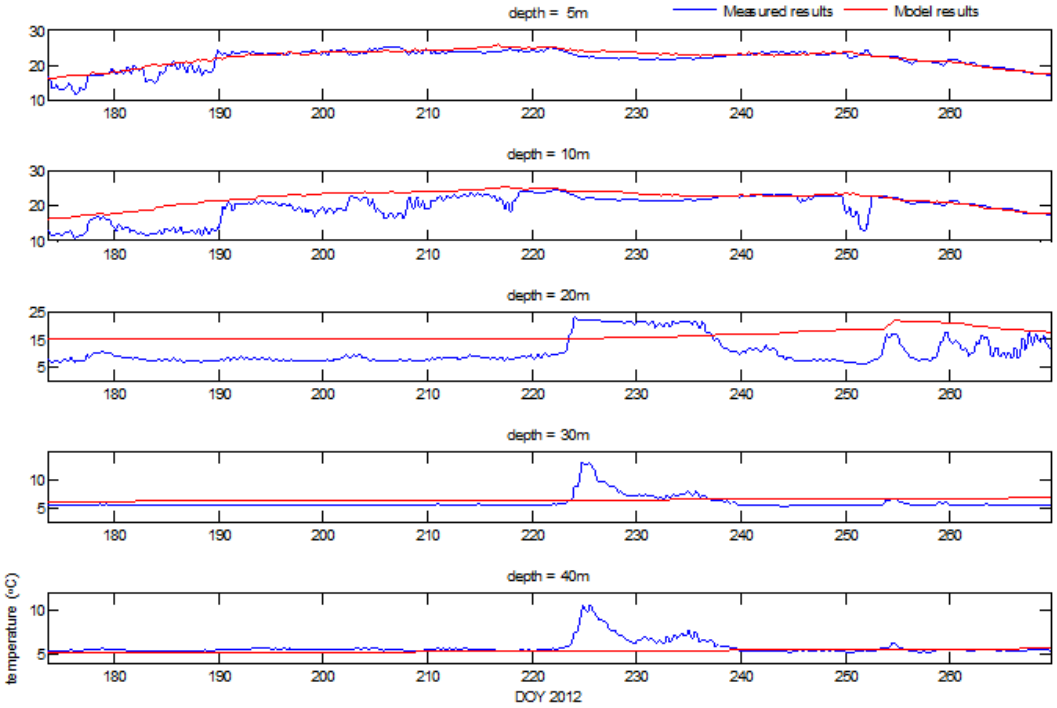

Fig.3.8 Time series of simulated (red) water temperature versus observed (blue) at depth of 5m, 10m, 20m, 30m, 40m.

As mentioned before, one-dimensional model is much preferable at horizontal homogeneous environment with strong vertical mixing. So model results can not reflect the true field data, especially at the shallow nearshore area where along shore and cross shore current are notable. In our simulation period, a strong along shore current is observed during DOY 223-230

which is impossible for the model to capture the dynamics of thermal structure and current velocity. This mismatch resulted from the horizontal effect can be well correlated with the imbalance between the heat storage through measured temperature profiles and that from the calculated surface heat flux (Fig.3.9). The measured heat storage equation can be expressed as:

$$H = \sum_{t=0}^{t=end}(\sum_{h=-H}^{h=0} C_p \rho \Delta T \, / \Delta t) \quad (67)$$

where, C_p is the heat capacity of water, ρ is the density, ΔT is the temperature difference between time step, Δt is the measurement time step. The dramatic increase of heat storage during DOY 223-230 can sufficiently explain downwelling effect on the suddenly increased mixing depth layer for the thermal structure and magnitude of velocity during that period.

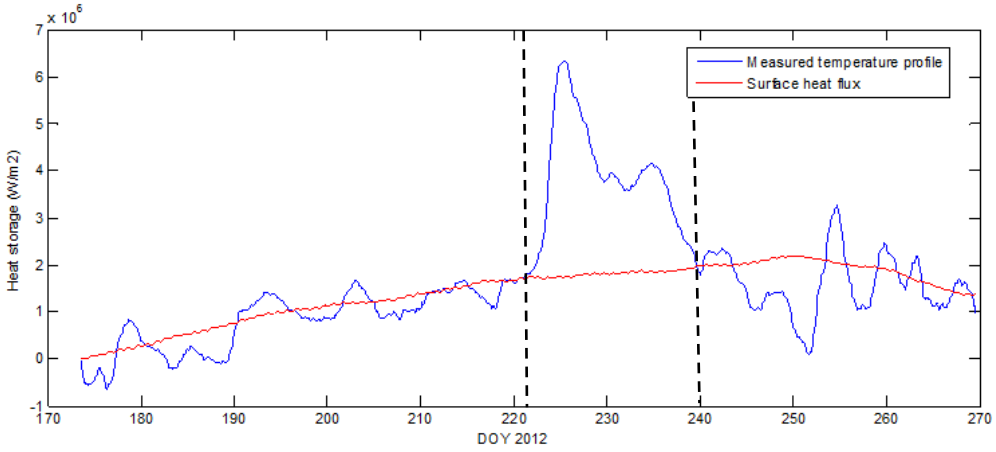

Fig.3.9 Heat storage obtained from measured temperature profiles (blue) and surface heat flux (red).

3.2 Biological Results

A one-dimensional column phytoplankton model was developed to investigate the effect of the mussels on the concentration of phytoplankton for the mid-depth site. The model was deployed for the simulation during the spring and the beginning of summer to see how mussels' filtration will affect the distribution of phytoplankton in the water column under different vertical

mixing conditions. In addition, during this time period, the nutrient is assumed to be a non-limiting factor, so the growth model of phytoplankton can be simplified. Field measurement data at this site is available for the spring and summer in 2013 and is applied to validate the model's accuracy. As shown in Fig.3.10, The simulation with mussel filtering activities produced observable reduction in the weak stratification vertical column in spring due to the sufficient delivery of food to the mussel bed by vertical mixing. In the summer stratified season, since the thermocline can significantly prevent the exchange of phytoplankton from the surface mixed layer to the hypolimnion, the effects of mussel is limited at a relatively thin bottom layer and the difference in the surface is little.

With the increase of water temperature and light penetration from Spring to Summer, our model results demonstrated a quick growth for the phytoplankton (Fig.3.11), especially in June with a very high concentration at the surface area. The difference of the simulation with/without mussel for Julian 60-200 is displayed in the bottom figure of Fig.3.11. It proved again that mussels have the potential to decrease the particles in the water column during well mixed time and their clearance rate is very limited in strong stratification time.

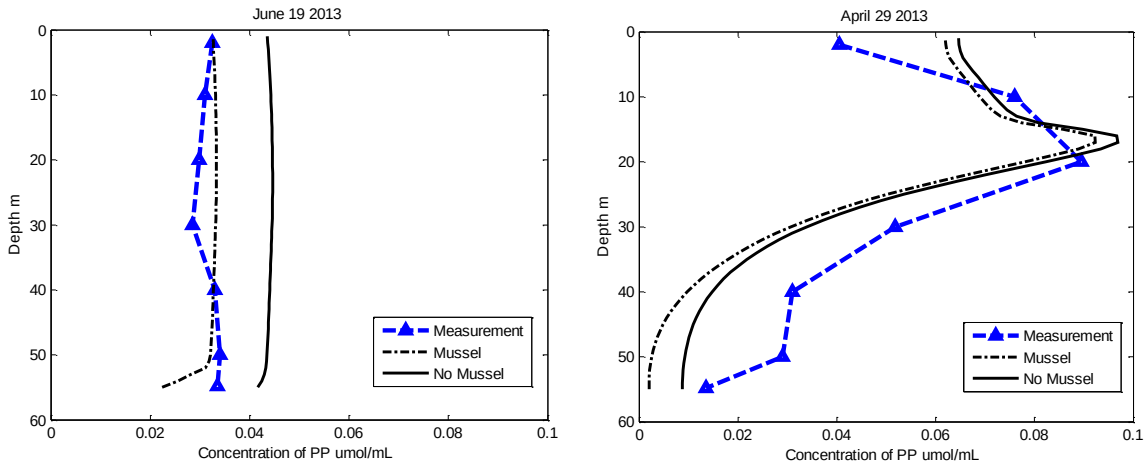

Fig.3.10 Comparison between the field measurement (triangle) and simulation results with (dash line) and without (solid line) mussel.

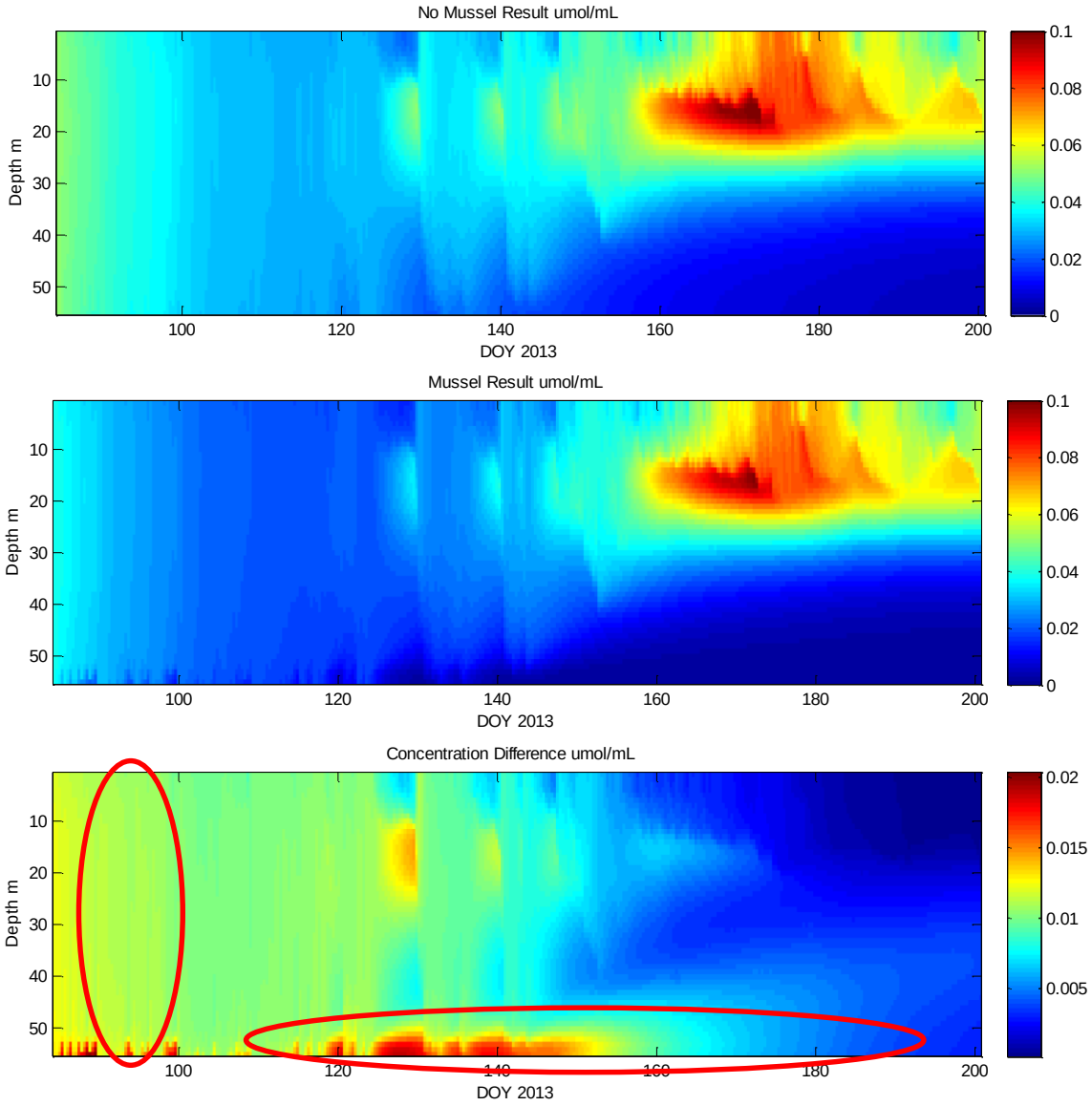

Fig.3.11 simulation results of particle phosphorus concentration time series distribution with and without mussels. The bottom is their difference.

3.3 Conclusion

In this Chapter, a 1D transport model for Lake Michigan is developed and the validity is tested as well with the comparison between the model results and filed observations. The five-year long water surface temperature indicated the importance of the dynamically calculated heat flux in improving the simulation results in our 1D model. A sink term of $3day^{-1}$ is introduced into the model to resolve the buildup of kinetic energy. Without that damp effect, the magnitude of the velocity in the whole column is much larger than the observed one. The model reproduced good velocity result with the sink term before the downwelling period and there is little effect on the thermal structure. The wave breaking and water current interaction is also tested in the model. Surface wave breaking is proved to increase the energy dissipation at the very surface while the wave current interaction can efficiently increase the mixing depth along with a relative surface temperature. Finally, compared to the observed thermal data from the deployment in summer of 2012, our model successfully reproduced the main features on the development of the thermal stratification. Time series of temperature at different depth agree with the field data well except during the downwelling period. At last, based on the well resolved physical condition, the 1D phytoplankton transport model was conducted and showed the ability to reproduce their distribution through the spring and beginning of summer. The mussel was incorporated at the bottom as well. With the existence of mussels, the simulation result is much closer to the field measurement, especially in the spring when the stratification is weak.

Even though a 1D model is constructed with a lot of simplifications, our investigation proved that the 1D model can sufficiently be applied in the Great Lakes, especially in the off shore area where horizontal effect is relative weak in comparison with the nearshore area. And the simplicity of the model will be very attractive as a convenient tool to investigate of the vertical distribution of physical mixing and ecological parameters of deep, stratified lakes, such

as Lake Michigan. However, more work need to be continued to improve the model performance. More investigation is needed to determine the sink term. An 8 day^{-1} value is applied in an ocean case based on the literature which is much smaller compared that in our model for Lake Michigan. Meanwhile, the determination of the specific sink term is relative empirical in order to match the magnitude of the observed velocity. Instead of a vertical uniform value, a depth dependent value could be more reasonable. The diffusive thermocline is another problem need to be addressed. Additional physical mechanism can be added into the model for future studies.

Chapter 4

4. 3D Biophysical model to investigate the effect of mussel on Lake Michigan

4.1 Physical results

The lake-averaged water surface temperature from satellite data as well as that observed at two buoys in the south (45007) and north (45002) sub-basin are downloaded to compare with the simulation results. Time series of modeled results versus observed water surface temperature for these 3 cases are presented in the Fig 4.1-4.3. The model is proved to be capable in accurately reproducing the seasonal thermal cycle for all these 3 cases from the stratification to convection period. The lake-wide surface temperature jump in the August is well captured. However, small bias after the beginning of the simulation was observed. It seems that the simulated surface temperature is relatively higher than the observation which was in accordance with that reported

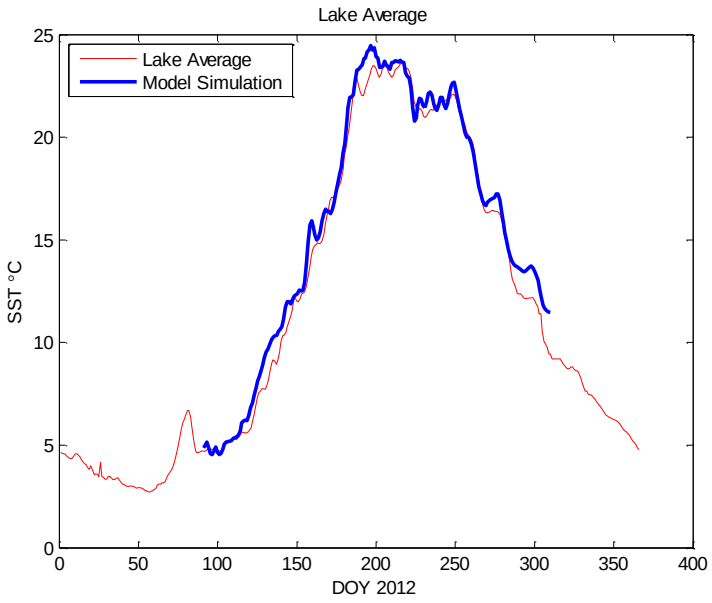

Fig.4.1 Comparison of lake average surface temperature. Satellite data (red), model results (blue).

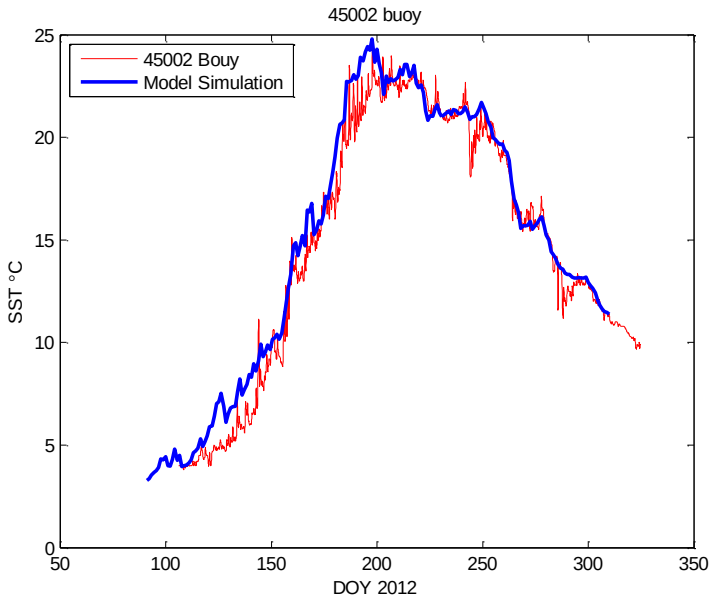

Fig.4.2 Comparison of north bouy 45002 in Lake Michigan. Field observation (red), model results (blue).

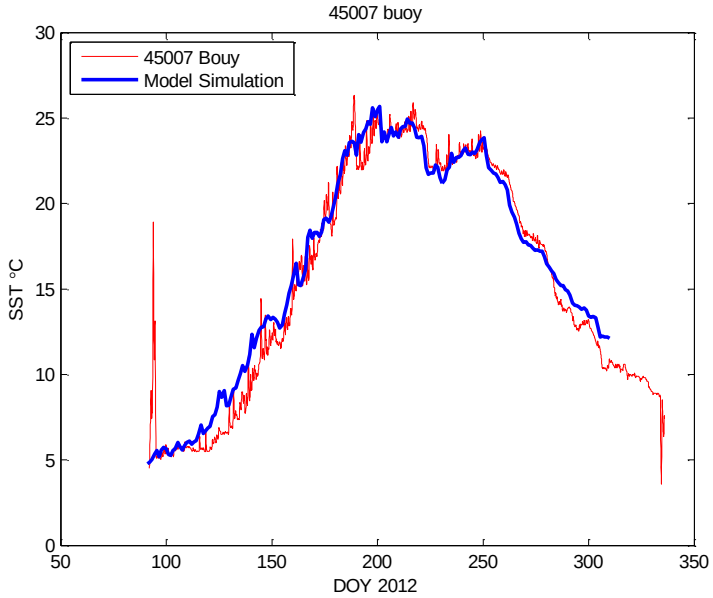

Fig.4.3 Comparison of south bouy 45007 in Lake Michigan. Field observation (red), model results (blue).

in the literature. And the main reason is most likely the inadequate prescription of initial conditions. Compared to the results at the buoy position, the average lake surface temperature result looks even more accurate. The simulated monthly lake average surface temperature generally well match with the satellite data (Fig. 4.4).

The average summer current for Lake Michigan is plotted to show the performance on the velocity field (Fig.4.5). The middle figure is the main summer long-term current observation pattern in Lake Michigan which reveals that the lake is featured with a cyclonic large-scale circulation pattern outside and two smaller cyclonic circulations at each sub-basin as well as some small circulations at the ridge under the southern wind. The red arrows in the left indicate vertical average circulation directions for the summer as the model simulation results. And the current patterns for the model results coincide with the observations very well. The magnitude of the summer average current is also depicted in the right figure. As presented for the whole lake, the average vertical current value is recorded as around 1 cm/s given the low speed wind during the summer time (Beletsky and Schwab, 2001). This value agrees well with the simulation average value for our model. In addition, relative larger current can be observed along the coastal lines which is very reasonable due to the shallower depth.

In the 1D model section, the simulation results are compared with the field measurement. In this section, the simulation result at the 55m site will also be extracted to check the 3D model's performance in the vertical thermal structure and velocity output. The comparison of thermal structure is shown in Fig.4.6. In general, the model result is in a good agreement with the observation by reproducing the thermocline depth change and fluctuation resulted from internal waves. Different to the 1D model, the horizontal advection and diffusion is well reflected in the 3D model. The uncommon downwelling effect in August which is not captured by the 1D model

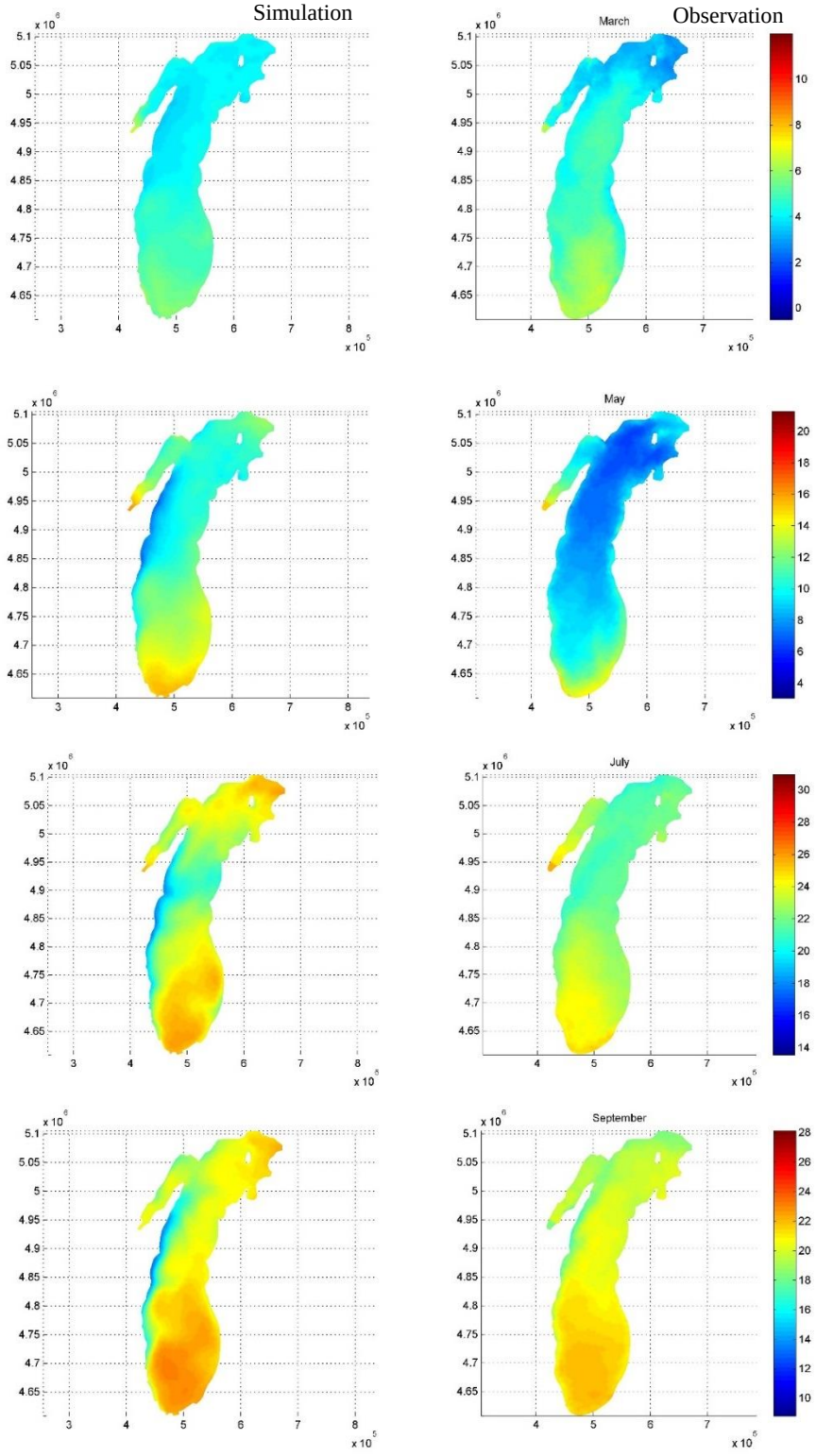

Fig.4.4 Comparison of monthly average water surface temperature in March, May, July and September. Simulation results (left), satellite data (right).

is clearly demonstrated here. However, as it is mentioned above, the diffusive thermocline still cannot be efficiently resolved and more work should be done to account for this effect.

The time series of velocity and temperature are also analyzed in detail here. The model results at 6m, 16m and 50m which represent the surface mixing layer, thermocline layer and bottom layer are compared with the field observation (Fig.4.7-4.9). Again, due to the diffusive thermocline, the temperature time series at 6m and 50m match better than the 16m result. Agreement between model and observations looks reasonable for the current speed and even the magnitude of the near-inertial oscillations with a period about 18 hours. However, the model seems overestimated the current speed at the surface while underestimate the current speed at the bottom layer.

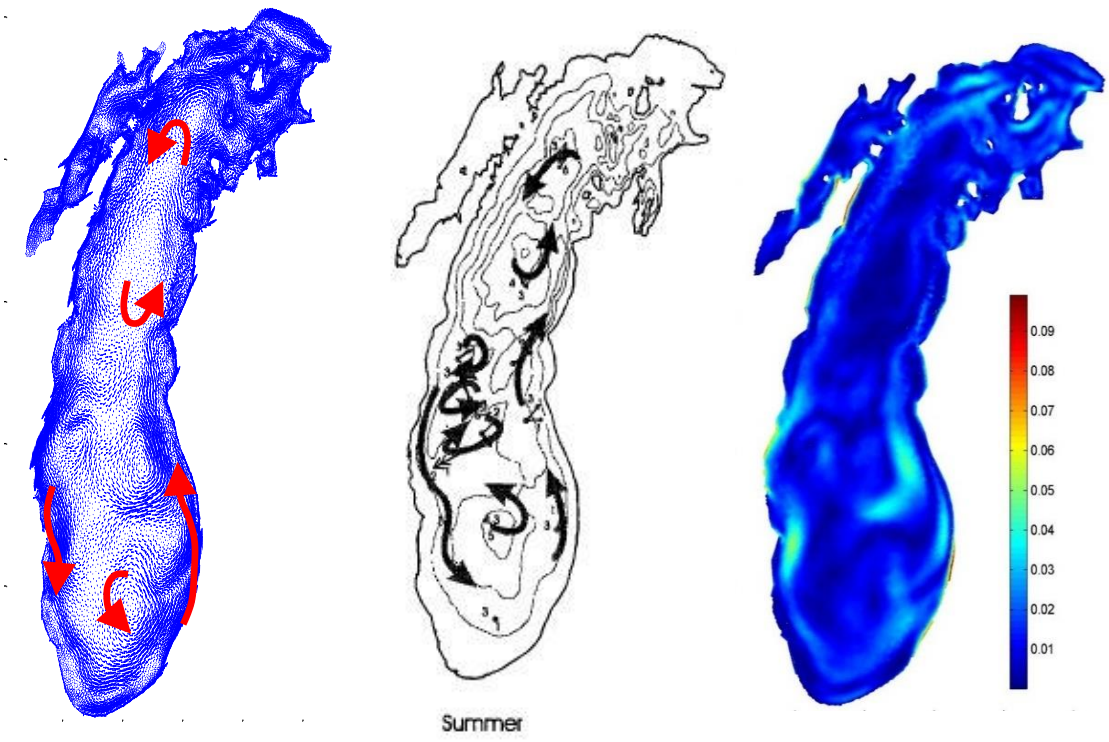

Fig.4.5 Summer vertical average circulation pattern and magnitude. Simulation circulation (left), observed circulation (mid), summer vertical average current speed (right).

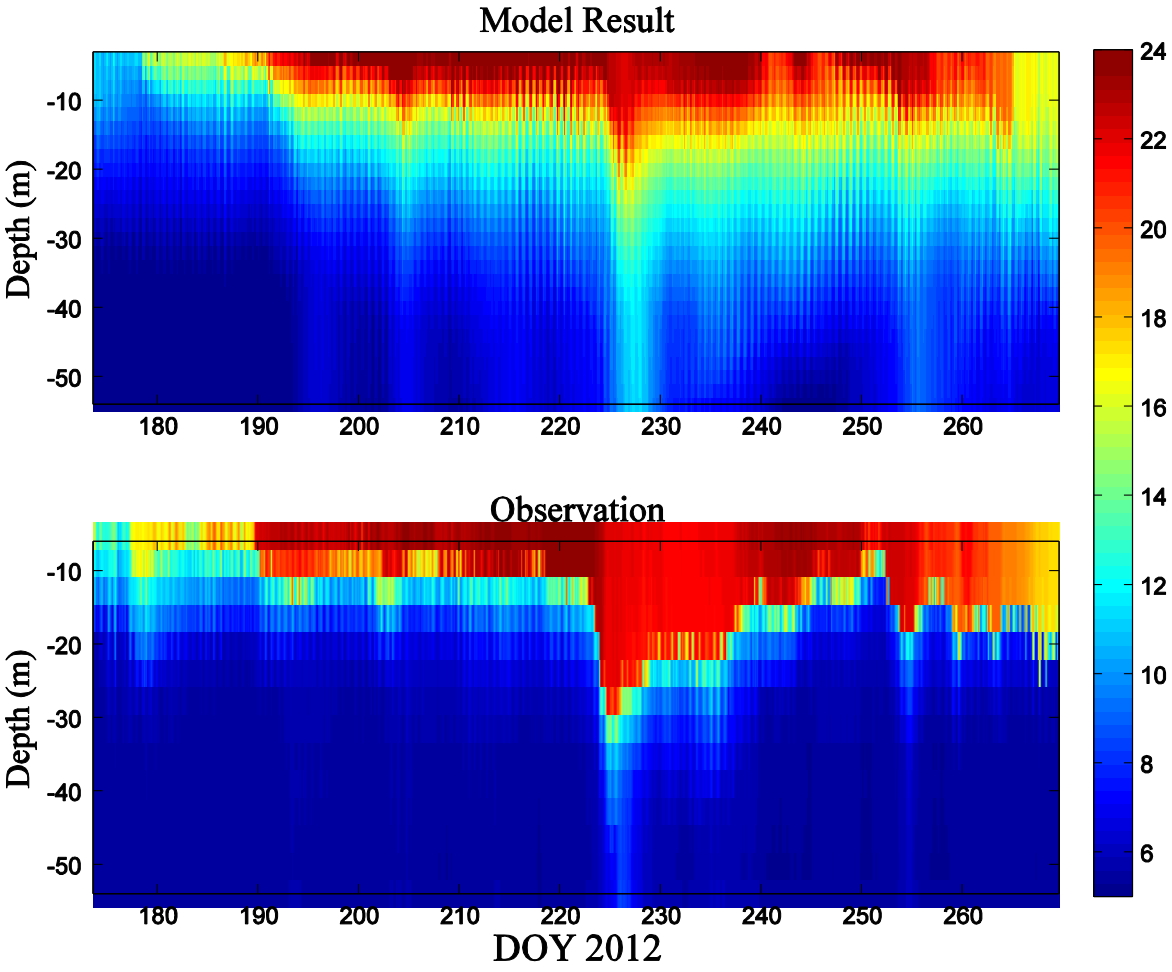

Fig.4.6 Thermal structure for the 55m site. Model output (above), field observation (bottom).

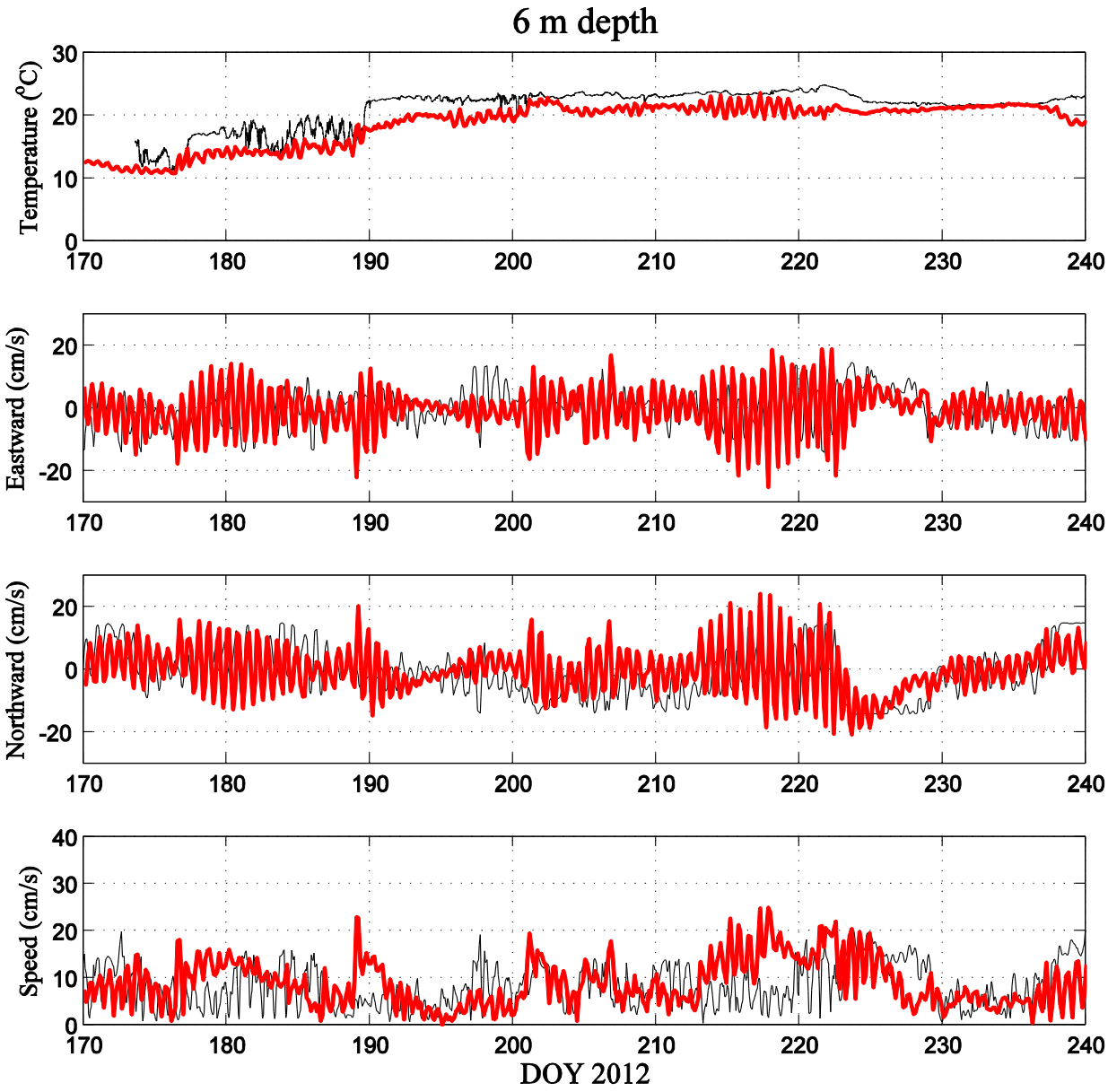

Fig.4.7 6m depth comparison for temperature and velocity.
Observation (black), model results (red).

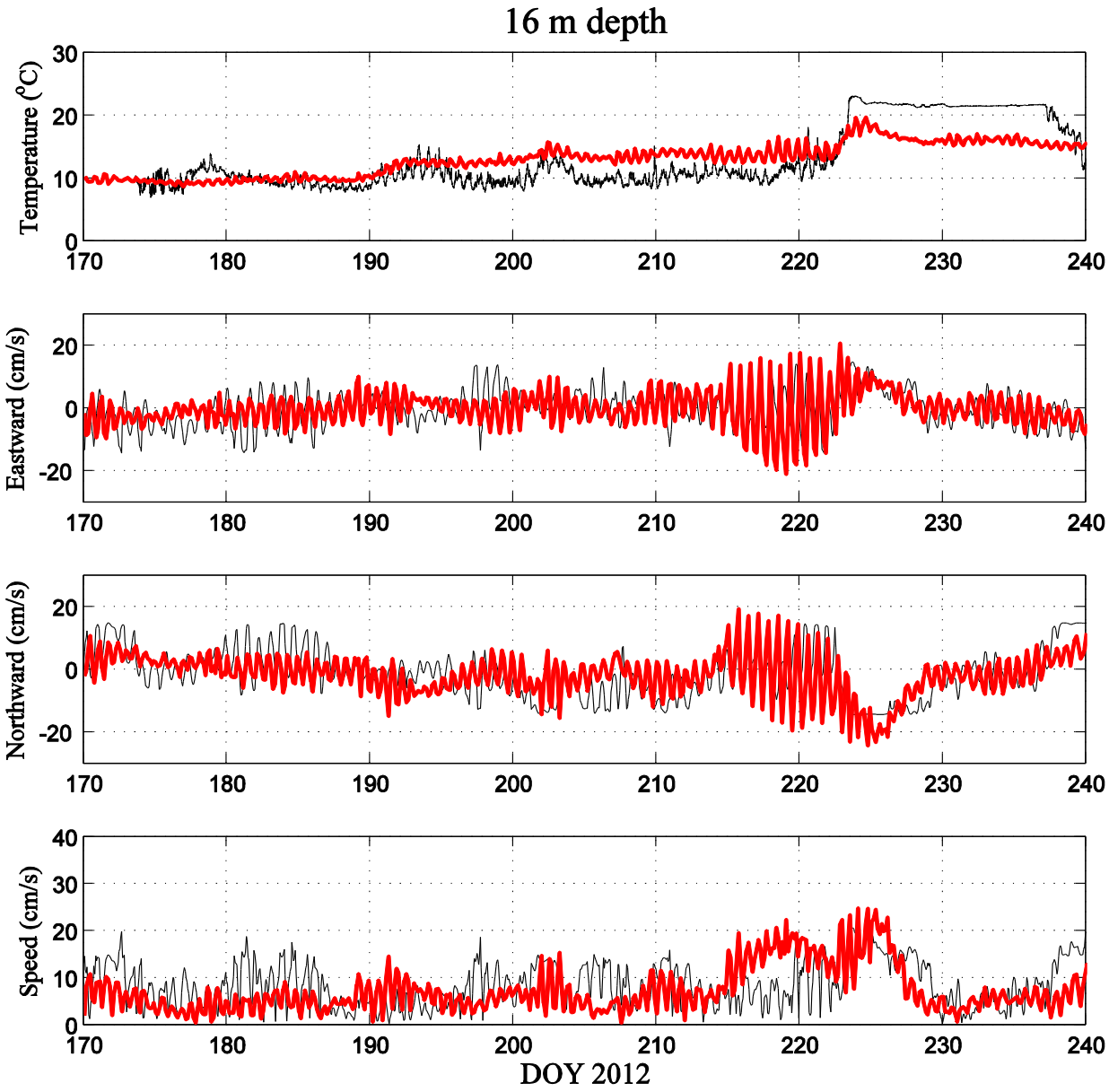

Fig.4.8 16m depth comparison for temperature and velocity. Observation (black), model results (red).

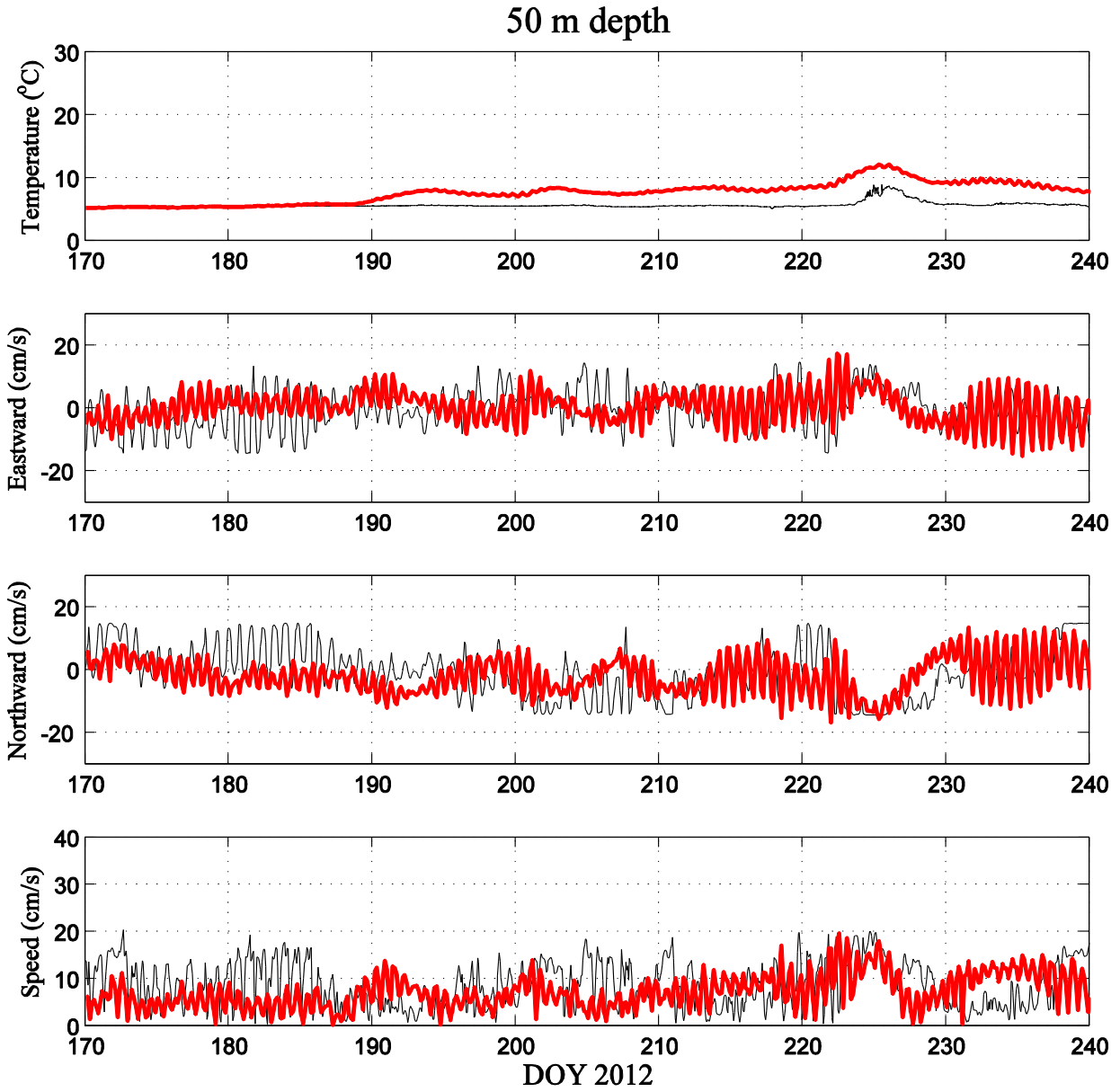

Fig.4.9 50m depth comparison for temperature and velocity. Observation (black), model results (red).

4.2 Biological results

The lake-wide vertical average concentration of phytoplankton is presented in Fig.4.10-4.11. High concentration of phytoplankton can be found generally at the nearshore area with

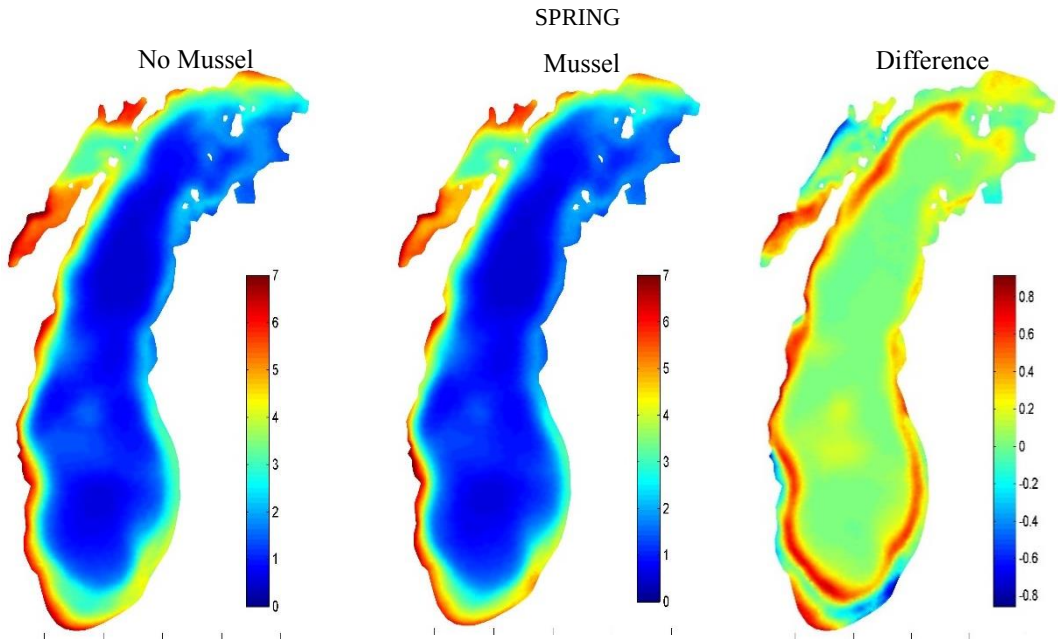

Fig.35 Spring vertical average phytoplankton concentration (mmol C/m^3).

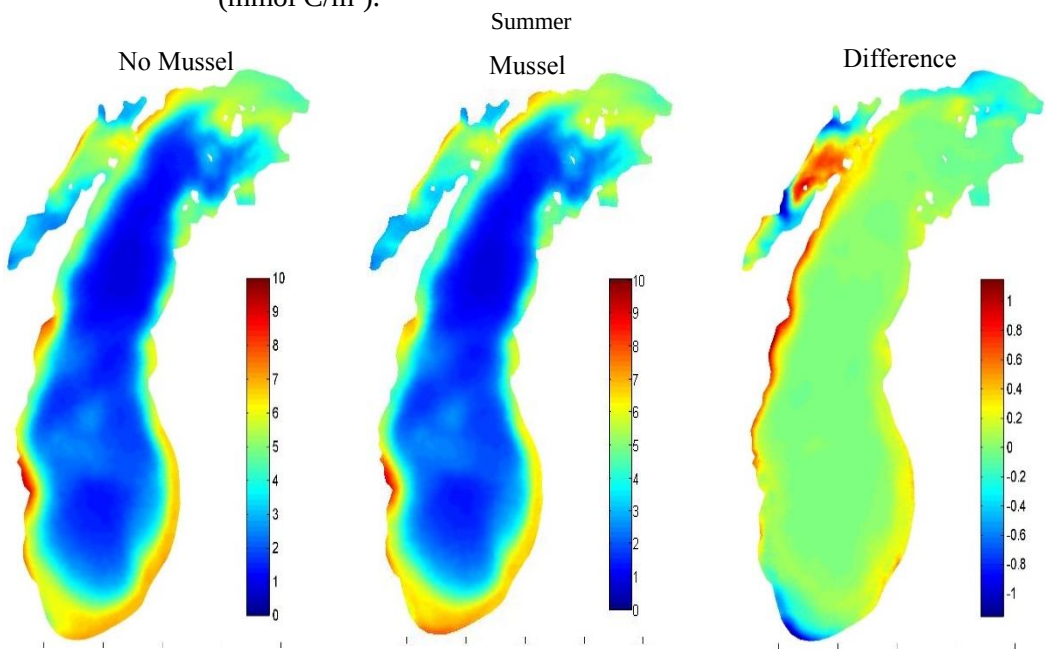

Fig.4.11 Summer vertical average phytoplankton concentration (mmol C/m^3).

sufficient nutrient supply, warmer water temperature and adequate light penetrating into the lake bottom. To better illustrate the effect of the mussel to the nutrient dynamic and the distribution of phytoplankton, the model was executed with and without the existence of mussels at the bottom. In addition, two-time series (spring and summer) results are analyzed to investigate the seasonal difference. In spring, the mussel is possible to get access to the entire water column given the weak stratification at that time while the mussel filter feeding activity is very limited in the hypolimnion zone for mussels in summer since the material exchange is significantly suppressed with the thermocline. During the spring, the lake-wide phytoplankton is found with obvious decrease at the nearshore shallow area where high density of mussels have been established. And 6% decrease of the phytoplankton can be derived for the whole lake by integrating the amount of total phytoplankton with mussels included in the model compared to the case without mussels. However, the decrease of phytoplankton in the summer is relative low even with the effect of mussel and the total lake-wide phytoplankton decrease is only 2% according the simulation.

The vertical distribution is also studied to reveal more details of how mussels affect the distribution of nutrient and phytoplankton. The 55m mid-depth site in the 1D model is again picked as the location of research target in the 3D model due to the high density of mussel there and availability of field data. The results are still distinguished as two seasons considering the physical mixing condition (Fig.4.12). For soluble reactive phosphorus (SRP), it seems there is little seasonal variation with nearly the same concentration in the upper layer for the two cases and a higher boundary concentration layer at the bottom in the existence of mussel. Concentration of SRP in the upper layer becomes very low in both spring and summer due to the uptake process of phytoplankton. Relative high concentration is observed from the model with the limit growth of phytoplankton and the excretion of mussels. At the very bottom, the SRP

concentration is almost 25 percent larger than that without mussel in spring. In summer, the difference is even larger, reaching to almost 47 percent.

On the opposite, particulate phosphorus (PP), mainly from the phytoplankton, is found in the distribution with a high concentration in the surface layer while a low value close to the bottom. In spring, a decrease in the whole water column is observed with the mussel incorporated in the model since their potential grazing effect can reach the very surface under

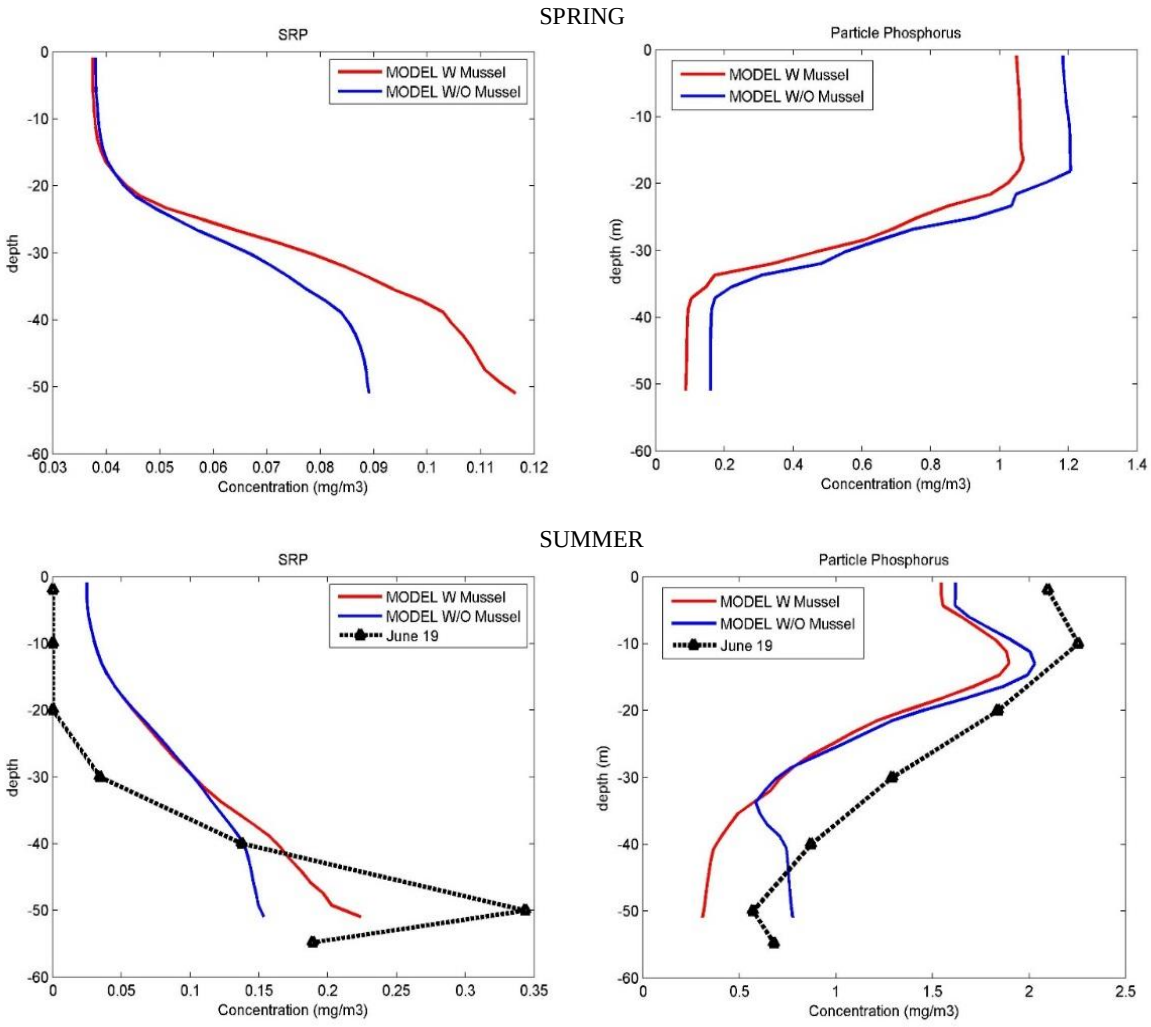

Fig.4.12 Comparison of vertical distribution of nutrient and phytoplankton. SRP (left), Particle Phosphorus (right).

weak stratification during this period. With the formation of strong stratification at the thermocline in summer, little difference is found at the surface mixing layer due to the limited access of mussels. However, a much lower boundary concentration layer of PP at bottom is modeled compared to the case without mussel. Meanwhile, field measurements at this site in summer of 2012 was performed, the simulation results showed reasonable magnitude and the results with mussel included displayed more accuracy compared to the observed data. However, the model still overestimated the concentration of SRP on the surface and underestimated that in the bottom.

As for the time series (spring and summer in 2012) of the vertical change at the 55m site (Fig.4.13-4.15), the SRP showed a low concentration at the surface layer based on the consumption of phytoplankton. And the difference of the simulation with/without mussel clearly demonstrated a high boundary concentration layer during spring and summer due to the excretion effect of mussels. The growth of large phytoplankton is limited on the light, water temperature, SRP as well as strong need of silicon. When the water surface temperature becomes warm at the end of spring in addition with the light, large phytoplankton was found in rapid growth compared to the small phytoplankton for the simulation results. When it stepped into the summer and silica was not well supplied, the growth of large phytoplankton is significantly suppressed. Our simulation results did prove an important role in the distribution of the large phytoplankton. In the spring, uniform decrease on the whole water column was simulated while strong decrease only happens in the bottom layer through the filtering activities. In other words, our model proved the mussel did a positive job in preventing the potential algae blooms in the spring time. Different to the large size phytoplankton, the small phytoplankton is in a low maximum growth rate and the growth is not dependent on silica. As the results showed, the

dramatic growth occurs primarily in the summer. So mussels' effect is little to the small phytoplankton on the surface with the strong stratification.

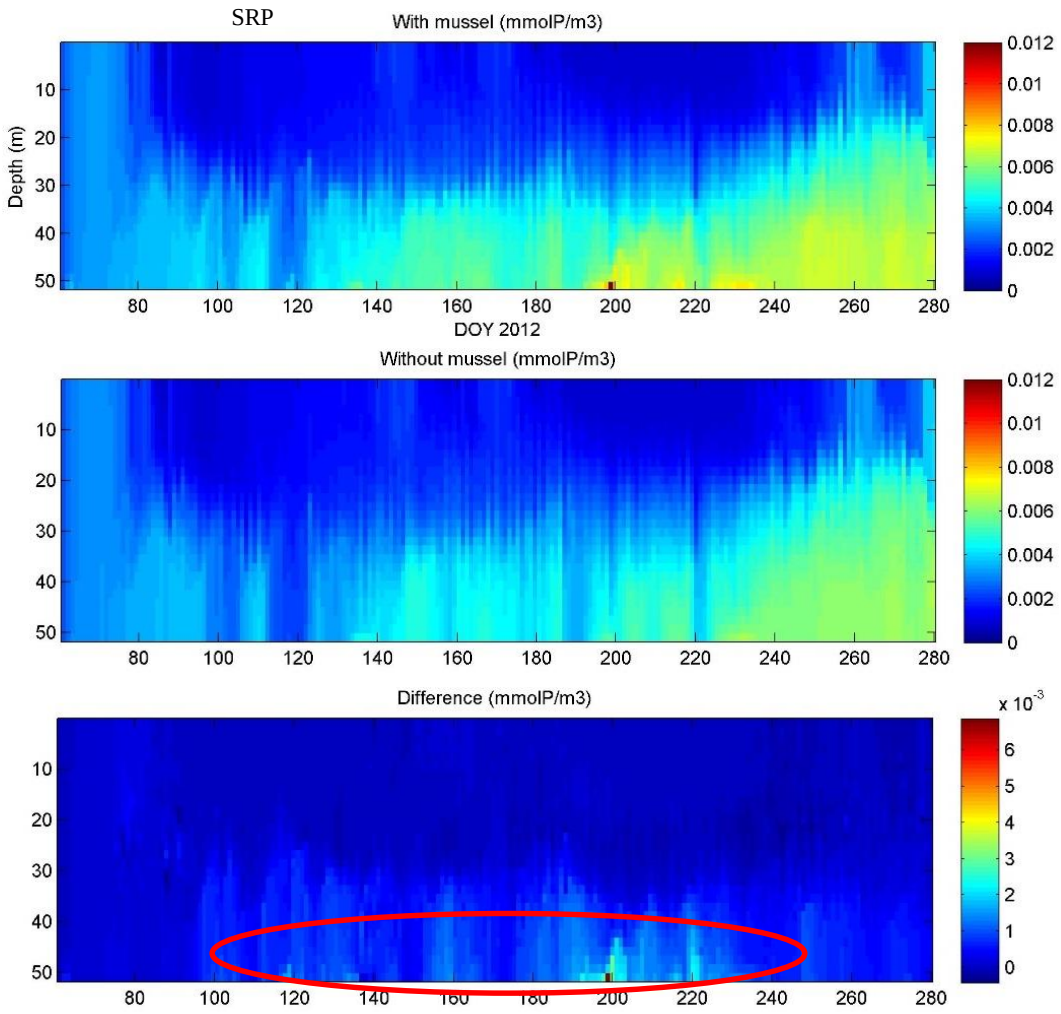

Fig.4.13 SRP concentration simulation in the 55m site in spring and summer. With mussel (above), without mussel (mid), their difference (bottom).

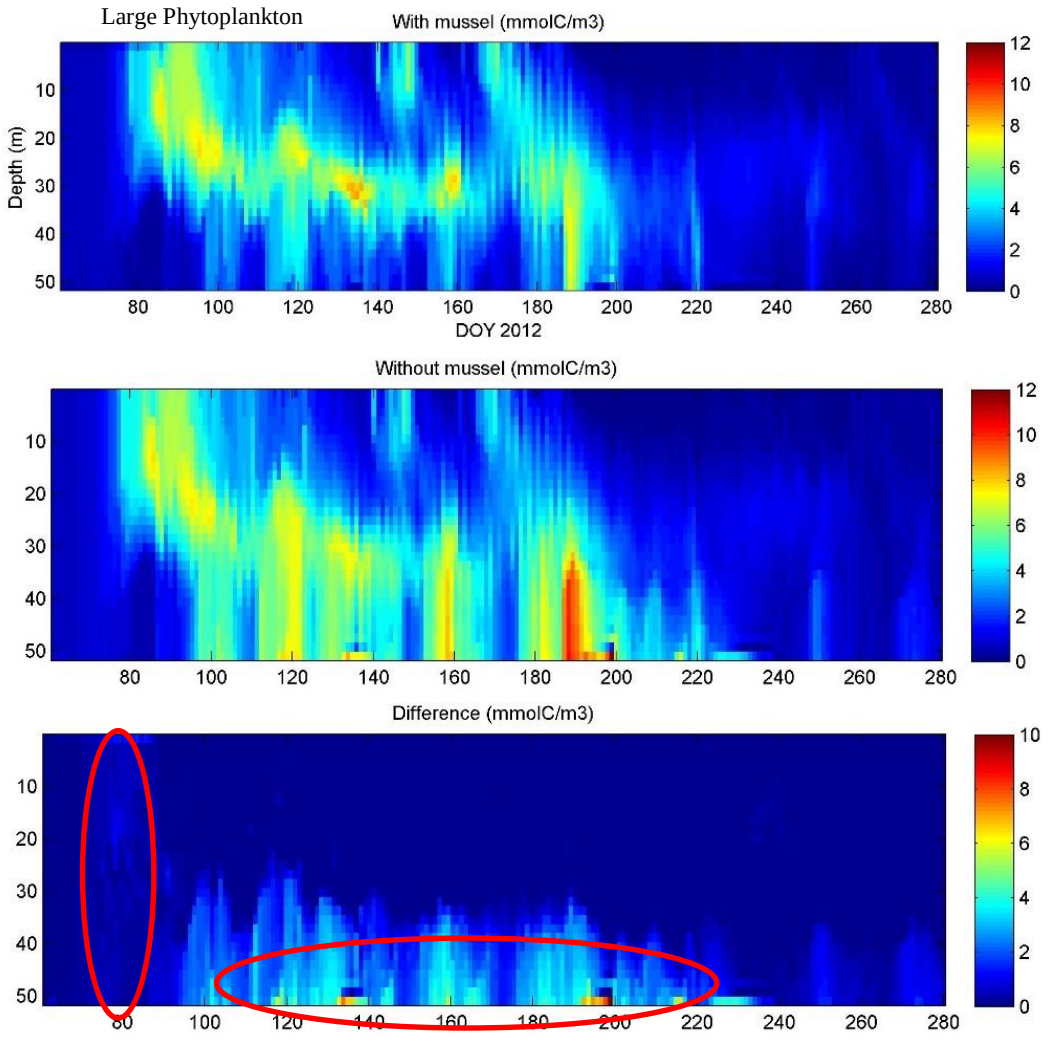

Fig.4.14 Large phytoplankton concentration simulation in the 55m site in spring and summer. With mussel (above), without mussel (mid), their difference (bottom).

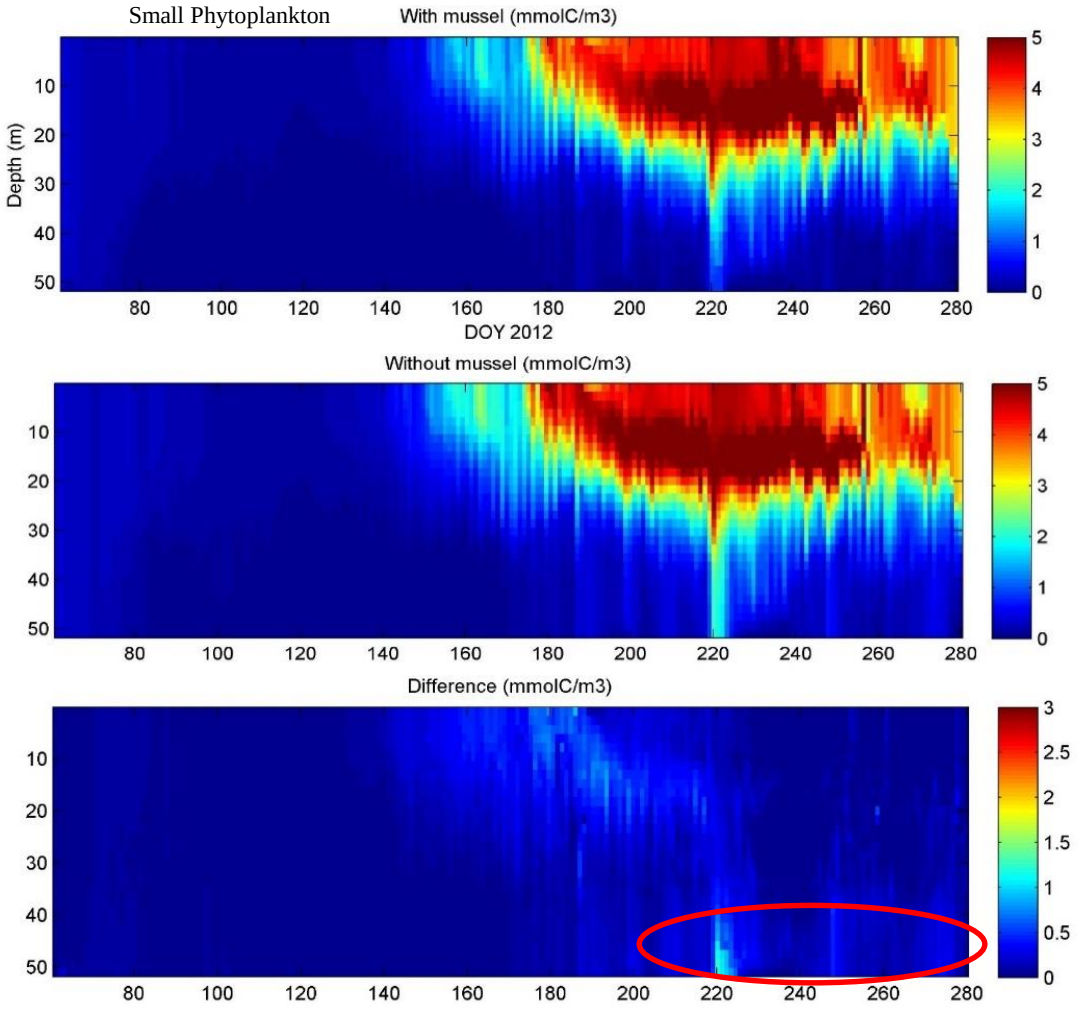

Fig.4.15 Small phytoplankton concentration simulation in the 55m site in spring and summer. With mussel (above), without mussel (mid), their difference (bottom).

As described in the “nearshore shunt” hypothesis (Hecky et al, 2004), mussels in the shallow area are not only like local “engineers”, but also are responsible for the low particle concentration in the offshore area. In order to understand the effect of the mussel in the nearshore and offshore exchange, the vertical transect of Lake Ferry Express (LFE) route is determined as the research target here. The LFE connects the city of Milwaukee in Wisconsin and the city of Muskegon in Michigan as shown in Fig.4.16. At the same time, the bottom mussel density is also plotted along the express route (Fig.4.17). This transect is featured with very low

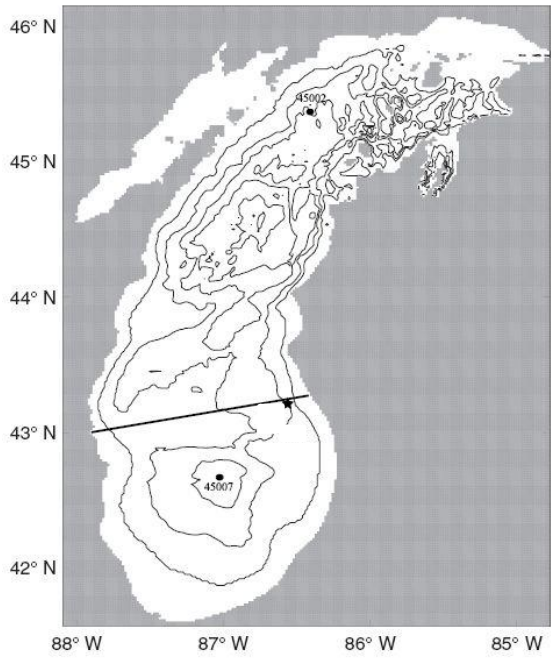

Fig.4.16 Lake ferry transect in Lake Michigan, isobaths are contoured at 50m intervals.

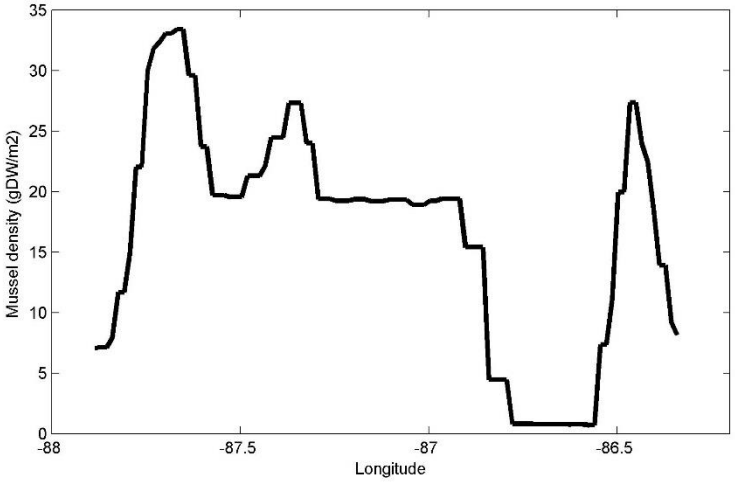

Fig.4.17 Bottom mussel density along the ferry route (g DW/m^2).

density of mussel at very shallow area as well as very deep positions. In the mid depth region, high density of mussels is established there. The phytoplankton and SRP results along this

transect are extracted at DOY 70, 110, 150, 180, 210 for the spring and summer period (Fig.4.18-4.19).

At the very beginning of DOY 70, the mussels' effect on phytoplankton distribution is very local, with phytoplankton concentration decreases in the whole water column due to the grazing effect. Difference at deep positon is nearly zero with no colonization of mussel there. However, as the time progresses, the concentration at the nearshore area become lower first under considerable filtering effect of mussel. With the horizontal advection and diffusion, the phytoplankton in the upper layer and bottom layer at the offshore area is very likely to transport to the nearshore area as depicted in DOY 150, and relative low concentration is observed even there in no colonization of mussel in this area. Given the high current speed at surface, the change is much stronger than that in the bottom. At depths near the thermocline, the hydrodynamic is very stable and little difference is found between the simulation with and without mussels. Very similar to the phytoplankton, SRP is featured with a local increase under the excretion effect of mussels in the well-mixed spring season. And with the bottom current effect, the high concentration boundary layer of SRP can be observed in the offshore area without mussel colonization as depict in DOY 180. At the surface, no obvious difference was observed since the SRP was kept in a very low concentration due to the uptake by the phytoplankton.

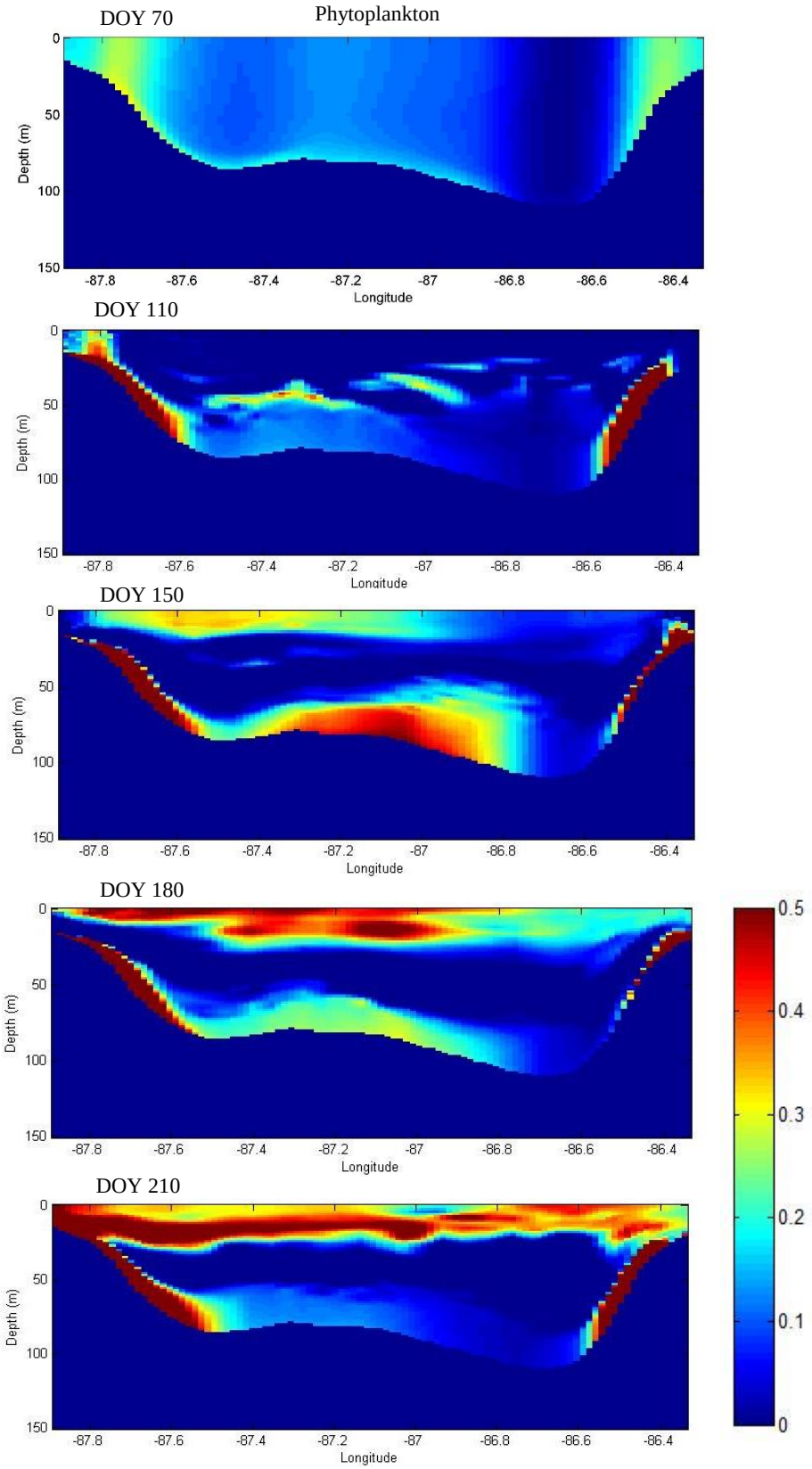

Fig.4.18 Time series of vertical phytoplankton concentration difference along the transect of with/without mussel (mmol/m^3).

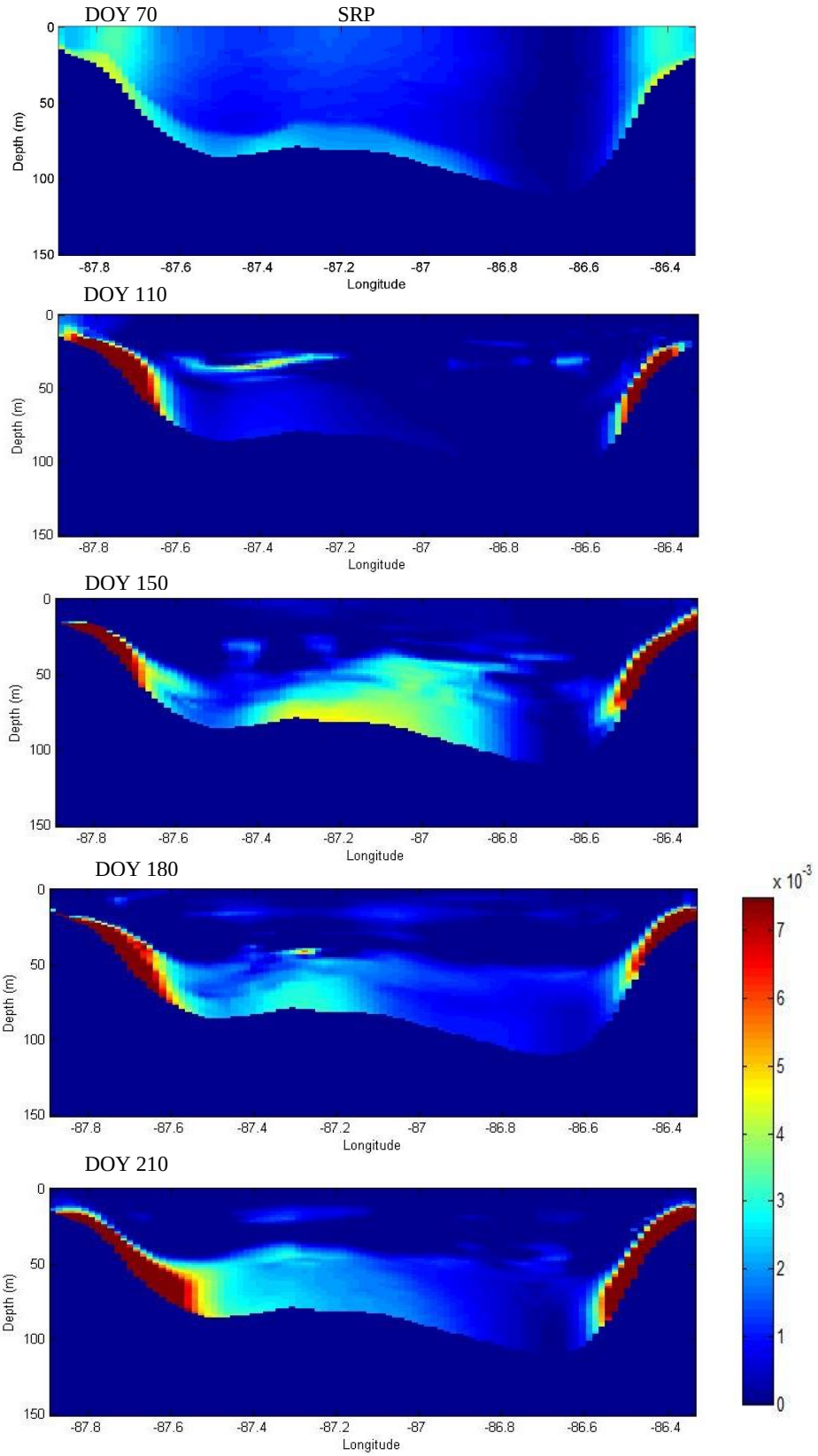

Fig.4.19 Time series of vertical SRP concentration difference along the transect of with/without mussel (mg/m^3).

4.3 Conclusion

In this chapter, the 3D biophysical model is proved to be capable in simulating the hydrodynamic environment and mussels' filtering effect on Lake Michigan. Based on the physical FVCOM model, lake surface temperature, thermal structure and current pattern were discussed with the comparison between the simulation results and observational data. Our model successfully reproduced the lake-wide spatial water surface temperature, seasonal vertical stratification and current circulation. Horizontal advection, diffusion and vertical mixing were well reproduced and applied to drive the biological model simulation. Besides the physical exchange, the NPZD model was established to well represent the biological paramters and mussels were incorporated in this model as a bottom boundary condition. To investigate how mussel will affect the ecosystem, the case with and without mussels was simulated respectively to check the difference. With the grazing and excretion process, the simulation with mussel showed almost 6 percent decrease in the total phytoplankton in spring while the 2 percent decrease in the summer time. In addition, the simulation results with mussel added featured with a high boundary concentration layer of nutrient and a low boundary concentration layer of phytoplankton near the bottom which agrees well with recent field observations. The vertical mixing was also demonstrated as an important factor for the mussel on the clearance rate. During the weak stratification in spring, the mussel is highly possible to access the whole water column while very limited depth over bottom can be influenced by mussels' filtering activities under strong stratification. At last, the transect time series were analyzed and the mussel was found not only to affect the local area, but can efficiently resulted in a lower phytoplankton concentration in offshore areas.

Chapter 5

5. *Cladophora* Particle Trajectory Simulation

5.1 Physical Result

The physical model that tracks sloughed Cladophora particle is driven by the physical output of FVCOM simulation as described in section 2.3. The key processes to track the particles are well resolve the flow field. Very dense mesh was applied for this area for high resolution output. Sleeping Bear Dune area is characterized with complicated bathymetry, so the simulated vertical

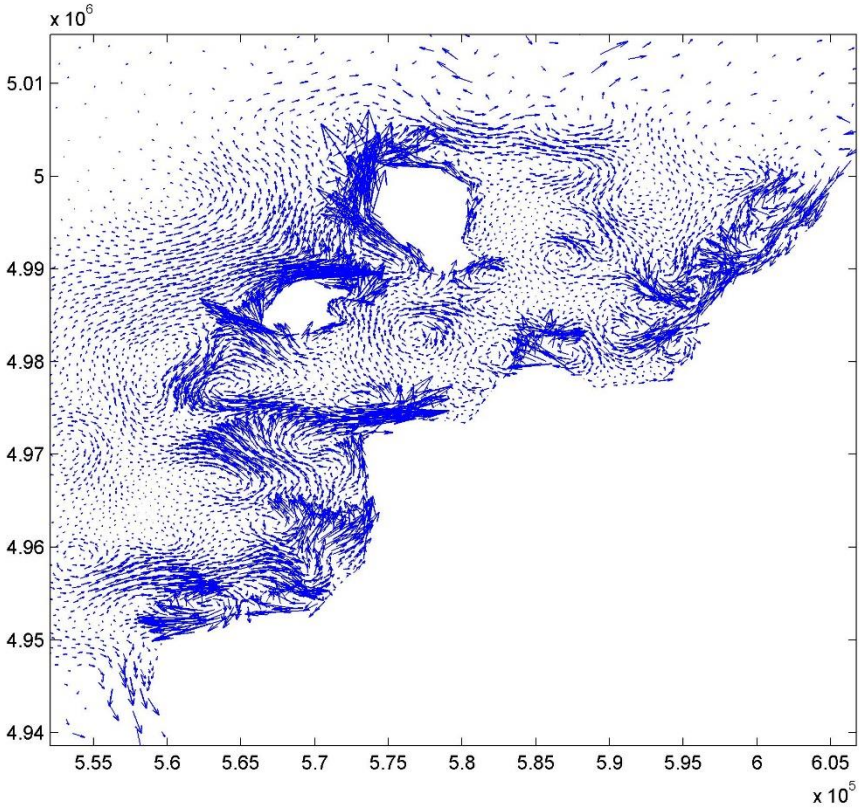

Fig.5.1 Vertical depth average flow pattern for SBD.

average velocity was featured with several gyres as shown in Fig.5.1. Field velocities were collected at the bottom of the 10m Good Harbor pit in 2013. Observed velocity speed at bottom is small, around 2cm/s. the model well reproduced the east component of velocity and show small bias in the north component compared to the field measurement (Fig.5.2).

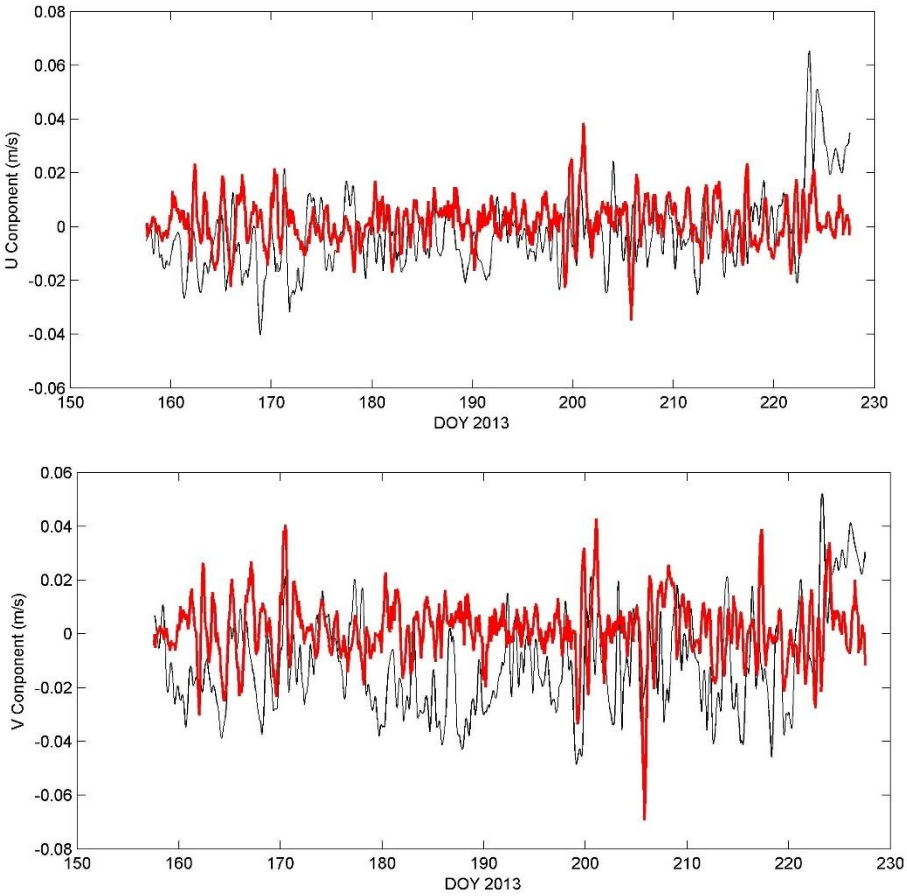

Fig.5.2 Comparison of velocity at the Good Harbor bottom. Observation (black), model simulation (red).

5.2 Trajectory Simulation

The trajectory simulation is based on the Lagrangian particle tracking method as described in section 2.5. In the particle model, we assume that the *Cladophora* all grow in the shallow area with depth less than 10m which is reasonable given the light requirement at the very bottom to support the growth. And when they are dead, they will be treated as a particle and move with the flowing water. The initial release position is as shown by blue dots in Fig.5.3. For the simulation, 5000 thousand particles will be released every day to track where they will be and their possible final destination. For the one-month model run from September to October, particles in general moved away from the original position and gradually deposited at nearby and deeper area (Fig. 5.4). Since the wave was treated as uniform for this area, so the wave induced bottom shear stress will be different with depth according to the linear wave equation. The shallow area would experience with much stronger bottom shear stress compared to the deep area. So in the shallow

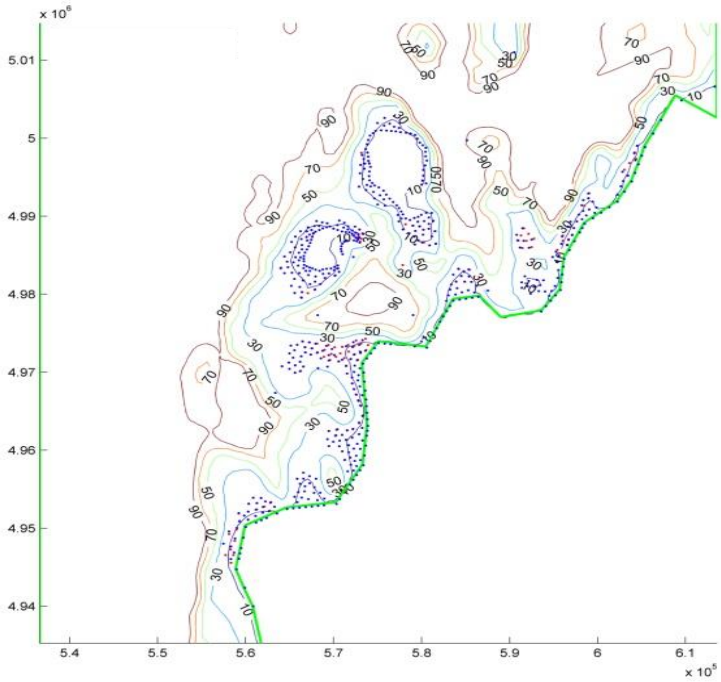

Fig.5.3 Initial positions (blue dots) to release the *Cladophora* particle for the SBD area.

area, the deposited particles are very likely to be suspended into the water body again while the in deep pit, the particles are difficult to be suspended unless they are under strong storm effects. Our particle model validated the assumption that dead *Cladophora* is possible to accumulate in the deep pit and will result in potential environmental problems.

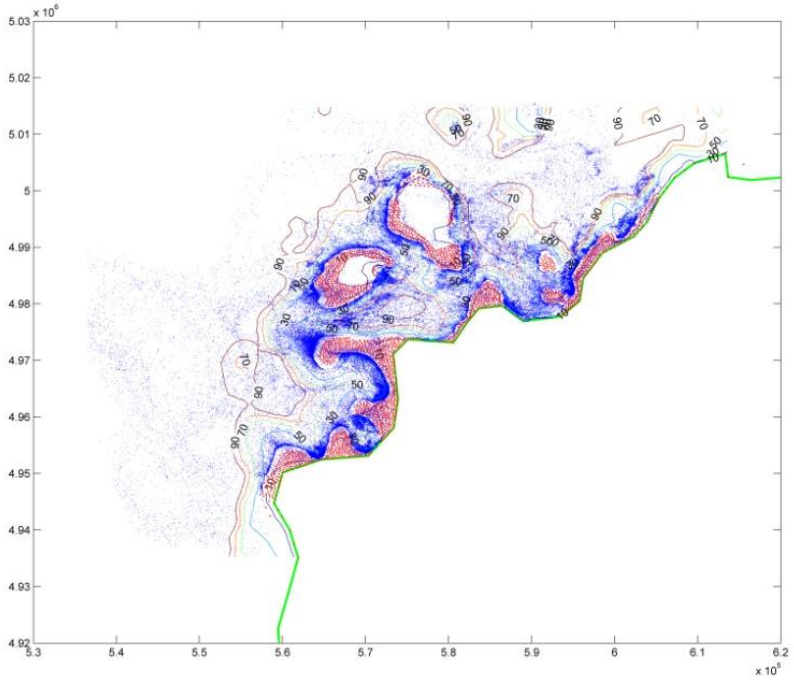

Fig.5.4 Final position (blue dots) of the particles after one month in the SBD area.

Chapter 6

6. Conclusion

6.1 Completed Work

The overall objective of my thesis study is to apply numerical models to investigate the ecosystem of Lake Michigan, specifically to investigate how invasive dreissenid mussels affect the nutrient dynamic and distribution of phytoplankton. An accurate representation of hydrodynamic circulation, horizontal advection and vertical mixing is key to explore the effect of mussels and the transport of sloughed *Cladophora*. Biogeochemical models coupled with the physical model have been demonstrated as a useful and efficient tool for the research objective. The following tasks have been completed in my thesis study:

1. A one-dimensional model with accurate vertical mixing parameters resolved was developed for Lake Michigan. It takes full consideration of momentum sink, wave and Coriolis effects to reproduce important physical processes. Biological and chemical processes can also be coupled with this model directly.
2. I have improved the FVCOM by adapting the dynamically calculated heat flux in the model run. More importantly, a three-dimensional biophysical model with mussels' filtration and excretion processes incorporated was established to investigate the impact of mussels on the ecosystem.
3. Based on simulation results from FVCOM, a *Cladophora* particle trajectory model was developed to track the path of the sloughed *Cladophora*.

6.2 Research Findings

The 1D model has been successfully developed at the 55m mid-depth region in my research work and it can be easily expanded to any other area with stable horizontal homogeneity. Incorporating the prognostic heat flux in the 1D model has been proved to improve the model performance compared to the precomputed heat flux in reproducing the water surface temperature. A momentum sink term was found to be important for the 1D model to account for some horizontal processes that are missing in the model, and to offset the artificially increased velocity, especially near the lake bottom. The wave effects were tested in the model as well. It is found that including wave breaking was necessary to correctly simulate the near-surface energy dissipation. The wave current interaction did help to increase the mixing depth. However, these improvements are not as significant as those reported in ocean wave mixing modeling. The 1D phytoplankton transport model demonstrated that mid-depth mussels can effectively access the entire water column under weak stratification conditions, which may attribute to the disappearance of algae blooms in the spring.

The 3D coupled physical-biogeochemical model can well reveal the impact of mussels to Lake Michigan. Based on the simulated 2012 case, the total amount of phytoplankton was estimated to decrease by 6 percent in spring and by 2 percent in summer with the mussel model included. Near the mid-depth lake bottom, a layer of high nutrient concentration and low particle concentration was observed, comparing simulation runs with and without mussels. It also suggests that mussels' effect is not local and mussels in shallow and mid-depth zones can affect the concentration of phytoplankton and nutrient in the offshore area. This result is also supported by the Ferry (Lake Express) route transect surveys. The particle tracing model suggests that sloughed *Cladophor*a particles will likely end up depositing at the nearby and deep areas. This

simulation result strongly supported the hypothesis that *Cladophora* may accumulate in deep pits of the Sleeping bear dune area and put a potential threat to the environment.

6.3 Future Work

In both 1D and 3D modelling work, an artificially diffusive thermocline from simulation results remains to be a problem. The structure of the thermocline, as the most important feature for the summer stratification, plays a critical role in determining the exchange of materials between the eplimnion and hypolimnion water. In addition to the numerical artifact, other missing important physical processes, such as the Langmiur circulation, may also attributed to the diffuse thermocline structure. In addition, a depth dependent momentum sink term rather than the uniform scheme currently employed should be considered to better resolve the momentum field.

The biogeochemical module can be improved in a number of ways. For example, the cycling of nutrient through the buried mussel feces and pseudofeces, as well as the dead *Cladophora* should be incorporated in to the model to partially complete the energy and nutrient fluxes between the substrate and the water column. At last, much more work should be done on the particle tracking model in the future. Instead of the constant particle release every day, the *Cladophora* growth model is definitely necessary to be incorporated to derive particle release with spatial and time variations. In addition, more validation work should be conducted to build the relationship between the variation of deposited particles and the recorded *Cladophora* mats depth.

Reference

Ackerman, J.D., Loewen, M.R., and P.F. Hamblin. 2001. Benthic-pelagic coupling over a zebra mussel bed in the western basin of Lake Erie. Limnology and Oceanography 46(4): 892-904.

Auer, M.T., Tomlinson, L.M., Higgins, S.N., Malkin, S.Y., Howell, E.T., Bootsma, H. a., 2010. Great Lakes Cladophora in the 21st century: same algae—different ecosystem. J. Great Lakes Res. 36, 248–255. doi:10.1016/j.jglr.2010.03.001

Babanin, A.V., 2006. On a wave-induced turbulence and a wave-mixed upper ocean layer. Geophysical Research Letters 33(L20605).

Babanin, A. V., et al. 2012. Surface waves and wave-coupled effects in lower atmosphere and upper ocean. Journal of Geophysical Research 117.

Bai, X.Z., Wang, J., 2013. Modelling 1993-2008 climatology of seasonal general circulation and thermal structure in the Great Lakes using FVCOM. Ocean Modelling 65:40-63.

Beletsky, D. and D. Schwab 2001. Modeling circulation and thermal structure in Lake Michigan: annual cycle and interannual variability. Journal of Geophysical Research 106: 19745-19771.

Beletsky, D., et al. 2006. Modeling the 1998-2003 summer circulation and thermal structure in Lake Michigan. Journal of Geophysical Research-Oceans 111(C10).

Bocaniov, S. a., Smith, R.E.H., Spillman, C.M., Hipsey, M.R., Leon, L.F., 2014. The nearshore shunt and the decline of the phytoplankton spring bloom in the Laurentian Great Lakes: insights from a three-dimensional lake model. Hydrobiologia 731, 151–172. doi:10.1007/s10750-013 1642-2

Boegman, L., Loewen, M.R., Culver, D.A., Hamblin, P.F., Charlton, M.N., 2008. Spatial-Dynamic Modeling of Algal Biomass in Lake Erie: Relative Impacts of Dreissenid Mussels and Nutrient Loads. J. Environ. Eng. 134, 456–468. doi:10.1061/(ASCE)0733-9372(2008)134:6(456)

Boegman, L., Loewen, M.R., Hamblin, P.F., Culver, D.A., 2008. Vertical mixing and weak stratification over zebra mussel colonies in western Lake Erie. Limnol.Oceanogr. 53, 1093–1110.

Bunnell, D.B., Madenjian, C.P., Holuszko, J.D., Adams, J. V., French, J.R.P., 2009a. Expansion of Dreissena into offshore waters of Lake Michigan and potential impact on fish populations. J. Great Lakes Res. 35, 74–80. doi:10.1016/j.jglr.2008.10.002

Bootsma, H.A., 2009. Causes, Consequences and Management of Nuisance *Cladophora*; Final Report Submitted to the Environmental Protection Agency Great Lakes National Program Office. Chicago, IL.

Bootsma, H., Liao, Q., 2013. Nutrient Cycling by Dreissenid Mussels, in: Quagga and Zebra Mussels. CRC Press, pp. 555–574. doi:doi:10.1201/b15437-43

Cha, Y., Stow, C. a, Nalepa, T.F., Reckhow, K.H., 2011. Do invasive mussels restrict offshore phosphorus transport in Lake Huron? Environ. Sci. Technol. 45, 7226–31. doi:10.1021/es2014715

Choi, J., et al. 2012. A year of internal Poincaré waves in southern Lake Michigan. Journal of Geophysical Research: Oceans 117(C7).

Connelly, N.A., O'Neill, C.R., Knuth, B.A., Brown, T.L., 2007. Economic zebra mussels on drinking water treatment and electric power generation Environ. Manage. 40, 105–112. doi:10.1007/s00267-006-0296-5

Chapra, S.C., Dolan, D.M., 2012. Great Lakes total phosphorus revisited: 2. Mass balance modeling. J. Great Lakes Res. 38, 741–754.

Craig, P.D, Banner, M.L., 1994. Modeling wave-enhanced turbulence in the ocean surface layer. Journal of Physical Oceanography 24:2546-2559.

Dayton, A.I., Auer, M.T., Atkinson, J.F., 2014. *Cladophora*, mass transport, and the nearshore phosphorus shunt. J. Great Lakes Res. 40, 790–799. doi:10.1016/j.jglr.2014.05.010

Edwards, W. J., C. R. Rehmann, et al. (2005). The impact of a benthic filter feeder: limitations imposed by physical transport of algae to the benthos. Can. J. Fish. Aquat. Sci. 62: 205-214.

Fahnenstiel, G., Pothoven, S., Vanderploeg, H., Klarer, D., Nalepa, T., Scavia, D., 2010b. Recent changes in primary production and phytoplankton in the offshore region of southeastern Lake Michigan. J. Great Lakes Res. 36, 20–29. doi:10.1016/j.jglr.2010.03.009

Hecky, R.E., Smith, R.E.H., Barton, D.R., Guildford, S.J., Taylor, W.D., Charlton, M.N., Howell, T., 2004. The nearshore phosphorus shunt: a consequence of ecosystem engineering by dreissenids in the Laurentian Great Lakes. Can. J. Fish. Aquat. Sci. 61, 1285–1293.

Higgins, S.N., Hecky, R.E., Guildford, S.J., 2006. Environmental controls of *Cladophora* growth dynamics in eastern Lake Erie: Application of the *Cladophora* growth model (CGM). J. Great Lakes Res. 32, 629–644.

Higgins, S.N., Pennuto, C.M., Howell, E.T., Lewis, T.W., Makarewicz, J.C., 2012. Urban influences on *Cladophora* blooms in Lake Ontario. J. Great Lakes Res. 38, 116–123. doi:10.1016/j.jglr.2011.11.017

Higgins, S.N., Malkin, S.Y., Todd Howell, E., Guildford, S.J., Campbell, L., Hiriart-Baer, V., Hecky, R.E., 2008b. An Ecological Review of *Cladophora Glomerata* (*Chlorophyta*) in the Laurentian Great Lakes. J. Phycol. 44, 839–854. doi:10.1111/j.1529-8817.2008.00538.x

Hu, H. and J. Wang 2010. Modeling effects of tidal and wave mixing on circulation and thermohaline structures in the Bering Sea: Process studies. Journal of Geophysical Research 115(C1).

Huang, C. J. and F. L. Qiao 2010. Wave-turbulence interaction and its induced mixing in the upper ocean. Journal of Geophysical Research-Oceans 115(C4).

Jiang, L., Xia, M., 2015. Dreissenid mussel impacts on plankton dynamics in western Lake Errie. Ecological Modelling 308: 18-33.

Jonsson, P.R., Petersen, J.K., Karlsson, Ö., Loo, L., Nilsson, S., 2014. Particle depletion above experimental bivalve beds : In situ measurements and numerical modeling of bivalve filtration in the boundary layer. Limnol. Oceanogr. 50, 1989–1998.

Fillingham, J.H., 2015. Modelling Lake Michigan nearshore carbon and phosphorus dynamics. University of Wisconsin-milwaukee

Karatayev, A.Y., Burlakova, L.E., Padilla, D.K., 2014. Zebra versus quagga mussels: a review of their spread, population dynamics, and ecosystem impacts. Hydrobiologia 97–112. doi:10.1007/s10750-014-1901-x

Leon, L.F, 2011. Application of a 3D hydrodynamic-biological model for seasonal and spatial dynamics of water quality and phytoplankton in Lake Erie. Journal of Great Lakes Research. 37(1): 41-53.

Limburg, K.E., Luzadis, V. a., Ramsey, M., Schulz, K.L., Mayer, C.M., 2010. The good, the bad, and the algae: Perceiving ecosystem services and disservices generated by zebra and quagga mussels. J. Great Lakes Res. 36, 86–92. doi:10.1016/j.jglr.2009.11.007

Luo, L., Wang, J., 2012. Simulating the 1998 spring bloom in Lake Michigan using a coupled physical-biological model. Journal of Geophysical Research: Ocean 117(C10011).

Madon, S.P., Schneider, D.W., Stoeckel, J. a, Sparks, R.E., 1998. Effects of inorganic sediment and food concentrations on energetic processes of the zebra mussel, Dreissena polymorpha : implications for growth in turbid rivers. Can. J. Fish. Aquat. Sci. 55, 401–413. doi:10.1139/f97-214

Malkin, S.Y., Guildford, S.J., Hecky, R.E., 2008. Modeling the growth response of *Cladophora* in a Laurentian Great Lake to the exotic invader Dreissena and to lake warming. Limnol. Oceanogr. 53, 1111–1124. doi:10.4319/lo.2008.53.3.1111

McCormic, M. and G. Meadows, 1998. An intercomparison of four mixed layer models in a shallow inland sea. Journal of Geophysical Research. 93:6774-6788.

Mellor G, Yamada, T, 1982. Development of a turbulence closure model for geophysical fluid problems. Review of Geophysics and Space Physics 20:851-875.

Mellor, G. 2000. One-dimensional, ocean surface layer modelling: a problem and a solution. Journal of Physical Oceanography. 31:790-809.

Mellor, G. and A. Blumberg, 2004. Wave breaking and ocean surface layer thermal response. Notes and Correspondence 34: 693-698.

Mosley, C., and H. Bootsma. "Phosphorus recycling by profunda quagga mussels (Dreissena rostriformis bugensis) in Lake Michigan." Journal of Great Lakes Research 41 (2015): 38-48.

Nuss, W. and D. Titley, 1994. Use of multiquadric interpolation for meteorological objects analysis. Monthly Weather Review 122: 1611-1631.

Mida, J.L., Scavia, D., Fahnenstiel, G.L., Pothoven, S. a., Vanderploeg, H. a., Dolan, D.M., 2010. Long-term and recent changes in southern Lake Michigan water quality with implications for present trophic status. J. Great Lakes Res. 36, 42–49. doi:10.1016/j.jglr.2010.03.010

Nalepa, T.F., Fanslow, D.L., Lang, G. a., 2009. Transformation of the offshore benthic community in Lake Michigan: recent shift from the native amphipod Diporeia spp. to the invasive mussel Dreissena rostriformis bugensis. Freshw. Biol. 54, 466–479. doi:10.1111/j.1365-2427.2008.02123.x

Nalepa, T. F., S. A. Pothoven, et al. 2009. Recent changes in benthic macroinvertebrate populations in Lake Huron and impact on the diet of lake whitefish (*Coregonus clupeaformis*). Aquatic Ecosystem Health & Management 12(1): 2-10.

Nalepa, T.F., Fanslow, D.L., Pothoven, S. a., 2010. Recent changes in density, biomass, recruitment, size structure, and nutritional state of Dreissena populations in southern Lake Michigan. J. Great Lakes Res. 36, 5–19. doi:10.1016/j.jglr.2010.03.013

Nalepa, T.F., Fanslow, D.L., Lang, G. a, Lamarand, D.B., Cummins, L.G., Carter, G.S., 2014. Lake-Wide Benthic Surveys in Lake Michigan in 1994-95, 2000, 2005, and 2010: Abundances of the Amphipod Diporeia spp. and Abundances and biomass of the Mussels Dreissena Polymorpha and Dreissena Rostiformis Bugensis, NOAA Technical Memorandum GLERL-164. Ann Arbor, Michigan.

Newell, R.I.E., 2004. Ecosystem influences of natural and cultivated populations of suspension-feeding bivalve molluscs: a review. J. Shellfish Res.

Ozersky, T., Malkin, S.Y., Barton, D.R., Hecky, R.E., 2009. Dreissenid phosphorus excretion can sustain C. glomerata growth along a portion of Lake Ontario shoreline. J. Great Lakes Res. 35, 321–328. doi:10.1016/j.jglr.2009.05.001

Pauer, J.J., Anstead, A.M., Melendez, W., Taunt, K.W., Kreis, R.G., 2011. Revisiting the Great Lakes Water Quality Agreement phosphorus targets and predicting the trophic status of Lake Michigan. J. Great Lakes Res. 37, 26–32. doi:10.1016/j.jglr.2010.11.020

Paulson, C. and J. Simpson, 1977. Irradiance measurements in the upper ocean. Journal of Physical Oceanography 7: 952-956.

Pothoven, S. a., Madenjian, C.P., 2008. Changes in Consumption by Alewives and Lake Whitefish after Dreissenid Mussel Invasions in Lakes Michigan and Huron. North Am. J. Fish. Manag. 28, 308–320. doi:10.1577/M07-022.1

Prins, T.C., Smaal, A.C., Dame, R.F., 1998. A review of the feedbacks between bivalve grazing and ecosystem processes. Aquat. Ecol. 31, 349–359. doi:10.1023/a:1009924624259

Raikow D.F, Sarnelle O, 2004. Dominance of the noxious cyanobacterium Microcystis aeruginosa in low-nutrient lakes is associated with exotic zebra mussels. Limnol. Oceanogr. 49:482-487.

Ramcharan, C. and C.B. Turner (2010). Influence of zebra (Dreissena polymorpha) and quagga (Dreissena rostriformis) mussel invasions on benthic nutrient and oxygen dynamics. Can. J. Fish. Aquat. Sci. 67(12), 1899-1908.

Rosati, A., Miyakoda, K., 1998. A general circulation model for upper ocean simulation. Journal of Physical Oceanography 18:1601-1626.

Rowe M.D, Obenour D.R, 2015. Mapping the spatial distribution of the biomass and filter-feeding effect of invasive dreissenid mussels on the winter-spring phytoplankton bloom in Lake Michigan. Freshwater Bioloy. 60: 2270-2285.

Schwalb, A.N., Bouffard, D., Ozersky, T., Boegman, L., Smith, R.E.H., 2013. Impacts of hydrodynamics and benthic communities on phytoplankton distributions in a large, *dreissenid*-colonized lake (Lake Simcoe, Ontario, Canada). Inl. Waters 3, 269–284.

Schwalb, A.N, 2014. 3D modelling of dreissenid mussel impacts on phytoplankton in a large lake supports the nearshore shunt hypothesis and the importance of wind-driven hydrodynamics. Aquatic. Sciences. 77(1): 95-114.

Strayer, D.L, Hattala, K.A, 2004. Effects of an invasive bivalve (*Dreissena polymorpha*) on fish in the Hudson River estuary. Can. J. Fish. Aquat. Sci. 61, 924-941.

Tomlinson, L.M., Auer, M.T., Bootsma, H.A., Owens, E.M., 2010. The Great Lakes *Cladophora* Model: Development, testing, and application to Lake Michigan. J. Great Lakes Res. 36, 287–297. doi:10.1016/j.jglr.2010.03.005

Troy, C. D., et al. 2012. Cross-shelf thermal variability in southern Lake Michigan during the stratified periods. Journal of Geophysical Research 117(C2).

Tyner, E.H., 2013. Nearshore Benthic Oxygen Dynamics in Lake Michigan. University of Wisconsin - Milwaukee.

Tyner, E.H., Bootsma, H.A., 2015. Dreissenid metabolism and ecosystem-scale effects as revealed by oxygen consumption. Journal of Great Lake Research 41:27-37.

Vanderploeg, H. a., Liebig, J.R., Nalepa, T.F., Fahnenstiel, G.L., Pothoven, S. a., 2010. Dreissena and the disappearance of the spring phytoplankton bloom in Lake Michigan. J. Great Lakes Res. 36, 50–59. doi:10.1016/j.jglr.2010.04.005

Vanderploeg, H., J. R. Liebig, et al. (2001). Zebra mussel (*Dreissena polymorpha*) selective filtration promoted toxic Microcystis blooms in Saginaw Bay (Lake Huron) and Lake Erie. Can.J. Fish. Aquat. Sci 58: 1208-1221.

Vanderploeg, H.A., Nalepa, T.F., Jude, D.J., Mills, E.L., Holeck, K.T., Liebig, J.R., Grigorovich, I.A., Ojaveer, H., 2002. Dispersal and emerging ecological impacts of Ponto-Caspian species in the Laurentian Great Lakes. Can. J. Fish. Aquat. Sci. 59, 1209–1228. doi:10.1139/F02-087

Vaughn, C.C., Nichols, S.J., Spooner, D.E., 2008. Community and foodweb ecology of freshwater mussels. J. North Am. Benthol. Soc. 27, 409–423. doi:10.1899/07-058.1

Wang, X. L., Y. Feng, and V. R. Swail, 2015. Climate change signal and uncertainty in CMIP5-based projections of global ocean surface wave heights. J. Geophys. Res. Oceans 120: 3859-3871.

Whitman, R.L., Shively, D.A., Pawlik, H., Nevers, M.B., Byappanahalli, M.N., 2003. Occurrence of Escherichia coli and Enterococci in *Cladophora* (*Chlorophyta*) in Nearshore Water and Beach Sand of Lake Michigan Occurrence of Escherichia coli and Enterococci in *Cladophora* (*Chlorophyta*) in Nearshore Water and Beach Sand of Lake Michigan. doi:10.1128/AEM.69.8.4714

Wu, C.H., Nepf, H.M., Breaking criteria and energy losses for three dimensional wave breaking. Journal of Geophysical Research: Ocean 107(C10).

Xue, P.F., Schwab, D.J., 2015. An investigation of the thermal response to meteorological forcing in a hydrodynamic model of Lake Superior. Journal of Geophysical Research: Oceans 120: 5233-5253.

Yu, N. and D. A. Culver (1999). Estimating the effective clearance rate and refiltration by zebra mussels, Dreissena polymorpha, in a stratified reservoir. Freshwater Biology. 41:481-492.

Zhang, H., Culver, D, Boegman, L., 2008. A two-dimensional ecological model of Lake Erie: Application to estimate *dreissenid* impacts on large lake plankton populations. Ecol. Modell. 214, 219–241. doi:10.1016/j.ecolmodel.2008.02.005

CURRICULUM VITAE

Name: Chunqi Shen

Place of Birth: Suzhou, China

Education

Ph.D. Civil and Environmental Engineering (08.2016)
University of Wisconsin-Milwaukee
Thesis: Modelling of *dreissenid* mussel impacts on Lake Michigan

M.S. Environmental Engineering (06.2012)
Hohai University, China
Thesis: Simulation of water diversion effect to water quality in Chaohu Lake based on the EFDC model

B.S. Environmental Engineering (06.2009)
Hohai University, China

Work Experience

University of Wisconsin-Milwaukee
Teaching Assistant Engineering Principles of Water Resources Design (Fall 2014, Spring 2015)
Research Assistant 2012-2014, 2015-2016

Research Techniques and Skills

Software: SPSS, Surfer, MapInfo, Tecplot, Microsoft office, Photoshop.
Programming Languages: Fortran, Matlab, Python, C/C++.

Honor & Awards

- Chancellor Award, Department of Civil Engineering, UW-Milwaukee. 2012-2015.
- Graduate major Scholarship, Department of Environmental Engineering, Hohai University, 2010.
- Academic Excellence Award, Department of Environmental Engineering, Hohai University, 2005-2009.

Research Experience

Alteration of Nutrient Cycling and Food Web Structure by Profundal Quagga Mussels in Lake Michigan: Establish the 1D and 3D biogeochemistry model to simulate the effect of mussel to the ecosystem in Lake Michigan (2013 till now).

Investigations of Type E Botulism at Sleeping Bear Dunes National Lakeshore: Using the Lagrangian particle trajectory method to track the movement of Cladorphora (2015 till now).
Fate and Transport of Biocolloids in Beach Sand: Field data measurement, sampling and data analysis (2012-2013).

The Effect of Water Diversion to Water Quality in Chaohu Lake: Applying the EFDC model to simulate the water quality situation in Chaohu Lake (2010-2012).

The National Key Project of Science and Technology: Management of Water Environment in Junction Area of Plain River Network Region in Taihu Lake Basin: Collecting basic data and evaluating the water quality of current situation in study area (2009-2010).

Conference Presentations

Shen, C.; Liao, Q; Tory, C; Bootsma, H.A., 2013. One dimensional turbulent mixing model in Lake Michigan with non-breaking wave induced mixing. International Association for Great Lakes Research Annual Conference. Purdue Unviersity, West Lafayette, IN. Jun 4, 2013.